Water exchange studies of lanthanide complexes and aqua ions

THÈSE N° 7116 (2016)

ÉCOLE POLYTECHNIQUE FÉDÉRALE DE LAUSANNE

POUR L'OBTENTION DU GRADE DE DOCTEUR ÈS SCIENCES

PAR

Shima KARIMI

ÉCOLE POLYTECHNIQUE
FÉDÉRALE DE LAUSANNE

Suisse
2016

"Don't be satisfied with stories of how things have gone for others. Unfold your own myth." Rumi

Table of Contents

Acknowledgements

First of all, I would like to express my deep gratitude to Prof. Lothar Helm for providing me with the great opportunity to do my PhD thesis under his supervision. I could have not imagined having a better advisor and mentor during my PhD. His patience, motivation, immense knowledge and his instructive advice was extremely valuable and without them the development of this thesis would have not been possible.

I am very grateful to the jury members Prof. Kay Severin, Prof. Gabor Laurenczy, Prof Carlos Geraldes and Prof. Eva Toth for accepting to expertise my thesis.

Part of the work discussed in this manuscript has been performed in collaboration with the Universidade da Coruña and Università del Piemonte Orientale "A. Avogadro". Great thank you to Prof. Carlos Platas-Iglesias, Prof. Mauro Botta and Dr. Lorenzo Tei for their help and corporation. Prof. André Merbach is acknowledged for many helpful and stimulating discussions.

I wish to express my sincere thanks to Dr. Loïck Moriggi as the former member of the group for his guidance during the first year of my PhD. Thanks to the other past members and co-workers of the group that contributed to an agreeable working environment. A special thanks to Gäelle Lapicoray for her help and friendship.

I am also very grateful to Yves Morier and Christophe Clément from the mechanical workshop for their technical support, Madeleine Steffen, the LCIB secretary and Anne-Lene Odegaard, the secretary of the PhD school for their help with the administrative work and the team of the ISIC chemical store: Gladys Pache, Annalise Carrupt and Benjamin Kronenberg. Thanks to Patrick Favre and Donald Zbinden for the IT support and special thanks to Dr. Pascal Miéville and Anto Barisic for their NMR technical support.

I would like to acknowledge deeply my parents and my brothers who were always behind me with all their love and worries. I can hardly express my sincere appreciation for their attention and support.

And finally I would like to thank my beloved husband, Anthony, for his constant support, inspiration, encouragement and unconditional love.

Abstract

Complexes of lanthanide (III) ions have been used in structural studies of biomolecules and as contrast agents (CA). Clinically approved CAs have only one water molecule in their first coordination sphere. Structure and water exchange rate of these complexes have been very well studied, however, water exchange kinetics of lanthanide complexes with two coordinated water molecules have not been investigated widely. In this regard, in the present work, a comprehensive study of water exchange kinetics of selected Ln^{3+} complexes with different ligands having two inner-sphere water molecules was conducted. In chapter III, selected lanthanide complexes of DO3A and DTTA-Me as representatives for macrocyclic and acyclic ligands have been studied by ^{17}O NMR spectroscopy and ^1H nuclear magnetic relaxation dispersion (NMRD). Water exchange rate constants measured on both complexes show a maximum at dysprosium and are much faster on DTTA-Me complexes than on the DO3A complexes. A change in water exchange mechanism is detected depending on both lanthanide and ligand structure.

When analyzing the water exchange rates of $[Ln(L)(H_2O)_2]^x$ complexes, a unique rate constant for the exchange of the two water molecules was considered, however, the individual rate constants can be either very similar or very different. In order to investigate this, in chapter IV, the replacement of coordinated water molecule(s) in $[Gd(DTTA-Me)(H_2O)_2]^-$ by fluoride anions using multinuclear NMR spectroscopy was studied. Variable pressure ^{17}O NMR measurements were also conducted for mechanistic assignment of the exchange reactions. It was found that fluoride binding facilitate the departure of the coordinated water molecule following a dissociative mechanism and accordingly cause a marked acceleration of the water exchange.

In chapter V, the water exchange properties of lanthanide complexes of AAZTAPh-NO_2 ligand was studied by ^1H NMR spectroscopy. Water exchange rate constants were found to change more than two orders of magnitude along the series. Moreover, $[Dy(AAZTAPh-NO_2)(H_2O)_2]^-$ was found to potentially be a very effective negative contrast agent for high magnetic fields imaging applications.

Chapter VI is dedicated to the water exchange kinetics of selected lanthanide perchlorate and chloride aqua ions at different concentrations of 0.5 m to 2 m in order to establish the extent to which the nature of the counter-ion and the concentration of the Ln^{3+} change the rate and mechanism of the water exchange. Our results measured on neodymium ion are the first direct experimental proof for the maximum of water exchange rate constant along the lanthanide series as well as the change of the mechanism for water exchange from a dissociative mechanism for aqua ions of the early lanthanides to an associative mechanism for those of the late lanthanides.

Keywords: lanthanide complexes, lanthanide aqua ions, water exchange rate, water exchange mechanism, ^{1}H, ^{17}O, ^{19}F and $^{35/37}Cl$ NMR spectrometry

Résumé

Les complexes d'ions lanthanides (III) ont été utilisés dans des études structurales des biomolécules et comme agents de contraste (AC). Les ACs approuvés cliniquement contiennent ont une seule molécule d'eau dans leur première sphère de coordination. La structure et le taux d'échange d'eau de ces complexes ont été très bien étudiés, cependant, la cinétique de l'échange d'eau des complexes de lanthanides avec deux molécules d'eau coordonnées n'a pas été beaucoup étudiée. À cet égard, dans le présent rapport, une étude complète de la cinétique de l'échange d'eau de certains complexes Ln^{3+} avec différents ligands ayant deux molécules d'eau dans leur sphère intérieure a été menée. Dans le chapitre III, les complexes de lanthanides DO3A et DTTA-Me sélectionnés en tant que représentants de ligands macrocycliques et acycliques ont été étudiés par spectroscopie RMN ^{17}O et par dispersion de relaxation magnétique nucléaire ^1H (DRMN). Les constantes de taux d'échange d'eau mesurées sur les deux complexes montrent un maximum à dysprosium et sont beaucoup plus rapides sur les complexes DTTA-Me que sur les complexes DO3A. Un changement dans le mécanisme d'échange d'eau est détecté en fonction de la structure des lanthanides et du ligand.

Lors de l'analyse des taux d'échange d'eau des complexes de $[Ln(L)(H_2O)_2]^x$, une constante de vitesse unique pour l'échange des deux molécules d'eau a été considérée, cependant, les constantes de vitesse individuelles peuvent être soit très similaires soit très différentes. Pour étudier cette question, au chapitre IV, le remplacement de la molécule d'eau coordonnée dans $[Gd(DTTA-Me)(H_2O)_2]^-$ par des anions fluorure à l'aide de la spectroscopie RMN multinucléaire a été étudié. Les mesures de RMN ^{17}O à pression variable ont également été effectuées pour l'assignation mécanistique des réactions d'échange. Il a été constaté que la liaison fluorure facilite le départ de la molécule d'eau coordinnée suivant un mécanisme dissociatif et par conséquent provoque une nette accélération de l'échange d'eau.

Dans le chapitre V, les propriétés d'échange d'eau de complexes de lanthanides AAZTAPh-NO$_2$ ont été étudiées par spectroscopie RMN ^1H. Il a été observé que les constantes de vitesse d'échange d'eau changent de plus de deux ordres de grandeur dans la

série. Par ailleurs, [Dy(AAZTAPh-NO$_2$)(H$_2$O)$_2$]$^-$ est révélé comme un agent de contraste négatif potentiellement très efficace pour des applications en imagerie à hauts champs magnétiques.

Le chapitre VI est consacré à la cinétique d'échange d'eau des perchlorates de lanthanide et des ions aqua chlorure sélectionnés, à différentes concentrations de 0,5 m à 2 m, afin d'établir dans quelle mesure la nature du contre-ion et la concentration en Ln^{3+} changent le taux et le mécanisme de l'échange d'eau. Nos résultats, mesurés sur l'ion néodyme, sont la première preuve expérimentale directe pour le maximum de la constante du taux d'échange d'eau dans la série des lanthanides, ainsi que le changement d'un mécanisme d'échange d'eau à partir d'un mécanisme dissociatif pour les ions aqua du début des lanthanides à un mécanisme associatif pour ceux de la fin des lanthanides.

Mots-clés: complexes de lanthanides, ions lanthanides aqua, taux de change de l'eau, mécanisme d'échange d'eau, spectrométrie RMN ^{1}H, ^{17}O, ^{19}F et $^{35/37}$Cl

Chapter I

Introduction

I.1   Lanthanide elements

I.1.1   General properties

The 15 f-block lanthanide elements, ranging from lanthanum to lutetium, atomic number of 57 to 71, show similar chemical properties. All lanthanide ions with the exception of La^{3+} to Lu^{3+} are paramagnetic at room temperature, having unpaired electrons located in the 4f orbitals. The inner 4f orbitals are filled progressively (Table I-1) along the lanthanide series. The radius of the lanthanide ions shrinks along the series from La^{3+} to Lu^{3+}, due to the shielding of the nuclear charge by the electrons of 4f.[1]

Lanthanides magnetic properties change along the series. It is now well accepted that the coordination number (CN) of Ln^{3+} ions changes along the series;[2] the heavier ions are eight-coordinate, whereas the lighter ions are nine-coordinate species and the change of CN occurs in the range of Nd^{3+} to Tb^{3+}, where equilibrium exists between the nine and eight coordinated species.

Table I-1. Lanthanide elements properties[3]

Element	Symbol	Atomic number	Atom	Ln^{3+}	Ln^{3+} ionic radius (Å)[4]	μ_{eff}
Lanthanum	La	57	$[Xe]\,5d^1\,6s^2$	$[Xe]$	1.25	0
Cerium	Ce	58	$[Xe]\,4f^1\,5d^1\,6s^2$	$[Xe]\,4f^1$	1.22	2.54
Praseodymium	Pr	59	$[Xe]\,4f^3\,6s^2$	$[Xe]\,4f^2$	1.2	3.58
Neodymium	Nd	60	$[Xe]\,4f^4\,6s^2$	$[Xe]\,4f^3$	1.175	3.68
Promethium	Pm	61	$[Xe]\,4f^5\,6s^2$	$[Xe]\,4f^4$	-	2.83
Samarium	Sm	62	$[Xe]\,4f^6\,6s^2$	$[Xe]\,4f^5$	1.14	0.85
Europium	Eu	63	$[Xe]\,4f^7\,6s^2$	$[Xe]\,4f^6$	1.12	0
Gadolinium	Gd	64	$[Xe]\,4f^7\,5d^1\,6s^2$	$[Xe]\,4f^7$	1.105	7.94
Terbium	Tb	65	$[Xe]\,4f^9\,6s^2$	$[Xe]\,4f^8$	1.09	9.72
Dysprosium	Dy	66	$[Xe]\,4f^{10}\,6s^2$	$[Xe]\,4f^9$	1.075	10.63
Holmium	Ho	67	$[Xe]\,4f^{11}\,6s^2$	$[Xe]\,4f^{10}$	1.055	10.6
Erbium	Er	68	$[Xe]\,4f^{12}\,6s^2$	$[Xe]\,4f^{11}$	1.04	9.59
Thulium	Tm	69	$[Xe]\,4f^{13}\,6s^2$	$[Xe]\,4f^{12}$	1.025	7.57
Ytterbium	Yb	70	$[Xe]\,4f^{14}\,6s^2$	$[Xe]\,4f^{13}$	1.01	4.53
Lutetium	Lu	71	$[Xe]\,4f^{14}\,5d^1\,6s^2$	$[Xe]\,4f^{14}$	0.995	0

I.1.1 Lanthanide application

Lanthanides have numerous applications such as optoelectronics applications,[5] luminescent materials (including probes in biology and medicine),[5-9] new magnetic materials,[10,11] catalysts[12,13] and vehicles for drug delivery in medicine. Cerium, praseodymium and lanthanum compounds have been used in China as feed additives as greater weight gain in sheep, chickens and pigs were observed when small amounts of these additives were used.[14,15] Moreover, lanthanide species have been used in pharmaceuticals for the treatment of various diseases. Lanthanide paramagnetic properties make their complexes a good candidate for contrast agents in Magnetic Resonance Imaging techniques.[8]

I.1.1.1 Magnetic Resonance Imaging (MRI)

Magnetic Resonance Imaging (MRI) is considered as a harmless and non-invasive diagnostic technique since MRI images are acquired without using ionising radiation normally used in ordinary x-ray/CAT (Computed Axial Tomography) scans or without the use of radiotracers as in PET and SPECT. Nowadays, over 1 million MRI scans are performed in the world every week. Most commercial MRI scanners utilise magnetic fields of $0.3 - 3$ Tesla. Such machines have become affordable even for small hospitals.

MRI consist of a super-conducting magnet producing a homogenous and strong magnetic field, a radio frequency (RF) transmitter and receiver system, a gradient coil system, and a computer which receive the signals sent from the receiver coil and process them to images (Figure I-1).
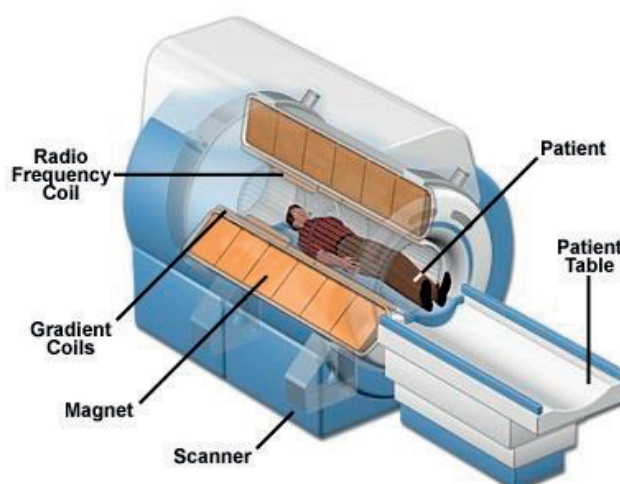
Figure I-1. MRI scanner.[16]

The resonance of water protons is mostly used for diagnostic purposes since water constitutes about 63% of the human weight and is present in all organs, tissues, muscles and fat. Moreover, ^1H isotope has a natural abundance of 99.98% and the highest nuclear gyromagnetic ratio among all stable isotopes. Other high natural abundance isotopes like ^{23}Na and ^{31}P can also be used. Inhaled hyperpolarised ^3He and ^{129}Xe are used for the MRI of lungs.

The magnetic moments of the protons in water molecules within the patients' tissues in the presence of a magnetic field will no longer be energetically equivalent and they will be oriented along the magnetic field creating a steady state magnetisation. A short radio frequency pulse can perturb this equilibrium. After the pulse, proton spins reorient to the original magnetic field direction. This recovering process is called relaxation. The relaxation of hydrogen nuclei after radiofrequency excitation takes from several hundred of milliseconds to a few seconds, depending on their surroundings. For instance, protons in water have longer relaxation time than in blood or in cerebrospinal fluid. In tissues, their relaxation times are much shorter and are the shortest in fat, about 200 milliseconds. These differences in relaxation times appear as degrees of brightness within the MR image.

I.1.1.1 MRI Contrast Agents

Although MRI is one of the mostly used diagnostic techniques, its low sensitivity is considered as its main drawback. An improvement could be achieved through acquiring more scans (increase of signal to noise) but the MRI acquisition is very long, normally tens of minutes and lengthening of the examination time would not be profitable. Acquisition time reduction and contrast enhancement can be achieved by the use of contrast agents (CAs) by accelerating the water protons relaxation, i.e. the time describing the return to the equilibrium magnetisation after a perturbation. Nowadays, almost 40% of MRI investigations use CAs[17,18] however it is estimated to increase due to the recent contrast agent development. An example of image improvement via the administration of a paramagnetic contrast agent can be seen in Figure I-2.
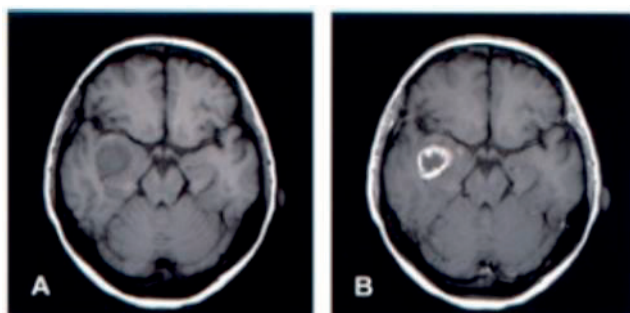
Figure I-2. MRI image of a human brain before (A) and after (B) injection of a Gd^{3+} contrast agent.[19]

The contrast in MR images is due to the differences in longitudinal, T_1, and transverse, T_2, relaxation times in different tissues. CAs are categorised as positive (T_1 weighted images) and negative (T_2 weighted images) based on brightening or darkening effects on the image. Since positive enhancement is normally easier to detect than the negative one, T_1 contrast agents are usually preferred. The main representatives of T_2 weighted images are the iron oxide nanoparticles.[20,21]

Gadolinium chelates demonstrated to be the best candidate for T_1 contrast agents[19] due to the large number of unpaired electrons ($4f^7$) and its slow electron spin relaxation, T_e ($\sim 10^{-9}$ s), compared to Ho^{3+} or Dy^{3+} which for example have larger magnetic moments

but the asymmetry of their electronic states leads to a very fast T_e ($\sim 10^{-13}$ s). The biggest drawback of Gd^{3+} is its toxicity. Administration of free Gd^{3+} is toxic even at low doses ($LD_{50} \sim 0.1$ mmol/kg body weight). Lanthanide aqua ions hydrolyze to form precipitating hydroxides, free Gd^{3+} ions are rapidly sequestered within the bone and the liver, with biologic half life of several weeks. This long term retention within the body leads to Gd^{3+} interactions with physiologic systems and the inhibition of the activity of numerous endogenous enzymes, mainly through Ca^{2+} replacement, which sizes approximate that of Gd^{3+}. Calcium channel inhibition would affect processes that depend upon Ca^{2+} influx, such as neural transmission. Furthermore, it has been proven that free gadolinium was closely related to the development of the serious syndrome nephrogenic systemic fibrosis (NSF).[22,23]

In order to prevent the Gd^{3+} toxicity, appropriate ligands such as poly(aminocarboxylates) have been developed to encapsulate Gd^{3+}.[19] These ligands bind to seven or eight of the nine available sites on the Gd^{3+} metal through their oxygen and nitrogen donor atoms, leaving one or two sites for water coordination. Gd^{3+} ions can form very stable complexes with polyaminocarboxylic acids. $Gd-DTPA$ (Magnevist®, Schering AG, Germany) ($log\,K_{ML} \sim 22.5$) as the first CA approved for clinical use in 1988 has been used for more than 20 million patients. $Gd-DOTA$ (Dotarem®, Guerbert SA, France) ($log\,K_{ML} \sim 24-25$), $Gd-HPDO3A$ (ProHance®, Bracco Imaging, Italy) and $Gd-DTPA-BMA$ (Omniscan®, GE Health, USA) are the other commercially available CAs, which are commonly used in clinics (Figure I-3). The more than ten fold lower toxicity value of Magnevist® or Dotarem® ($LD_{50} = 5.6$ mmol/kg body weight and 11 mmol/kg body weight, respectively) compared to the bare Gd^{3+} ion clearly illustrates the stability increase induced by chelate effect.[24,25] Although Gd^{3+} chelates are supposed to be cleared from the body by the kidneys, processes such as impaired kidney function may slow the excretion providing enough time for gadolinium complex dechelation. *In vivo* toxic effects can result from transmetallation, the ligand selectivity for the other endogenous ions (e.g. Zn^{2+}, Fe^{2+}, Mg^{2+} or Ca^{2+}) over the Gd^{3+}. The CAs efficiency is evaluated by its relaxivity enhancement. Commercial CAs as Dotarem, Magnevist, Omniscan and Prohance have relaxivity around 3.5 mM^{-1} s^{-1} at 20 MHz and 39°C.[26]

$$[Gd(DOTA)(H_2O)]^- \qquad [Gd(HP-DO3A)(H_2O)] \qquad [Gd(DTPA)(H_2O)]^{2-} \qquad [Gd(DTPA-BMA)(H_2O)]$$

Dotarem®   ProHance®,   Magnevist®   Omniscan®,
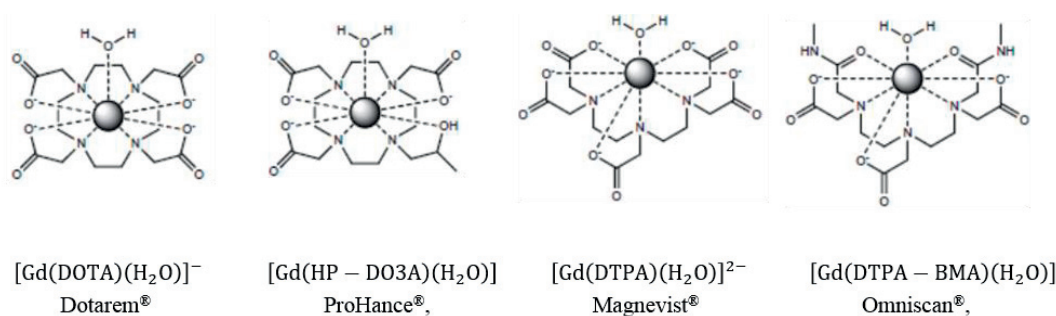
Figure I-3. Chemical structure of some commercially available MRI contrast agents.[19]

Some other lanthanides are also used as imaging agents. $[Eu(DTPA)(H_2O)]^{2-}$ chelate is investigated for target cells labeling.[27] $[Dy(DTPA-BMA)(H_2O)]$ is proposed for myocardial investigations[28] and $[Dy(HP-DO3A)(H_2O)]$ in brain investigations.[29]

As mentioned before, MRI contrast agent efficiency is evaluated in terms of relaxivity. The faster the relaxation, the shorter the exam and smaller amounts of contrast agents will be injected. An impressive amount of work has been carried out aimed at elucidating the relationship between the structural and dynamic characteristics of the Gd^{3+} complexes and parameters of the water relaxation enhancement. Some of these parameters can be tuned to maximise the relaxivity by ligand design.[8,30] These parameters are the rotational correlation time (τ_R), the number of directly bound water molecules to the metal ion (q) and the residence time of the water molecule in the first coordination sphere (τ_m).

The influence of rotational correlation time, τ_R, the time constant describing the tumbling of the Ln-water proton or oxygen vector,[31] depends on the magnetic field. In general, the slower the rotation, the more effective is the interaction between the Ln^{3+} electron spin and the nuclear spin of water protons/oxygens. Increasing τ_R mainly consisting in the synthesis of higher molecular weight ligands by the attachment of poly(amino carboxylate) chelate to macromolecules such as insulins,[32,33] dendrimers,[34-38] micelles,[36,39-42] metalostars,[43] or proteins,[31,44-47] however such an expected enhancement of relaxivity is often "quenched" due to the slow exchange of the bound water.[34]

The inner-sphere relaxivity is directly proportional to the number of bound water molecules. The bound water molecules relaxed by the lanthanide ions will be exchanged with surrounding water molecules, transmitting the relaxation to the bulk water. Hence, the more bound water molecules, the more solvent waters can be exchanged with inner-sphere water molecules. Using hepta- or hexadentate ligands would provide Ln^{3+} complexes with respectively 2 and 3 inner-sphere water molecules. However, this will lead to a decrease in thermodynamic stability of the compound due to the decrease of the denticity of the ligands. Furthermore, the coordinated water molecules may be replaced by bidentate endogeneous anions.[48] Few thermodynamically and kinetically stable Gd^{3+} chelates having two coordinated water molecules have been investigated (Figure I-4). In the case of Gd − HOPO complexes, developed by Raymond and co-workers,[49] their coordinating geometry prevents water molecule replacement with other ligands. Gd − AAZTA complexes developed by Aime and co-workes[50] show inertness towards endogenous anions.[50]
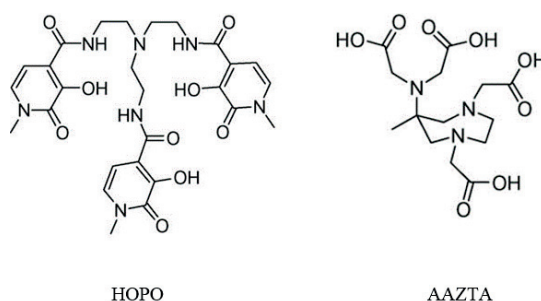
Figure I-4. Structure of HOPO and AAZTA ligand.

The water exchange rate is another parameter that has been investigated in great detail.[51,52] Complexes having the same number of inner-sphere water molecules might have different relaxivities, based on the difference in water molecule residency time. Increase in relaxivity is expected at high water exchange rates, however, the exchange rate between the bound water molecule(s) and the bulk water molecules needs to be situated within an optimal value,[17,34,53,54] as if the exchange is too slow, the paramagnetic effect will not be properly propagated throughout the solution and if it is too fast, the coordinated water molecule will not have enough time to feel the interaction with the electron spin of the metal.[55-57] For Gd^{3+} complexes, the relaxivity reaches it's maximum when water exchange rate is larger than the longitudinal relaxation rate of the bound water[58] $\left(k_{ex} \gg \frac{1}{T_{1m}}\right)$. Water exchange value of about 5×10^7 s^{-1} at 298 K is expected to lead to the highest relaxivity for large Gd^{3+} compounds at 0.47 T.[59] Different strategies have been considered to enhance the slow water exchange rate of the commercial CA[17,33,55,60-66] such as increasing the steric compression at the water binding site[55,61] or synthesis of a new class of chelates.[67]

It has to be noted that the rational design of highly efficient CAs resides in the simultaneous optimisation of all parameters to attain maximum relaxivities, *i.e.* 100 mM^{-1} s^{-1} instead of 4-5 mM^{-1} s^{-1} for commercial drugs, as predicted by the Solomon-Bloembergen-Morgan equations. Taking into account the effect of the MR scanner magnetic field, the requirements for high relaxivity at low magnetic fields ($\leq$ 1.5T) are fast k_{ex} and slow τ_R (> 5 ns), whereas at high magnetic fields (≥ 3 T) they are fast water exchange and intermediate τ_R (0.5−2 ns).[68]

I.2   Nuclear Magnetic Resonance Spectroscopy (NMR)

NMR has been used as an effective tool to study the relaxivity of MRI contrast agents. In fact, in 1946 Bloch[69] introduced the concept of relaxation times. He presumed that when the spins in a strong static field (B_0) are excited from equilibrium by a radiofrequency pulse, the magnetisation will return to its equilibrium position along the *z*-axis, representing the return of the spin populations to the Boltzmann equilibrium. This

implies a transition from the high energy state to the low energy state, known as relaxation.

The two main relaxation processes are longitudinal relaxation (T_1) and transverse relaxation (T_2). Longitudinal relaxation describes the restoration process of magnetisation M_0 in the direction of the external magnetic field (B_0 assumed to be along the z-axis), as the evolution of the M_z component along z in which the spins return to thermal equilibrium with the surrounding lattice (spin–lattice relaxation) (Figure I-5). The NMR pulse sequence used to measure T_1 is called *inversion recovery* (IR). In this method, a 180° pulse inverts equilibrium magnetisation along the z axis (from M_0 to $-M_0$). The magnetisation undergoes a longitudinal relaxation during a variable time τ, leading to the magnetisation $M_z(\tau)$ then a 90° pulse rotates the magnetisation z component to the xy plane in order to detect the free induction decay (FID). One can calculate the longitudinal relaxation time T_1, due to the exponential evolution of the magnetisation with respect to the variable delays τ:

$$\frac{dM_z}{d\tau} = -\frac{(M_z - M_0)}{T_1} \tag{I-1}$$

$$M_z(\tau) = M_z^0(1 - e^{-\tau/T_1}) \tag{I-2}$$
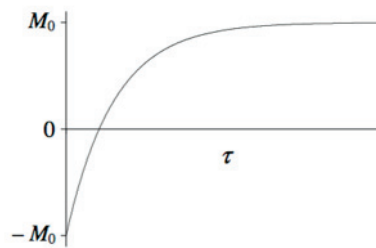
Figure I-5. The evolution of the magnetisation respect to the variable delays during T$_1$ measurement.

Transverse relaxation (T_2) is the time constant for relaxation along a direction perpendicular to the static magnetic field, describing the evolution of M_{xy} toward zero in which the spins return to equilibrium with other spins (spin–spin relaxation). This process does not require energy transitions but depends on the local variation of the magnetic

field strength that leads to the dispersion of phase coherence of the precessing spins. The *Carr-Purcell-Meiboom-Gill* ($CPMG$) sequence can be used to measure the transverse relaxation time T_2, which is composed of one 90° pulse along the x axis in order to rotate the magnetisation into the xy plane followed by two 180° pulses along the y axis. M_{xy} is decreasing and decaying to zero. By plotting the amplitude $M_{xy}(\tau)$ of the second echo against τ (Figure I-6) one can measure the T_2:

$$\frac{dM_{xy}}{d\tau} = -\frac{M_{xy}}{T_2} \tag{I-3}$$

$$M_{xy}(\tau) = M_{xy}^0 e^{-\tau/T_2} \tag{I-4}$$
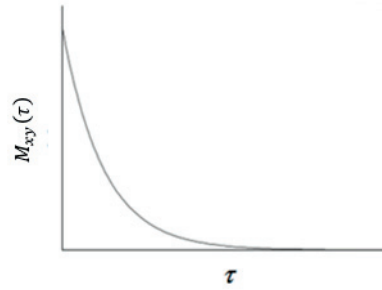
Figure I-6. The evolution of the magnetisation respect to the variable delays during T_2 measurement.

I.2.1 Relaxation Mechanism

NMR relaxation is mainly caused by fluctuating magnetic fields at the nuclear spin. The fluctuations are created by the random motions of the molecules and can arise from several mechanisms generating time dependent magnetic interactions, such as dipolar coupling, scalar coupling and electric quadrupole interaction. The contribution of the various mechanisms differs depending on the type of the nucleus, the chemical environment or the magnetic field strength.

I.1.1.2   The Dipolar Mechanism

Dipole-dipole interaction is a trough space interaction of the magnetic fields of two spins (I and S, they can be like or unlike spins) which can be either an intramolecular or an intermolecular interaction if the nuclear spins are on the same molecule or on different molecules, respectively. Dipolar interactions are distance dependence (Figure I-7), proportional to the sixth power of the inverse of the distance between the dipoles (r^{-6}) making the intramolecular interactions more effective than the intermolecular ones.
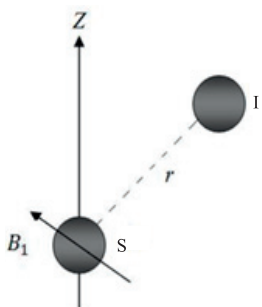
Figure I-7. Spin S experiences fluctuation of the magnetic field, B_1, due to the magnetic moment of the neighbor spin I.

When small molecules in solution tumble, the relative orientation of the two vectors changes with time creating a fluctuating magnetic field at each nucleus, which will create dipolar relaxation. In fact, when small molecules tumble rapidly, dipolar relaxation will be less effective and T_1 becomes longer. On the other hand, when large molecules move too slowly, they will have the opposite relationship between molecular motions and T_1: in this case the relaxation is more effective when the molecules move faster.

Furthermore, the magnetic moment is proportional to the square of the gyromagnetic ratio of the spin. Thus the larger the gyromagnetic ratio, the larger the magnetic moment and the larger the fluctuating local magnetic field will be. Since proton has a very high magnetic dipole moment, it is one of the most effective nuclei for causing dipolar relaxation. However, an electron has an about 658 times higher magnetic dipole moment than a proton and therefore creates a much stronger dipolar relaxation.

I.1.1.3   Quadrupolar Relaxation

Quadrupolar relaxation is a dominant mechanism for spin $> \frac{1}{2}$ nuclei having nonspherical charge distributions. Such nuclei interact with surrounding electron clouds (electric field gradients) resulting in splitting of the quadrupolar energy levels. In high symmetry systems (cubic, spherical, octahedral, tetrahedral), the electric field gradient generated by surrounding charges cancels out, resulting in no quadrupolar interaction. There are two quantities to consider when dealing with quadrupolar nuclei, the nuclear quadrupole moment (eQ), the asymmetric charge distribution within a nucleus, and the electric field gradient (efg), the Laplacian of the potential of the electrons surrounding the nucleus which depends on the random rotational reorientation. Rotation of the molecule will therefore influence quadrupolar relaxation.

I.1.1.4   Scalar Relaxation

Scalar interaction considers the probability of finding the spin of the unpaired electrons on an interacting nucleus and occurs when the nucleus-electron distance is about the nuclear radius (~ 10 fm). Only nuclei bound directly to a paramagnetic species undergo scalar interaction.

I.1.1.5   Curie Relaxation

In paramagnetic systems, the differences in populations of the electron spin energy levels due to the Boltzmann distribution induces a magnetic moment. There is always a slight excess of electron spins in the spin state of lower energy, causing the sample to have a finite static magnetic moment along the external magnetic field. Curie relaxation increases with increasing magnetic field since the difference in spin state population increases. The nuclear spin interacts with the static magnetic moment. The relaxation arising from this interaction is known as the Curie relaxation.

I.3 References

(1)   Marcus, Y. *Chem. Rev.* **1988**, *88*, 1475.
(2)   D'Angelo, P.; Zitolo, A.; Migliorati, V.; Persson, I. *Chem. Eur. J.* **2010**, *16*, 684.
(3)   Cotton, S. In *Lanthanide and actinide chemistry*; John Wiley & Sons, 2013.
(4)   D'Angelo, P.; Zitolo, A.; Migliorati, V.; Chillemi, G.; Duvail, M.; Vitorge, P.; Abadie, S.; Spezia, R. *Inorg. Chem.* **2011**, *50*, 4572.
(5)   Elhabiri, M.; Scopelliti, R.; Bünzli, J.-C. G.; Piguet, C. *J. Am. Chem. Soc.* **1999**, *121*, 10747.
(6)   Delbianco, M.; Lamarque, L.; Parker, D. *Org. Biomol.Chem.* **2014**, *12*, 8061.
(7)   Bunzli, J.-C. G.; Piguet, C. *Chem. Soc. Rev.* **2005**, *34*, 1048.
(8)   Caravan, P.; Ellison, J. J.; McMurry, T. J.; Lauffer, R. B. *Chem. Rev.* **1999**, *99*, 2293.
(9)   Harte, A. J.; Jensen, P.; Plush, S. E.; Kruger, P. E.; Gunnlaugsson, T. *Inorg. Chem.* **2006**, *45*, 9465.
(10)   Feltham, H. L. C.; Brooker, S. *Coord. Chem. Rev.* **2014**, *276*, 1.
(11)   Sharples, J. W.; Collison, D. *Coord. Chem. Rev.* **2014**, *260*, 1.
(12)   Aspinall, H. C. *Chem. Rev.* **2002**, *102*, 1807.
(13)   Lee, J.; Farha, O. K.; Roberts, J.; Scheidt, K. A.; Nguyen, S. T.; Hupp, J. T. *Chem. Soc. Rev.* **2009**, *38*, 1450.
(14)   He, M. L.; Rambeck, W. A. *Arch. Anim. Nutr.* **2000**, *53*, 323.
(15)   Thacker, P. A. *J. Anim. Sci. Biotechnol.* **2013**, *4*, 35.
(16)   http://www.magnet.fsu.edu/education/tutorials/magnetacademy/mri.
(17)   Rudovský, J.; Cígler, P.; Kotek, J.; Hermann, P.; Vojtíšek, P.; Lukeš, I.; Peters, J. A.; Vander Elst, L.; Muller, R. N. *Chem. Eur. J.* **2005**, *11*, 2373.
(18)   Řehoř, I.; Kubíček, V.; Kotek, J.; Hermann, P.; Lukeš, I.; Száková, J.; Vander Elst, L.; Muller, R. N.; Peters, J. A. *J. Mater. Chem.* **2009**, *19*, 1494.
(19)   Tóth, é.; Helm, L.; Merbach, A. In *The Chemistry of Contrast Agents in Medical Magnetic Resonance Imaging*; John Wiley & Sons, Ltd: Chichester, U.K., 2013.
(20)   Laurent, S.; Forge, D.; Port, M.; Roch, A.; Robic, C.; Vander Elst, L.; Muller, R. N. *Chem. Rev.* **2008**, *108*, 2064.
(21)   Laurent, S.; Bridot, J.-L.; Elst, L. V.; Muller, R. N. *Future Med. Chem.* **2010**, *2*, 427.
(22)   Ersoy, H.; Rybicki, F. J. *J. Magn. Reson. Imaging* **2007**, *26*, 1190.
(23)   Grobner, T. *Nephrol. Dial. Transplant.* **2006**, *21*, 1104.
(24)   Cacheris, W. P.; Quay, S. C.; Rocklage, S. M. *Magn. Reson. Imaging* **1990**, *8*, 467.
(25)   Meyer, D.; Schaefer, M.; Doucet, D. *Invest. Radiol.* **1990**, *25*, S53.
(26)   Aime, S.; Crich, S. G.; Gianolio, E.; Giovenzana, G. B.; Tei, L.; Terreno, E. *Coord. Chem. Rev.* **2006**, *250*, 1562.
(27)   Pacifici, R.; Di Carlo, S.; Bacosi, A.; Altieri, I.; Pichini, S.; Zuccaro, P. *J. Immunol. Methods* **1993**, *161*, 135.
(28)   Nilsson, S.; Wikström, G.; Ericsson, A.; Wikström, M.; Øksendal, A.; Waldenström, A.; Hemmingsson, A. *Acta Radiol.* **1996**, *37*, 27.
(29)   Runge, V. M.; Wells, J. W. *Invest. Radiol.* **1996**, *31*, 395.
(30)   Caravan, P. *Chem. Soc. Rev.* **2006**, *35*, 512.
(31)   Caravan, P.; Cloutier, N. J.; Greenfield, M. T.; McDermid, S. A.; Dunham, S. U.; Bulte, J. W. M.; Amedio, J. C.; Looby, R. J.; Supkowski, R. M.; Horrocks, W. D.; McMurry, T. J.; Lauffer, R. B. *J. Am. Chem. Soc.* **2002**, *124*, 3152.

(32)   Corsi, D. M.; Vander Elst, L.; Muller, R. N.; van Bekkum, H.; Peters, J. A. *Chem. Eur. J.* **2001**, *7*, 64.

(33)   Lebdušková, P.; Kotek, J.; Hermann, P.; Vander Elst, L.; Muller, R. N.; Lukeš, I.; Peters, J. A. *Bioconjugate Chem.* **2004**, *15*, 881.

(34)   Tóth, É.; Pubanz, D.; Vauthey, S.; Helm, L.; Merbach, A. E. *Chem. Eur. J.* **1996**, *2*, 1607.

(35)   Rudovský, J.; Botta, M.; Hermann, P.; Hardcastle, K. I.; Lukeš, I.; Aime, S. *Bioconjugate Chem.* **2006**, *17*, 975.

(36)   Nicolle, G.; Tóth, É.; Eisenwiener, K.-P.; Mäcke, H.; Merbach, A. *J. Biol. Inorg. Chem.* **2002**, *7*, 757.

(37)   Bryant, L. H.; Brechbiel, M. W.; Wu, C.; Bulte, J. W. M.; Herynek, V.; Frank, J. A. *J Magn. Reson. Imaging* **1999**, *9*, 348.

(38)   Lebduskova, P.; Sour, A.; Helm, L.; Toth, E.; Kotek, J.; Lukes, I.; Merbach, A. E. *Dalton Trans.* **2006**, *0*, 3399.

(39)   Hovland, R.; Glogard, C.; Aasen, A. J.; Klaveness, J. *J. Chem. Soc. Perkin Trans. 2* **2001**, *0*, 929.

(40)   André, J. P.; Tóth, É.; Fischer, H.; Seelig, A.; Mäcke, H. R.; Merbach, A. E. *Chem. Eur. J.* **1999**, *5*, 2977.

(41)   Torres, S.; Martins, J. A.; André, J. P.; Geraldes, C. F. G. C.; Merbach, A. E.; Tóth, É. *Chem. Eur. J.* **2006**, *12*, 940.

(42)   Hovland, R.; Glogard, C.; Aasen, A. J.; Klaveness, J. *Org. Biomol. Chem.* **2003**, *1*, 644.

(43)   Livramento, J. B.; Tóth, É.; Sour, A.; Borel, A.; Merbach, A. E.; Ruloff, R. *Angew. Chem. Int. Ed.* **2005**, *44*, 1480.

(44)   Caravan, P.; Greenfield, M. T.; Li, X.; Sherry, A. D. *Inorg. Chem.* **2001**, *40*, 6580.

(45)   Aime, S.; Botta, M.; Crich, S. G.; Giovenzana, G. B.; Pagliarin, R.; Piccinini, M.; Sisti, M.; Terreno, E. *J. Biol. Inorg. Chem.* **1997**, *2*, 470.

(46)   Tóth, É.; Connac, F.; Helm, L.; Adzamli, K.; Merbach, A. E. *J. Biol. Inorg. Chem.* **1998**, *3*, 606.

(47)   Vander Elst, L.; Chapelle, F.; Laurent, S.; Muller, R. N. *J. Biol. Inorg. Chem.* **2001**, *6*, 196.

(48)   Aime, S.; Gianolio, E.; Terreno, E.; Giovenzana, B. G.; Pagliarin, R.; Sisti, M.; Palmisano, G.; Botta, M.; Lowe, P. M.; Parker, D. *J. Biol. Inorg. Chem.* **2000**, *5*, 488.

(49)   Hajela, S.; Botta, M.; Giraudo, S.; Xu, J.; Raymond, K. N.; Aime, S. *J. Am. Chem. Soc.* **2000**, *122*, 11228.

(50)   Aime, S.; Calabi, L.; Cavallotti, C.; Gianolio, E.; Giovenzana, G. B.; Losi, P.; Maiocchi, A.; Palmisano, G.; Sisti, M. *Inorg. Chem.* **2004**, *43*, 7588.

(51)   Powell, D. H.; Dhubhghaill, O. M. N.; Pubanz, D.; Helm, L.; Lebedev, Y. S.; Schlaepfer, W.; Merbach, A. E. *J. Am. Chem. Soc.* **1996**, *118*, 9333.

(52)   Aime, S.; Botta, M.; Fasano, M.; Paoletti, S.; Terreno, E. *Chem. Eur. J.* **1997**, *3*, 1499.

(53)   Laus, S.; Sour, A.; Ruloff, R.; Tóth, É.; Merbach, A. E. *Chem. Eur. J.* **2005**, *11*, 3064.

(54)   Aime, S.; Botta, M.; Fasano, M.; Terreno, E. *Acc. Chem. Res.* **1999**, *32*, 941.

(55)   Laus, S.; Ruloff, R.; Tóth, É.; Merbach, A. E. *Chem. Eur. J.* **2003**, *9*, 3555.

(56)   Xu, J.; Franklin, S. J.; Whisenhunt, D. W.; Raymond, K. N. *J. Am. Chem. Soc.* **1995**, *117*, 7245.

(57)   Doble, D. M. J.; Botta, M.; Wang, J.; Aime, S.; Barge, A.; Raymond, K. N. *J. Am. Chem. Soc.* **2001**, *123*, 10758.

(58)   Terreno, E.; Boniforte, P.; Botta, M.; Fedeli, F.; Milone, L.; Mortillaro, A.; Aime, S. *Eur. J. Inorg. Chem.* **2003**, *2003*, 3530.

(59)   Aime, S.; Fasano, M.; Terreno, E. *Chem. Soc. Rev.* **1998**, *27*, 19.

(60)   Jaszberenyi, Z.; Sour, A.; Toth, E.; Benmelouka, M.; Merbach, A. E. *Dalton Trans.* **2005**, *0*, 2713.

(61)   Ruloff, R.; Toth, E.; Scopelliti, R.; Tripier, R.; Handel, H.; Merbach, A. E. *Chem. Commun.* **2002**, *0*, 2630.

(62)   Kotek, J.; Rudovský, J.; Hermann, P.; Lukeš, I. *Inorg. Chem.* **2006**, *45*, 3097.

(63)   Polasek, M.; Rudovsky, J.; Hermann, P.; Lukes, I.; Elst, L. V.; Muller, R. N. *Chem. Commun.* **2004**, *0*, 2602.

(64)   Kotek, J.; Lebdušková, P.; Hermann, P.; Vander Elst, L.; Muller, R. N.; Geraldes, C. F. G. C.; Maschmeyer, T.; Lukeš, I.; Peters, J. A. *Chem. Eur. J.* **2003**, *9*, 5899.

(65)   Woods, M.; Kovacs, Z.; Zhang, S.; Sherry, A. D. *Angew. Chem. Int. Ed.* **2003**, *42*, 5889.

(66)   Woods, M.; Botta, M.; Avedano, S.; Wang, J.; Sherry, A. D. *Dalton Trans.* **2005**, *0*, 3829.

(67)   Pierre, V. C.; Botta, M.; Raymond, K. N. *J. Am. Chem. Soc.* **2004**, *127*, 504.

(68)   Caravan, P.; Farrar, C. T.; Frullano, L.; Uppal, R. *Contrast Media Mol. Imaging* **2009**, *4*, 89.

(69)   Bloch, F. *Phys. Rev.* **1957**, *105*, 1206.

Chapter II

Theory of relaxation rates in paramagnetic systems

II.1 Paramagnetic Relaxation Enhancement

As discussed in the previous chapter, upon addition of paramagnetic ions or complexes of paramagnetic ions with bound water molecules to an aqueous medium, the rates of both longitudinal and transverse relaxations of ^{1}H and ^{17}O nuclear spins of water are increased, this phenomenon is known as Paramagnetic Relaxation Enhancement (PRE). The observed solvent relaxation rate, $1/T_{i,obs}$, is the sum of the paramagnetic, $1/T_{i,p}$, and the diamagnetic, $1/T_{i,d}$, relaxation rates which are the relaxation rate of the solvent nuclei respectively in the presence and the absence of paramagnetic ions:

$$\frac{1}{T_{i,obs}} = \frac{1}{T_{i,p}} + \frac{1}{T_{i,d}}, \quad \text{where } i = 1, 2 \tag{II-1}$$

The paramagnetic term can be divided into inner-sphere (IS) and outer-sphere (OS) components:

$$\frac{1}{T_{i,p}} = \left(\frac{1}{T_{i,p}}\right)^{IS} + \left(\frac{1}{T_{i,p}}\right)^{OS} \tag{II-2}$$

II.1.1 Inner-sphere relaxation

Inner-sphere relaxation is due to directly coordinated water molecule(s) to the paramagnetic ion, which is obtained by eqs II-3 and II-4[1] where P_m is the mole fraction and τ_m is the residence lifetime of the bound water ($\tau_m = 1/k_{ex}$). $\Delta\omega_m$ is the chemical shift difference between the bound water and the bulk water in rad s^{-1}. $1/T_{1m}$ and $1/T_{2m}$ are respectively the bound water longitudinal and transverse relaxation rates.

$$\left(\frac{1}{T_{1,p}}\right)^{IS} = P_m \frac{1}{T_{1m} + \tau_m} \tag{II-3}$$

$$\left(\frac{1}{T_{2,p}}\right)^{IS} = \frac{P_m}{\tau_m} \cdot \frac{T_{2m}^{-2} + \tau_m^{-1} T_{2m}^{-1} + \Delta\omega_m^2}{\left(\tau_m^{-1} + T_{2m}^{-1}\right)^2 + \Delta\omega_m^2} \tag{II-4}$$

Following the Solomon-Bloembergen-Morgan (SBM) theory, inner-sphere relaxation rates in the bound water are considered to be the sum of a dipolar ($1/T_{i,dd}$), scalar ($1/T_{i,Sc}$), Curie ($1/T_{i,Cu}$) and for ^{17}O spins also quadrupolar ($1/T_{i,q}$) contribution:[1,2]

$$\frac{1}{T_{im}} = \frac{1}{T_{i,dd}} + \frac{1}{T_{i,Sc}} + \frac{1}{T_{i,Cu}} + \frac{1}{T_{i,q}} \text{ where } i = 1,2 \tag{II-5}$$

Longitudinal relaxation rates:

$$\frac{1}{T_{1,dd}} = \frac{2}{15}\left(\frac{\mu_0}{4\pi}\right)^2 \frac{\gamma_I^2 \mu_B^2 \mu_{eff}^2}{r_{LnX}^6}\left[\frac{7\tau_{c2}}{1+\omega_S^2\tau_{c2}^2} + \frac{3\tau_{c1}}{1+\omega_I^2\tau_{c1}^2}\right] \tag{II-6}$$

$$\frac{1}{T_{1,Sc}} = \frac{2S(S+1)}{3}\left(\frac{A}{\hbar}\right)^2\left[\frac{\tau_{e2}}{1+\omega_S^2\tau_{e2}^2}\right] \tag{II-7}$$

$$\frac{1}{T_{1,Cu}} = \frac{1}{5}\left(\frac{\mu_0}{4\pi}\right)^2 \frac{\omega_I^2 \mu_B^4 \mu_{eff}^4}{(3kT)^2 r_{LnX}^6}\left[\frac{6\tau_{cs}}{1+\omega_I^2\tau_{cs}^2}\right] \tag{II-8}$$

$$\frac{1}{T_{1,q}} = \frac{3\pi^2}{10}\left(\frac{2I+3}{I^2(2I-1)}\right)\chi^2(1+\eta^2/3)\left[0.2\left(\frac{\tau_R}{1+\omega_I^2\tau_R^2}\right) + 0.8\left(\frac{\tau_R}{1+4\omega_I^2\tau_R^2}\right)\right] \tag{II-9}$$

Transverse relaxation rates:

$$\frac{1}{T_{2,dd}} = \frac{1}{15}\left(\frac{\mu_0}{4\pi}\right)^2 \frac{\gamma_I^2 \mu_B^2 \mu_{eff}^2}{r^6}\left[4\tau_{c1} + \frac{13\tau_{c2}}{1+\omega_S^2\tau_{c2}^2} + \frac{3\tau_{c1}}{1+\omega_I^2\tau_{c1}^2}\right] \tag{II-10}$$

$$\frac{1}{T_{2,Sc}} = \frac{S(S+1)}{3}\left(\frac{A}{\hbar}\right)^2\left[\tau_{e1} + \frac{\tau_{e2}}{1+\omega_S^2\tau_{e2}^2}\right] \tag{II-11}$$

$$\frac{1}{T_{2,cu}} = \frac{1}{5}\left(\frac{\mu_0}{4\pi}\right)^2 \frac{\omega_I^2 \mu_B^4 \mu_{eff}^4}{(3kT)^2 r^6}\left[4\tau_{cs} + \frac{3\tau_{cs}}{1+\omega_I^2\tau_{cs}^2}\right] \tag{II-12}$$

$$\frac{1}{T_{2,q}} = \frac{3\pi^2}{10}\left(\frac{2I+3}{I^2(2I-1)}\right)\chi^2(1+\eta^2/3)\left[0.3\tau_R + 0.5\left(\frac{\tau_R}{1+\omega_I^2\tau_R^2}\right) + 0.2\left(\frac{\tau_R}{1+4\omega_I^2\tau_R^2}\right)\right] \tag{II-13}$$

with $\mu_{eff}^2 = g_L^2 J(J+1)$ (for Ln^{3+} other than Gd^{3+}) and $\mu_{eff}^2 = g_L^2 s(s+1)$ (for Gd^{3+})

where γ_I is the nuclear gyromagnetic ratio, J is the total angular quantum number, g_L is the Landé g factor, μ_B is the Bohr magneton, ω_S and ω_I are respectively the electron and nucleus Larmor frequencies ($\omega = \gamma B$ and B is the magnetic field). η is an asymmetry parameter. $A/\hbar$ is the hyperfine or scalar coupling constant. r_{Lnx} is the distance between the electron spins and the ^{17}O or ^{1}H nucleus and χ is the quadrupolar coupling constant.

The correlation times are:

$$\frac{1}{\tau_{ci}} = \frac{1}{T_{ie}} + \frac{1}{\tau_m} + \frac{1}{\tau_R} \quad \text{where } i = 1, 2 \tag{II-14}$$

$$\frac{1}{\tau_{ei}} = \frac{1}{T_{ie}} + \frac{1}{\tau_m} \quad \text{where } i = 1, 2 \tag{II-15}$$

$$\frac{1}{\tau_{cs}} = \frac{1}{\tau_m} + \frac{1}{\tau_R} \tag{II-16}$$

T_{1e} and T_{2e} are respectively the longitudinal and transverse electronic relaxation times. T_{ie} for Gd^{3+} ions in solution are governed by the zero-field splitting (ZFS) modulated by random fluctuations and the rates can be expressed by the Bloembergen-Morgan theory of paramagnetic electron spin relaxation (eqs II-17 and II-18)[3,4] when $\Delta^2\tau_v^2 \ll 1$; Δ^2 is the mean square fluctuation of the ZFS, τ_v is the correlation time for the modulation of the ZFS and E_v is the activation energy.

$$\left(\frac{1}{T_{1e}}\right)^{ZFS} = \frac{1}{25}\Delta^2\tau_v[4S(S+1) - 3]\left(\frac{1}{1+\omega_s^2\tau_v^2} + \frac{4}{1+4\omega_s^2\tau_v^2}\right) \tag{II-17}$$

$$\left(\frac{1}{T_{2e}}\right)^{ZFS} = \frac{1}{50}\Delta^2\tau_v[4S(S+1) - 3]\left(\frac{5}{1+\omega_s^2\tau_v^2} + \frac{2}{1+4\omega_s^2\tau_v^2} + 3\right) \tag{II-18}$$

For other Ln^{3+} ions strong spin-orbit coupling leads to very efficient electron spin relaxation. A single electronic relaxation time T_e may be introduced as the values of T_{2e} are reported[5] to be very small and near to those of T_{1e} which leads to $\frac{1}{\tau_{ci}} \approx \frac{1}{\tau_{ei}} \approx \frac{1}{T_{ie}} \approx \frac{1}{T_e}$. Moreover, since in small complexes τ_m is usually longer than τ_R, the Curie component is mainly affected by τ_R and hence $\frac{1}{\tau_{cs}} = \frac{1}{\tau_R}$.

For nuclear relaxation of proton spins, since proton is far from the paramagnetic center and Ln^{3+} forms ionic bonds, the scalar coupling is very weak.[6,7] Moreover the $\tau_{e2}/(1 + \omega_s^2\tau_{e2}^2)$ term at frequencies above 10 MHz vanishes.[1] Consequently, the relaxation due to scalar coupling can be neglected.[8] Dipolar relaxation often dominates because it is proportional to γ_I^2 (which is big for ^1H). The Curie spin relaxation becomes important when T_e is short enough to let spins return to the equilibrium state before a change in the molecular orientation[9] which requires $\tau_R \gg T_e$.[9] For small complexes, τ_R is

about 10^{-10} s, therefore for Gd^{3+} complexes, $\tau_R \ll T_e$ and the Curie spin relaxation is negligible. For the Ln^{3+} ions with high magnetic moments, Curie spin relaxation can become significant[2,10-12] at high magnetic field strengths $\left(\frac{1}{T_{2,cu}} \propto \omega_I^2\right)$ due to their subpicosecond electronic relaxation time[8,13-16], $\tau_R \gg T_e$.

If another nuclear spin than proton like ^{17}O is observed, due to a direct contact between the Ln^{3+} ion and the water oxygen, the scalar contribution can become significant because the scalar coupling constant $\left(\frac{A}{\hbar}\right)^2$ is large. For lanthanides other than Gd^{3+} due to the very fast electronic relaxation the scalar term is smaller than the quadrupolar term, and can thus be neglected.[8]

II.1.2 Outer-sphere relaxation

The outer sphere water molecules are constituted by two distinct types of molecules: the second-sphere water molecules, which remain in the proximity of the complex by interacting with the hydrophilic groups, and the bulk water molecules, whose random translational motion can bring them to the vicinity of the paramagnetic species. In the present study, no special second sphere water will be considered and outer-sphere relaxation will be described exclusively by intermolecular interactions.

The outer-sphere relaxation rates are given as the sum of dipolar and Curie relaxations[17] (eq II-19). The dipole-dipole relaxation is described by eqs II-20 and II-22 as developed by Freed[18,19] and Ayant[20] and the Curie relaxation has been described by Fries[21] (eqs II-21 and II-23), where N_A is the Avogadro constant, a is the distance of closest approach of an outer-sphere water oxygen or proton to the metal center, D is the mutual diffusion of bulk water and the complex, τ_d is the correlation time for translational diffusion such that $\tau_d = a^2/D$, and $J(\omega)$ is the spectral density function.

$$\left(\frac{1}{T_{i,p}}\right)^{OS} = \left(\frac{1}{T_{i,dd}}\right)^{OS} + \left(\frac{1}{T_{i,Cu}}\right)^{OS} \text{ where } i = 1, 2 \tag{II-19}$$

Longitudinal relaxation rates:

$$\left(\frac{1}{T_{1,dd}}\right)^{OS} = \frac{32\pi}{405}\left(\frac{\mu_0}{4\pi}\right)^2 \frac{N_A\,[Ln]}{aD}\gamma_I^2\mu_B^2\mu_{eff}^2[3\,J(\omega_I) + 7\,J(\omega_S)] \tag{II-20}$$

$$J(\omega) = Re\left[\frac{1+\frac{1}{4}\left(i\omega\tau_d+\frac{\tau_d}{T_e}\right)^{1/2}}{1+\left(i\omega\tau_d+\frac{\tau_d}{T_e}\right)^{1/2}+\frac{4}{9}\left(i\omega\tau_d+\frac{\tau_d}{T_e}\right)+\frac{1}{9}\left(i\omega\tau_d+\frac{\tau_d}{T_e}\right)^{3/2}}\right]$$

$$\left(\frac{1}{T_{1,Cu}}\right)^{OS} = \frac{96\pi}{405}\left(\frac{\mu_0}{4\pi}\right)^2 \frac{N_A\,[Ln]}{aD}\frac{\omega_I^2\mu_B^4\mu_{eff}^4}{(3k_BT)^2}\,[3\,J(\omega_I)] \tag{II-21}$$

$$J(\omega) = Re\left[\frac{1+\frac{1}{4}(i\omega\tau_d)^{1/2}}{1+(i\omega\tau_d)^{1/2}+\frac{4}{9}(i\omega\tau_d)+\frac{1}{9}(i\omega\tau_d)^{3/2}}\right]$$

Transverse relaxation rates:

$$\left(\frac{1}{T_{2,dd}}\right)^{OS} = \frac{16\pi}{405}\left(\frac{\mu_0}{4\pi}\right)^2 \frac{N_A\,[Ln]}{aD}\gamma_I^2\mu_B^2\mu_{eff}^2[4J_1(0) + 3\,J_1(\omega_I) + 13\,J_2(\omega_S)] \tag{II-22}$$

$$J_k(\omega) = Re\left[\frac{1+\frac{1}{4}\left(i\omega\tau_d+\frac{\tau_d}{T_{ke}}\right)^{1/2}}{1+\left(i\omega\tau_d+\frac{\tau_d}{T_{ke}}\right)^{1/2}+\frac{4}{9}\left(i\omega\tau_d+\frac{\tau_d}{T_{ke}}\right)+\frac{1}{9}\left(i\omega\tau_d+\frac{\tau_d}{T_{ke}}\right)^{3/2}}\right], k = 1, 2$$

$$\left(\frac{1}{T_{2,Cu}}\right)^{OS} = \frac{48\pi}{405}\left(\frac{\mu_0}{4\pi}\right)^2 \frac{N_A\,[Ln]}{aD}\frac{\omega_I^2\mu_B^4\mu_{eff}^4}{(3k_BT)^2}\,[4\,J(0) + 3\,J(\omega_I)] \tag{II-23}$$

$$J(\omega) = Re\left[\frac{1+\frac{1}{4}(i\omega\tau_d)^{1/2}}{1+(i\omega\tau_d)^{1/2}+\frac{4}{9}(i\omega\tau_d)+\frac{1}{9}(i\omega\tau_d)^{3/2}}\right]$$

Outer sphere contribution to both transverse and longitudinal ^{17}O relaxation rates are negligible[22] (γ_I is small). For ^{1}H relaxation rates, in case of Gd^{3+}, the Curie contribution can be neglected, however for other Ln^{3+} solutions, Curie contribution becomes important at high magnetic fields.

II.1.3 Chemical shift

The paramagnetic chemical shift ($\Delta\omega_p$) is a function of the shift due to the inner-sphere water ($\Delta\omega_m$), and the shift of waters in the outer coordination sphere ($\Delta\omega_{OS}$):

$$\Delta\omega_p = P_m \left[\frac{\Delta\omega_m}{\left(\tau_m T_{2m}^{-1}+1\right)^2 + \tau_m^2 \Delta\omega_m^2} + \Delta\omega_{OS} \right] \tag{II-24}$$

The outer-sphere contribution to the chemical shift is assumed to be linearly related to $\Delta\omega_m$, through an empirical constant C_{OS}.

$$\Delta\omega_{OS} = C_{OS}\Delta\omega_m \tag{II-25}$$

$\Delta\omega_m$ is considered to have a contact[23,24] and a pseudocontact[25,26] component:

$$\Delta\omega_m = \Delta\omega_m^{con} + \Delta\omega_m^{pseud} \tag{II-26}$$

The contact shift is due to a through bond interaction between the unpaired electron spin and the oxygen or proton of the bound water molecule[27] which can be large for directly bound nuclei to the paramagnetic ion.[28] The pseudocontact shift is due to a through space interaction between the ^{17}O or ^1H nucleus and the magnetic moments of the unpaired electrons at the Ln^{3+} ion.[27]

II.2 ^1H NMR relaxation

II.2.1 Relaxivity

The term 'relaxivity' refers in general to longitudinal relaxivity and is used in MRI contrast agent context, indicating their efficiency to increase the relaxation rate of water protons.

$$r_1 = \frac{1}{[Ln^{3+}]} \frac{1}{T_{1,p}} \tag{II-27}$$

In eq II-27 the concentration of the lanthanide ion, $[Ln^{3+}]$, is in millimoles per liter (mM = mmol l^{-1}). For dilute systems the concentration in mM is equal to the concentration given in millimoles per kilogram solvent (mm = mmol kg^{-1}).[1] At high concentration this is however no longer the case. The calculation of the mole fraction of bound water, P_m, is calculated from the concentration of the paramagnetic species c and the number of bound water molecules q as $P_m = qc/55.56$. The concentration is given in mmol kg^{-1} in this case to avoid density corrections. The term relaxivity should always be accompanied by a specification of the magnetic field and the temperature.

II.2.2 Nuclear Magnetic Relaxation Dispersion (NMRD)

The relaxation of a nuclear magnetic spin changes due to temperature, pressure and magnetic field variation. Thermodynamic parameters influence the physical or chemical properties of the sample, however, the magnetic field does not influence the sample chemistry,[1] hence it can be used as a tool for separation of different parameters affecting the relaxation. Relaxation rate measurements, usually the longitudinal relaxation rate, as a function of the magnetic field is called relaxometry and the resulting curve is called Nuclear Magnetic Relaxation Dispersion profile (NMRD). NMRD profiles enable the determination of electronic relaxation times and rotational correlation times[29,30] and they have been mostly measured on the ^{1}H nucleus.

The temperature dependence of NMRD profiles gives some information regarding the parameters limiting the relaxivity. The r_1 values decrease with increasing temperature when rotation is governing relaxivity, whereas an opposite temperature effect will be observed when water exchange is the limiting factor.[1] However, as there are too many parameters influencing the relaxation rates, interpretation of only NMRD profiles would not result in accurate data, hence, independent information from other techniques like ^{17}O NMR and then a simultaneous fitting of all the data will help to determine reliable parameters.[1]

II.3 ^{17}O NMR relaxation

Variable temperature, pressure and magnetic field ^{17}O NMR relaxation rates and chemical shifts permit estimations of the rotational correlation time, the number of inner-sphere water molecules, and the electronic relaxation rate. Moreover, the analysis of variable temperature ^{17}O data is a well-established procedure to obtain an accurate water exchange rate constant.

II.4 Variable temperature

The temperature dependence of the water exchange rate constant at constant pressure is described by eq II-28,[31] where k_{ex}^{298} is the water exchange at 298 K, $\Delta S^{\ddagger}$ and $\Delta H^{\ddagger}$ are the entropy and enthalpy of activation. R and h are respectively the perfect gas and Planck constant.

$$(k_{ex}^T)_p = \frac{1}{\tau_m} = \frac{k_B T}{h} exp\left(\frac{\Delta S^{\ddagger}}{R} - \frac{\Delta H^{\ddagger}}{RT}\right) = \frac{(k_{ex}^{298})_p T}{298.15} exp\left[\frac{\Delta H^{\ddagger}}{R}\left(\frac{1}{298.15} - \frac{1}{T}\right)\right] \quad \text{(II-28)}$$

Temperature variation of the chemical shift $(\Delta\omega_m^T)_P$ at a constant pressure P can be presented with an empirical power series (eq II-29) where T is the experimental temperature. B_1 and B_2 are constants described by Lewis[32] and Bleaney[25] respectively and ω_0 is the nuclear spin resonance frequency (in rad s^{-1}). It has to be noted that for Gd^{3+} compounds, B_2, the pseudocontact contribution is zero, hence $A/\hbar$ can be obtained from the chemical shifts:

$$(\Delta\omega_m^T)_p = \omega_0\left(\frac{B_1}{T} + \frac{B_2}{T^2}\right) \quad \text{(II-29)}$$

$$B_1 = \frac{g_L \mu_B J(J+1)}{3 k_B \gamma}\frac{A}{\hbar} \quad \text{(II-30)}$$

Correlation times and the diffusion constant are supposed to obey an Arrhenius law in respect to temperature variation:

$$\tau_R = \tau_R^{298} exp\left[\frac{E_R}{R}\left(\frac{1}{298.15} - \frac{1}{T}\right)\right] \quad \text{(II-31)}$$

$$\tau_v = \tau_v^{298} exp\left[\frac{E_v}{R}\left(\frac{1}{298.15} - \frac{1}{T}\right)\right] \tag{II-32}$$

$$D_{Lnx} = D_{Lnx}^{298} exp\left[\frac{E_{Lnx}}{R}\left(\frac{1}{298.15} - \frac{1}{T}\right)\right] \tag{II-33}$$

II.5 Variable pressure

Classification of the ligand substitution mechanisms was suggested by Langford and Gray.[33] Three categories has been considered: associative A with an increased coordination number intermediate, dissociative D with a reduced coordination number intermediate, and interchange I subdivided to I_a and I_d when the exchange is associative-like and dissociative-like, respectively.[34] This classification was later extended by Merbach and coworkers based on the degree of expansion or contraction of the hydration sphere during the exchange using the same notation $A, I_a, I, I_d,$ and D (Figure II-1).
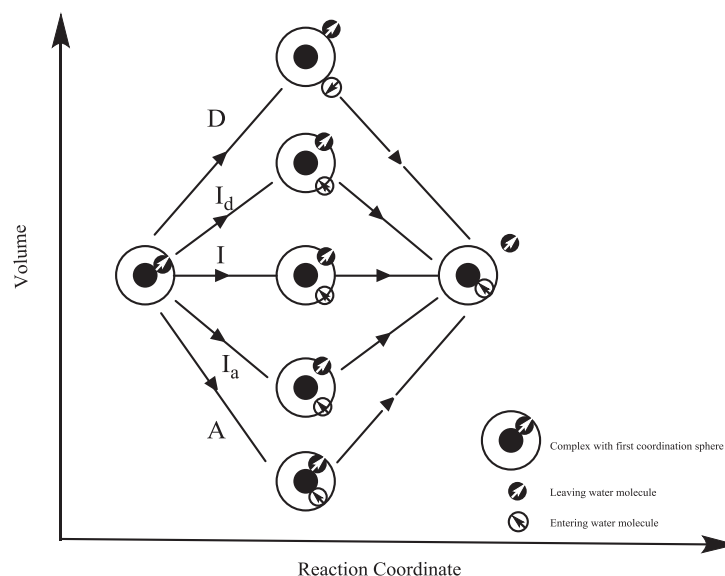
Figure II-1. Volume profiles for the water exchange process on Ln^{3+} compounds.[34]

Water exchange reactions mechanism can be obtained from variable pressure transverse ^{17}O NMR relaxation rate measurements, giving a direct access to the activation volume,[35] ($\Delta V^{\ddagger}$) through eq II-34.

$$\Delta V^{\ddagger} = -RT \left(\frac{\partial lnK}{\partial P} \right)_T \tag{II-34}$$

Water exchange reaction mechanisms can be assigned from the sign of activation volume, dissociative mechanism **D** is indicated by an expanded transition state (large positive $\Delta V^{\ddagger}$, rate constant slows down by pressure), an associative mechanism **A** is indicated by a contracted transition state[1] (large negative $\Delta V^{\ddagger}$, rate constant accelerates by pressure) and an interchange mechanism **I** when the bond making and bond breaking cancel each other in contributing[1] to the activation volume.

The maximum absolute activation volume has been estimated to be 13 ± 1 cm^3 mol^{-1} corresponding to the moving of a water molecule in or out of the solution.[36] It has to be mentioned that the activation entropy can be used to provide information about the reaction mechanism. Large negative values of the activation entropy usually indicate associative mechanisms, while dissociative reactions tend to have positive activation entropies.

The pressure dependence of the water exchange rate constant is given by:

$$ln(k_{ex}^P)_T = ln(k_{ex}^0)_T - \frac{P\,\Delta V^{\ddagger}}{RT} + \frac{P^2\,\Delta\beta^{\ddagger}}{RT} \tag{II-35}$$

where $\Delta\beta^{\ddagger}$ is the compressibility of activation which is very small for aqueous complexes,[37] and k_{ex}^0 refers to the rate constant at zero pressure.

$\Delta\omega_m$ variation with pressure is also considered to be linear (eq II-36)[38] where $\left(\Delta\omega_m^0\right)_T$ refers to $\Delta\omega_m$ at zero pressure and P_1 is the proportionality factor.

$$(\Delta\omega_m^P)_T = (\Delta\omega_m^0)_T \, (1 + P_1P) \tag{II-36}$$

It has to be noted that since for variable pressure measurements, samples are in cylindrical tubes the contribution of the bulk magnetic susceptibility (BMS) shift for paramagnetic species has to be considered. The BMS shift contribution (δ_{BMS}) can be calculated using II-37:

$$\delta_{BMS} = \frac{4\pi cs}{T}\left(\frac{\mu_{eff}}{2.84}\right)^2 \times 10^3 \tag{II-37}$$

where s depends on the sample shape and position in the magnetic field; $s = \frac{1}{3}$ for a cylinder parallel to the static magnetic field. c is the paramagnetic solute concentration in moles per liter (mol l^{-1}). Moreover, it has to be highlighted that a concentration change is expected as the pressure changes. Hence, considering density variation with pressure is necessary for an accurate calculation of BMS shift.

II.6 Water exchange rate constants

Water exchange rate constants can be obtained from variation with temperature of relaxation rates measured on the complex solution. For dilute Gd^{3+} compounds, the reduced transverse relaxation rate, $1/T_{2r}$ (eq II-38), can be used to calculate the water exchange rate constants:[39]

$$\frac{1}{T_{2r}} = \frac{1}{P_m}\left(\frac{1}{T_{2,obs}} - \frac{1}{T_{2,d}}\right) = \frac{1}{P_m}\left(\frac{1}{T_{2,p}}\right) \tag{II-38}$$

For dilute and fast exchanging lanthanide systems except Gd^{3+}, Cossy suggested[40] to use the transverse and longitudinal relaxation rate differences for water exchange rate determination (eq II-39) assuming that $1/T_{2m} - 1/T_{1m} \ll \Delta\omega_m^2\tau_m$.

$$\frac{1}{T_{2,obs}} - \frac{1}{T_{1,obs}} = P_m\Delta\omega_m^2\tau_m \tag{II-39}$$

However, for non-dilute and fast exchanging[41] lanthanide systems (except Gd^{3+}), the $1/T_{1m} \approx 1/T_{2m}$ assumption will not be applicable. Hence, under the conditions that $1/\tau_m \gg |(1/T_{iA}) - (1/T_{im})|\ i = 1, 2$ and $1/\tau_m \gg \Delta\omega_m$, one can write:

$$\frac{1}{T_{1,obs}} = \frac{P_A}{T_{1A}} + \frac{P_m}{T_{1m}} \tag{II-40}$$

$$\frac{1}{T_{2,obs}} = \frac{P_A}{T_{2A}} + \frac{P_m}{T_{2m}} + P_A P_m \Delta\omega_m^2 \tau \tag{II-41}$$

$$\omega_{obs} = \omega_A P_A + \omega_m P_m \tag{II-42}$$

$$\Delta\omega_m = \omega_m - \omega_A = \frac{\omega_{obs} - \omega_A}{P_m} \tag{II-43}$$

with $P_A = \frac{\tau_A}{\tau_A + \tau_m}$, $\quad \frac{1}{\tau} = \frac{1}{\tau_A} + \frac{1}{\tau_m}$, $\quad \frac{\tau_m}{\tau_A} = \frac{P_m}{P_A}$

By convention one uses A for unbound or bulk water molecules. Here P_A is the mole fraction of water on site A, ω_A is the chemical shift of the bulk water and ω_{obs} is the chemical shift observed on the coalesced signal. Considering that the relaxation rates of bulk water, $1/T_{1A}$ and $1/T_{2A}$ are equal under the extreme narrowing condition[42] subtraction of eq II-41 from eq II-40 gives:

$$\frac{1}{T_{2,obs}} - \frac{1}{T_{1,obs}} = P_m \left(\frac{1}{T_{2m}} - \frac{1}{T_{1m}}\right) + P_A P_m \Delta\omega_m^2 \tau \tag{II-44}$$

which can be further simplified to give:

$$\frac{1}{T_{2,obs}} - \frac{1}{T_{1,obs}} = P_m \left[\left(\frac{1}{T_{2m}} - \frac{1}{T_{1m}}\right) + P_A{}^2 \Delta\omega_m^2 \tau_m\right] \tag{II-45}$$

Another simplification of the general Swift and Connick equation eq II-4 can be obtained for the lanthanide ions other than Gd^{3+}. In this case relaxation of bound water molecules $1/T_{2m}$ is relatively small and we have $\tau_m \Delta\omega_m^2 \gg 1/T_{2,m}$. In this case eq II-4 can be simplified to eq II-46:

$$\left(\frac{1}{T_{2,p}}\right)^{IS} = P_m \cdot \frac{\tau_m \Delta\omega_m^2}{1 + \tau_m^2 \Delta\omega_m^2} \tag{II-46}$$

Under the fast exchange condition, where $\tau_m^2 \Delta\omega_m^2 \ll 1$, eq II-46 will simplify to eq II-47. Under the slow exchange condition (where $\tau_m^2 \Delta\omega_m^2 \gg 1$ and $\tau_m \gg T_{im}$, $i = 1, 2$), the longitudinal and transverse relaxation rates will be equal (eq II-48). In this case the inner-sphere transverse relaxation rate will be independent of $\Delta\omega_m$ and will decreases with

decreasing water exchange rate. Hence, no chemical shift data will be necessary for the assessment of water exchange rate.

$$\left(\frac{1}{T_{2,p}}\right)^{IS} = P_m \tau_m \Delta \omega_m^2 \tag{II-47}$$

$$\left(\frac{1}{T_{2,p}}\right)^{IS} = \left(\frac{1}{T_{1,p}}\right)^{IS} = \frac{P_m}{\tau_m} \tag{II-48}$$

II.7 References

(1)   Tóth, é.; Helm, L.; Merbach, A. In *The Chemistry of Contrast Agents in Medical Magnetic Resonance Imaging*; John Wiley & Sons, Ltd: Chichester, U.K., 2013.

(2)   Bertini, I.; Capozzi, F.; Luchinat, C.; Nicastro, G.; Xia, Z. *J. Phys. Chem* **1993**, *97*, 6351.

(3)   McLachlan, A. D. *Proc. R. Soc. Lond. A* **1964**, *280*, 271.

(4)   Powell, D. H.; Merbach, A. E.; González, G.; Brücher, E.; Micskei, K.; Ottaviani, M. F.; Köhler, K.; Von Zelewsky, A.; Grinberg, O. Y.; Lebedev, Y. S. *Helv. Chim. Acta.* **1993**, *76*, 2129.

(5)   Fries, P. H.; Belorizky, E. *J. Chem. Phys.* **2012**, *136*.

(6)   Yazyev, O. V.; Helm, L.; Malkin, V. G.; Malkina, O. L. *J. Phys. Chem. A* **2005**, *109*, 10997.

(7)   Esteban-Gómez, D.; de Blas, A.; Rodríguez-Blas, T.; Helm, L.; Platas-Iglesias, C. *ChemPhysChem.* **2012**, *13*, 3640.

(8)   Peters, J. A.; Huskens, J.; Raber, D. J. *Prog. Nucl. Magn. Reson. Spectrosc.* **1996**, *28*, 283.

(9)   Norek, M.; Peters, J. A. *Prog. Nucl. Magn. Reson. Spectrosc.* **2011**, *59*, 64.

(10)   Caravan, P.; Greenfield, M. T.; Bulte, J. W. M. *Magn. Reson. Med.* **2001**, *46*, 917.

(11)   Gueron, M. *J. Magn. Reson.* **1975**, *19*, 58.

(12)   Vega, A. J.; Fiat, D. *Mol. Phys.* **1976**, *31*, 347.

(13)   Alsaadi, B. M.; Rossotti, F. J. C.; Williams, R. J. P. *J. Chem. Soc. Dalton Trans.* **1980**, 2151.

(14)   Alsaadi, B. M.; Rossotti, F. J. C.; Williams, R. J. P. *J. Chem. Soc. Dalton Trans.* **1980**, 2147.

(15)   Burns, P. D.; La Mar, G. N. *J. Magn. Reson.* **1982**, *46*, 61.

(16)   Aime, S.; Barbero, L.; Botta, M.; Ermondi, G. *J. Chem. Soc., Dalton Trans.* **1992**, 225.

(17)   Gillis, P.; Roch, A.; Brooks, R. A. *J. Magn. Reson.* **1999**, *137*, 402.

(18)   Hwang, L. P.; Freed, J. H. *J. Chem. Phys.* **1975**, *63*, 118.

(19)   Freed, J. H. *J. Chem. Phys.* **1978**, *68*, 4034.

(20)   Ayant, Y.; Belorizky, E.; Fries, P.; Rosset, J. *J. Phys. France* **1977**, *38*, 325.

(21)   Vigouroux, C.; Belorizky, E.; Fries, P. H. *EPJD.* **1999**, *5*, 243.

(22)   Micskei, K.; Helm, L.; Brucher, E.; Merbach, A. E. *Inorg. Chem.* **1993**, *32*, 3844.

(23)   Golding, R.; Halton, M. *Aust. J. Chem.* **1972**, *25*, 2577.

(24)   Pinkerton, A. A.; Rossier, M.; Spiliadis, S. *J. Magn. Reson.* **1985**, *64*, 420.

(25)   Bleaney, B. *J. Magn. Reson.* **1972**, *8*, 91.

(26)   Golding, R. M.; Pyykkö, P. *Mol. Phys.* **1973**, *26*, 1389.

(27)   Djanashvili, K.; Platas-Iglesias, C.; Peters, J. A. *Dalton Trans.* **2008**, 602.

(28)   Viswanathan, S.; Kovacs, Z.; Green, K. N.; Ratnakar, S. J.; Sherry, A. D. *Chem. Rev.* **2010**, *110*, 2960.

(29)   Lauffer, R. B. *Chem. Rev.* **1987**, *87*, 901.

(30)   Koenig, S. H. *Magn. Reson. Med.* **1991**, *22*, 183.

(31)   Eyring, H. *J. Chem. Phys* **1935**, *3*, 107.

(32)   Lewis, W. B.; Jackson, J. A.; Lemons, J. F.; Taube, H. *J. Chem. Phys* **1962**, *36*, 694.

(33)   Langford, C. H.; Gray, H. B. In *Ligand substitution Processes*; W. A. Benjamin, Inc: New York, **1966**.

(34)   Helm, L.; Merbach, A. E. *J. Chem. Soc., Dalton Trans.* **2002**, 633.

(35)   Lincoln, S. F.; Merbach, A. E. *Adv. Inorg. Chem.* **1995**, *42*, 1.
(36)   Swaddle, T. W. *Inorg. Chem.* **1980**, *19*, 3203.
(37)   Merbach, A. E. *Pure Appl. Chem.* **1982**, *54*, 1479.
(38)   Pisaniello, D. L.; Helm, L.; Meier, P.; Merbach, A. E. *J. Am. Chem. Soc.* **1983**, *105*, 4528.
(39)   Swift, T. J.; Connick, R. E. *J. Chem. Phys* **1962**, *37*, 307.
(40)   Cossy, C.; Helm, L.; Merbach, A. E. *Inorg. Chem.* **1988**, *27*, 1973.
(41)   McLaughlin, A. C.; Leigh Jr, J. S. *J. Magn. Reson.* **1973**, *9*, 296.
(42)   Halle, B.; Wennerström, H. k. *J. Magn. Reson.* **1981**, *44*, 89.

Chapter III

Water exchange kinetics on $[\text{Ln}(\text{DO3A})(\text{H}_2\text{O})_2]$ and $[\text{Ln}(\text{DTTA}-\text{Me})(\text{H}_2\text{O})_2]^-$ studied by variable temperature, pressure and magnetic field NMR
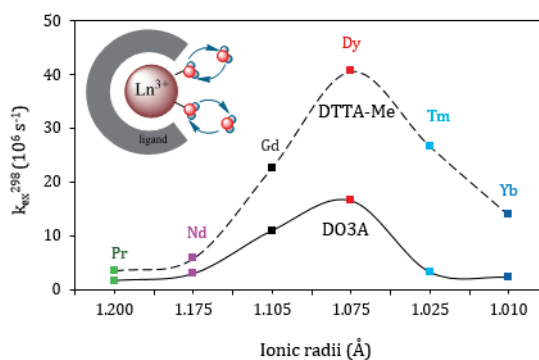
III.1 Introduction

As mentioned in chapter I, complexes of lanthanide(III) ions have been shown to behave as effective NMR shift and relaxation probes, allowing them to be used in structural studies of biomolecules and also as contrast agents (CA). Clinically approved CAs contain only one water molecule in their first coordination sphere.[1,2] Structure and water exchange rate of these complexes have been already well studied for DOTA[3,4] and DTPA[5] as the two important chelators used in MRI contrast agents. However, this is not the case for $[Ln(L)(H_2O)_2]^x$ complexes with a hydration number of two. Hence, in this study we focus on $[Ln(L)(H_2O)_2]^x$ complexes with L = DO3A and DTTA − Me (Scheme III-1) as representatives for macrocyclic and acyclic ligands, respectively.
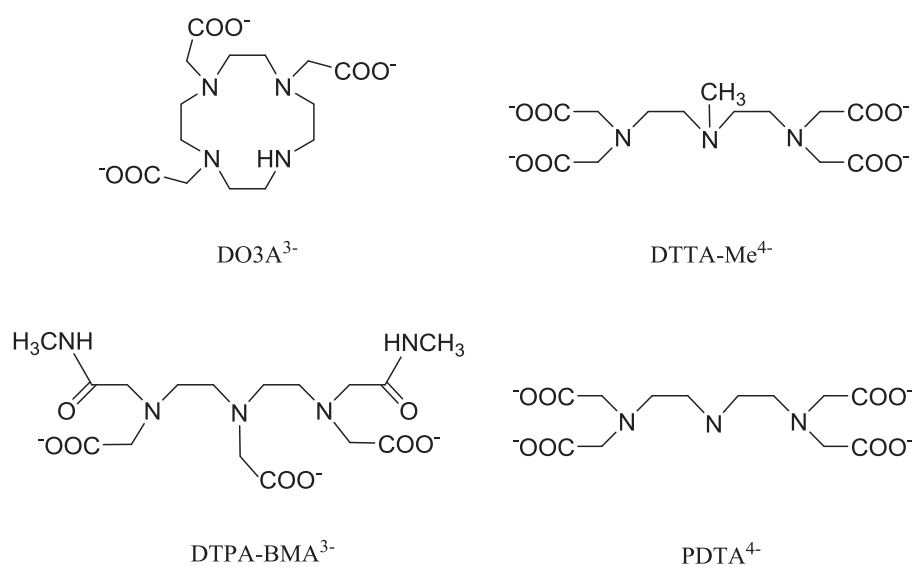
Scheme III-1. Structure of ligands.

In spite of high relaxivity values obtained with compounds using Gd^{3+} complexes of DO3A and DTTA − Me, these cannot be considered as a new lead for the synthesis of contrast agents due to their insufficient thermodynamic and kinetic stability. The lack of these important requirements limits their use as CA to *in vitro* studies. For a better understanding of the relationship between structure, exchange rate constant, and the mechanism of the water exchange, we conducted a comprehensive study of water exchange kinetics of selected Ln^{3+} complexes by ^{17}O NMR spectroscopy performed as a function of temperature, pressure and frequency and ^{1}H nuclear magnetic relaxation dispersion (NMRD). Mechanistic conclusions based on activation parameters are drawn, and comparisons are made with other lanthanide ion complexes.

III.2 Theory and data treatment

III.2.1 ^{1}H NMR relaxation

The measured longitudinal proton relativities are analyzed as discussed in chapter II using eqs II-27, II-3 and II-5. The longitudinal relaxation rate of inner-sphere water protons is considered to be the sum of a dipolar (eq II-6) and a Curie relaxation (eq II-8) contribution. In the case of lanthanide ions except Gd^{3+} the latter can become significant[6,7] at high magnetic field strengths due to their large quantum number and the subpicosecond electronic relaxation time.[8-12] Since the water protons have negligible scalar coupling to the electron spins, the relaxation due to scalar coupling can be neglected.[8] The outer-sphere relaxivity is also considered as the sum of the dipolar (eq II-20) and Curie relaxation (eq II-21) contribution. The correlation times and the diffusion constant are supposed to obey an Arrhenius law in respect to temperature variation (eqs II-31 and II-33).

III.2.2 ^{17}O NMR relaxation

^{17}O NMR relaxation rates and chemical shifts were analyzed using eq II-45, for the non-dilute and fast exchanging[13] lanthanide systems (except Gd^{3+}), where the $1/T_{1m} \approx 1/T_{2m}$ assumption is not applicable. In this case $(1/T_{2m} - 1/T_{1m})$ is taken

into account, considering that both are the sum of contributions due to dipole-dipole, Curie and quadrupolar mechanisms. The temperature and pressure dependence of the water exchange rate constant is calculated using eqs II-28 and II-35. Moreover, the temperature and pressure variation of $\Delta\omega_m$ was assessed using eqs II-29 and II-36. It has to be noted that for variable pressure ^{17}O NMR measurements, the contribution of the bulk magnetic susceptibility (BMS) shift for paramagnetic species has been considered (eq II-37).

III.2.3 Number of inner-sphere water molecules

In an UV-visible study on $\left[Eu(DO3A)(H_2O)_q\right]$, Tóth et al found a hydration equilibrium with $q = 1.8 \pm 0.1$.[14] In a luminescence study, Zhang et al found a similar value of $q = 1.8 \pm 0.2$ for $\left[Tb(DO3A)(H_2O)_q\right]$.[15] In order to investigate the possible change in the number of inner-sphere water molecules along the series, ^1H nuclear magnetic relaxation dispersion (NMRD) and ^{17}O chemical shift data have been investigated. Considering only one inner sphere water molecule for $\left[Ln(L)(H_2O)_q\right]^x$ compounds (Ln = Dy^{3+}, Tm^{3+} and Yb^{3+}) when analyzing the NMRD data, the model would not give a reasonable fit of the experimental data or would lead to unreasonable parameters ($T_e > 1$ ps and $\tau_R > 250$ ps). Furthermore, considering that the observed ^{17}O chemical shifts are linearly proportional to the hydration number of the Ln^{3+} ions and arise from the contact and pseudocontact shifts,[16] one can write:

$$\delta_m = \frac{\delta_{obs} - \delta_A}{q \cdot f_m} = \frac{\delta_p}{q} \; , \; f_m = [Ln^{3+}]/[H_2O] \tag{III-1}$$

$$\delta_p = \langle S_z \rangle \cdot (qF) + C^D \cdot (qG) \tag{III-2}$$

where F and G are ligand dependent parameters and C^D and $\langle S_z \rangle$ are lanthanide ion dependent parameters. When δ_p for a particular ligand is available for different lanthanides eq III-2 can be written in two linear forms.[16]

$$\frac{\delta_p}{C^D} = \frac{\langle S_z \rangle}{C^D} \cdot (qF) + qG \tag{III-3}$$

$$\frac{\delta_p}{\langle S_z \rangle} = qF + \frac{C^D}{\langle S_z \rangle} \cdot (qG) \tag{III-4}$$

A change in the number of inner sphere water molecules along the series results in a break in the plots of δ_p according to eqs III-3 and III-4 due to the change of the slope and the intercept.[16] As shown in Figure III-1, no break is observed suggesting that q is constant along the series. Hence, in this study, the number of inner sphere water molecules is considered to be constant with $q = 2$ for all $[Ln(L)(H_2O)_q]^x$ complexes. In addition we assume that the coordination number remains constant by temperature and pressure variation. The small absorption band at $\sim$ 580.6 nm found for $[Eu(DO3A)(H_2O)_2]$ [18] could be due to the presence of a steric isomer also with $q = 2$ similar to the SAP/TSAP isomers found for DOTA complexes.[10]
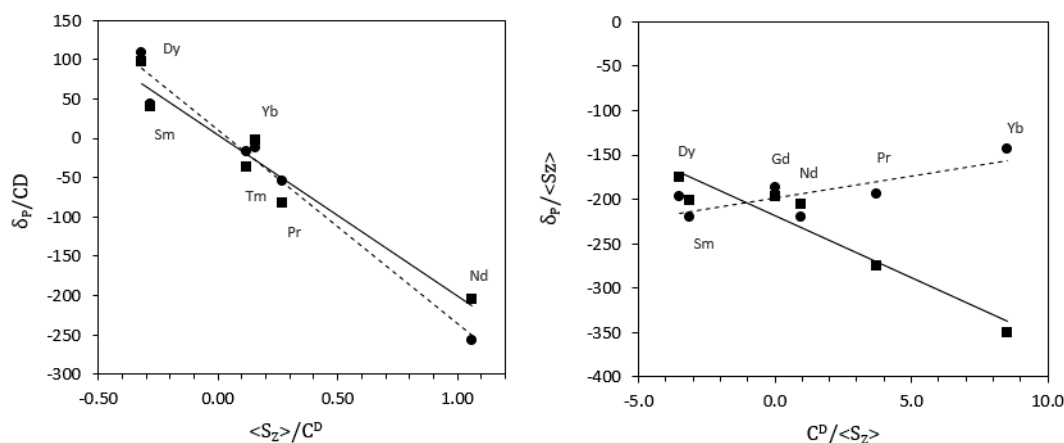
Figure III-1. ^{17}O NMR shifts in $[Ln(DO3A)(H_2O)_q]$ ($\bullet$, dashed line) and $[Ln(DTTA - Me)(H_2O)_q]^-$ ($\blacksquare$, solid line), $[Ln^{3+}] \sim 100$ mM, $B_0 = 18.8$ T, T = 25°C, pH = 5.7.

III.2.4 Variable temperature data

Dipolar and Curie relaxation rates used to calculate inner-sphere contributions to ^{1}H relaxivity or ^{17}O relaxation, depends on the distance between the electron spin and the corresponding nuclear spin as r_{LnX}^{-6}. The only relaxation mechanism independent of the distance is the quadrupolar relaxation, which is the dominant contribution to $1/T_1$ of ^{17}O. No experimental information is available for Ln-O and for Ln-H distances on the compounds studied. To overcome this lack of information we adopted the following strategy.

In a first round of fitting we fitted ^{17}O $1/T_1$ for all $[Ln(L)(H_2O)_2]^x$ solutions. For these fits we used the quadrupole coupling constant of pure water (7.58 MHz).[17] The other relaxation mechanisms contributed to less than 15% of the overall relaxation of bound water molecules. The Ln-O distances were fixed to the values reported by D'Angelo for lanthanide aqua ions.[18] From these fits we obtained rotational correlation times $\tau_{R,O}$ for the rotational diffusion of the Ln-O vectors.

In a second round, we performed a simultaneous fit of $ln[(1/T_2 - 1/T_1)/P_m]$ (^{17}O), $\Delta\omega_m$ (^{17}O), and r_1 (^{1}H) including inner-sphere (^{17}O, ^{1}H) and outer-sphere (^{1}H) contributions to relaxation. Dipolar and Curie relaxation for both ^{1}H and ^{17}O were considered. The quadrupolar relaxation for ^{17}O relaxation cancels in the difference $1/T_2 - 1/T_1$. The correlation time of the Ln-H vectors, $\tau_{R,H}$, is equal or shorter than the correlation time of the Ln-O vectors, $\tau_{R,O}$, due to internal rotation of inner-sphere water molecules.[19] In a first test $\tau_{R,O}$ was fixed to values obtained from the previous fit and the program was let to adjust the $\tau_{R,H}/\tau_{R,O}$-ratio which should be in the range of $0.6 - 1$.[19] The fit gave values between 0.8 to 1 with an error of ~ 0.2. We therefore decided to fix this ratio to one. The Ln-H distance, r_{LnH}, which is a sixth power weighted mean of the four Ln-H distances in $[Ln(L)(H_2O)_2]^x$, has been fitted. As last approximation, we considered a unique rate constant for the exchange of the two water molecules in the $q = 2$ complexes. Moreover, the following parameters have been fixed: $a_{LnH} = 3.6 \times 10^{-10}$ m, $D_{LnH}^{298} = 25 \times 10^{-10}$ m^{2}s^{-1} and the diffusion constant is assumed to obey Arrhenius law.

III.3 Results and discussion

The experimental data and calculated curves are shown in Figure III-2 to Figure III-3 and the corresponding fitted parameters are reported in Table III-1 and Table III-2. It has to be noted that for $[Sm(DTTA - Me)(H_2O)_2]^-$ and $[Sm(DO3A)(H_2O)_2]$ the chemical shifts were too small ($\Delta\omega_m \leq 0.1$ ppm) to enable the determination of the water exchange rate by ^{17}O NMR measurements even at the high magnetic field of 18.8 T and high concentration of metal ion chelate (100 mM) (see Table VIII-5).
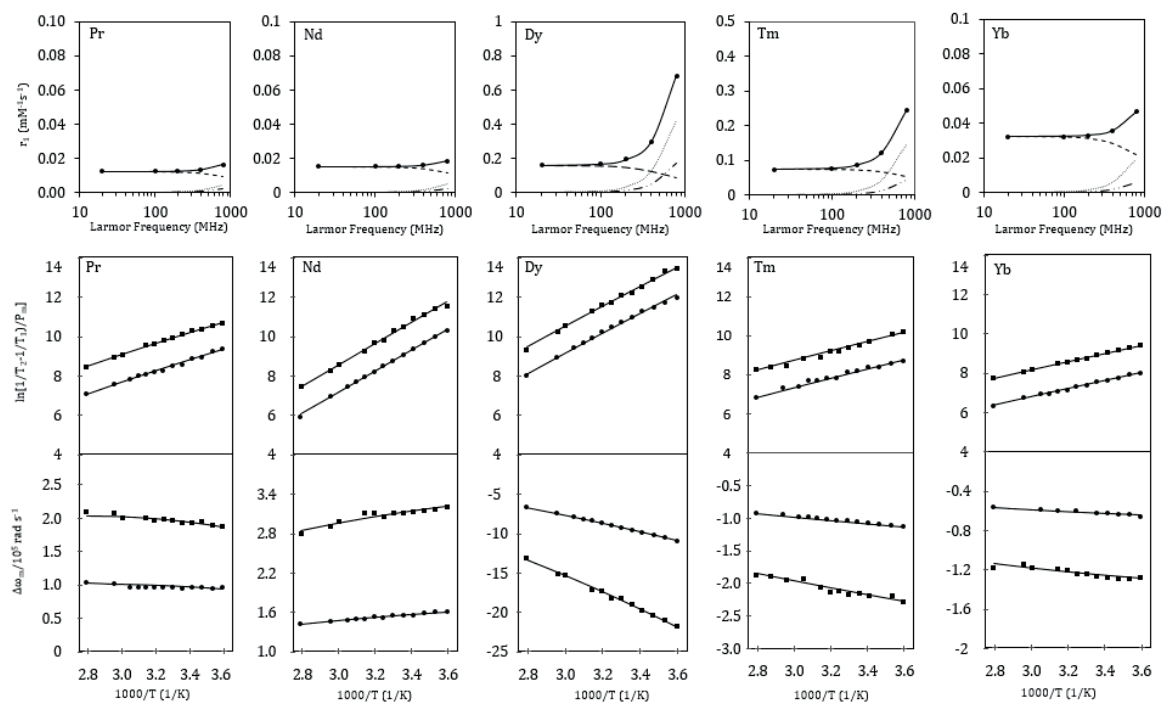
Figure III-2. ^{1}H NMRD profiles at 298 K (top) and ^{17}O NMR temperature dependence of $\ln[(1/T_2 - 1/T_1)/P_m]$ (middle) and chemical shifts $(\Delta\omega_m)$ (bottom) of $[Ln(DO3A)(H_2O)_2]$ complexes with Ln = Pr^{3+}, Nd^{3+}, Dy^{3+}, Tm^{3+}, Yb^{3+}, $[Ln^{3+}]$ ~100 mM, $B_0 = 9.4$ (●) and $B_0 = 18.8$ T (■), pH = 5.7. Lines correspond to the best fitting of the experimental data using parameters listed in Table III-1. The dashed, dotted and dash-dotted lines in ^{1}H NMRD profiles show the contributions $r_{1,d}^{IS}$, $r_{1,Cu}^{IS}$ and r_1^{OS} to r_1.
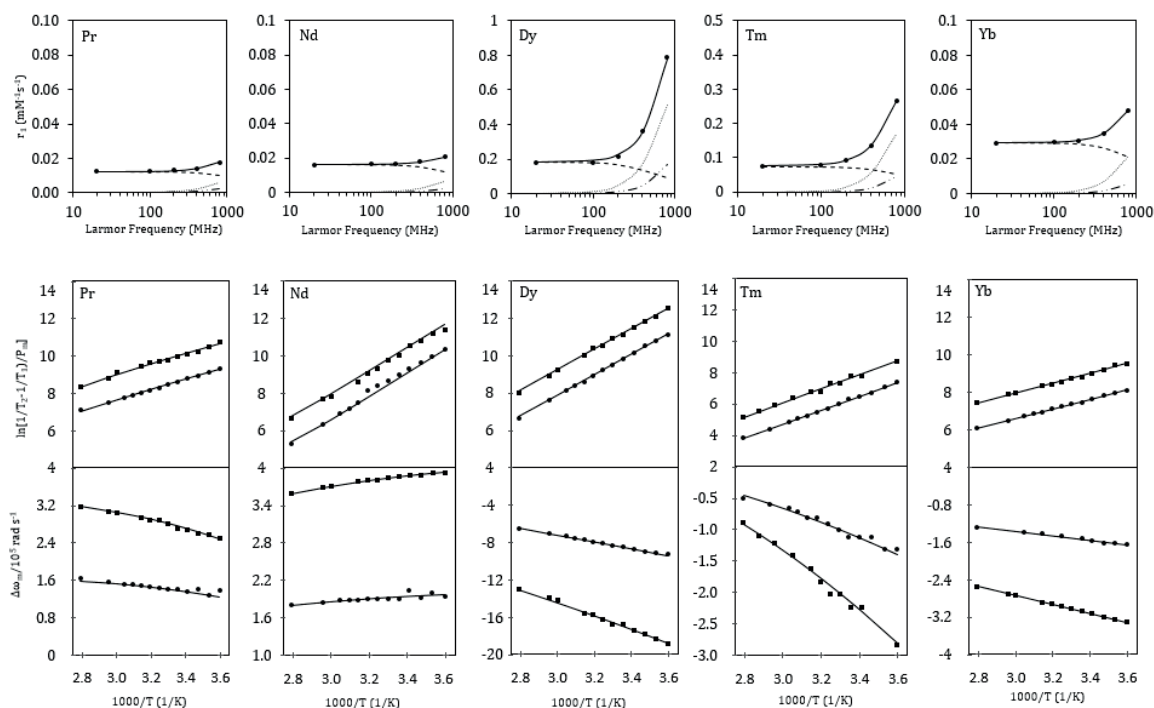
Figure III-3. ^{1}H NMRD profiles at 298 K (top) and ^{17}O NMR temperature dependence of $\ln[(1/T_2 - 1/T_1)/P_m]$ (middle) and chemical shifts ($\Delta\omega_m$) (bottom) of $[Ln(DTTA-Me)(H_2O)_2]^-$ complexes with Ln = Pr^{3+}, Nd^{3+}, Dy^{3+}, Tm^{3+}, Yb^{3+}, $[Ln^{3+}] \sim 100$ mM, $B_0 = 9.4$ (●) and $B_0 = 18.8$ T (■), pH = 5.7. Lines correspond to the best fitting of the experimental data using parameters listed in Table III-2. The dashed, dotted and dash-dotted lines in ^{1}H NMRD profiles show the contributions $r_{1,d}^{IS}$, $r_{1,Cu}^{IS}$ and r_1^{OS} to r_1.
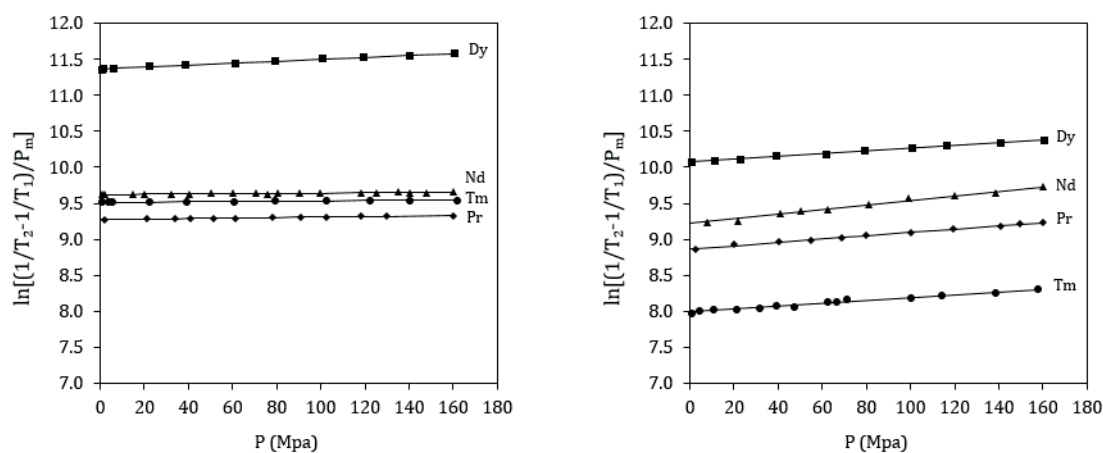
Figure III-4. ^{17}O NMR pressure dependence of $\ln[(1/T_2 - 1/T_1)/P_m]$ of $[Ln(DO3A)(H_2O)_2]$ (left) and $[Ln(DTTA-Me)(H_2O)_2]^-$ (right) complexes with Ln = Pr^{3+}, Nd^{3+}, Dy^{3+}, Tm^{3+}, $[Ln^{3+}] \sim 100$ mM, $B_0 = 9.4$ T, T = 22°C, pH = 5.7. Lines correspond to the best fitting of the experimental data using parameters listed in Table III-1 and Table III-2.
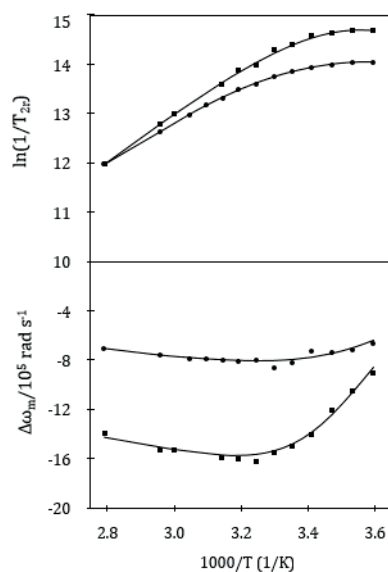
Figure III-5. ^{17}O NMR temperature dependence of $\ln(1/T_{2r})$ (top) and chemical shifts ($\Delta\omega_m$) (bottom) of $[Gd(DTTA - Me)(H_2O)_2]^-$ complex, $[Gd^{3+}]$ = 135.5 mM, B_0 = 9.4 (●) and B_0 = 18.8 T (■), pH =5.7. Lines correspond to the best fitting of the experimental data using parameters listed in Table III-2.
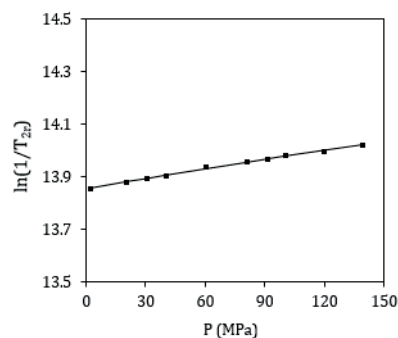
Figure III-6. ^{17}O NMR pressure dependence of $\ln(1/T_{2r})$ of $[Gd(DTTA - Me)(H_2O)_2]^-$ complex, $[Gd^{3+}]$ = 135.5 mM, B_0 = 9.4 T, pH = 5.7. Line correspond to the best fitting of the experimental data using parameters listed in Table III-2.

Table III-1. Parameters obtained from the nonlinear least squares fit of ^{1}H and ^{17}O NMR data for $[Ln(DO3A)(H_2O)_2]$ complexes.[a] Reported errors correspond to one standard deviation obtained by statistical analysis

		Pr^{3+}	Nd^{3+}	Gd^{3+} [14]	Dy^{3+}	Tm^{3+}	Yb^{3+}
$\Delta H^{\ddagger}$	(kJ mol^{-1})	23 ± 1	40 ± 1	33.3 ± 1.6	29 ± 1	13 ± 1	12 ± 1
k_{ex}^{298}	(10^6 s^{-1})	1.6 ± 0.1	2.9 ± 0.1	11 ± 1	16.6 ± 0.3	3.2 ± 0.1	2.2 ± 0.1
$\Delta S^{\ddagger}$	(J mol^{-1}K^{-1})	-50 ± 2	+12 ± 2	+1.4 ± 0.5	-9 ± 3	-77 ± 3	-83 ± 3
$\Delta V^{\ddagger}$	(cm^{3}mol^{-1})	-0.4 ± 0.2	-0.5 ± 0.2	-	-0.5 ± 0.3	-0.9 ± 0.5	-
$\tau_{R,O}^{298}$	(ps)	107 ± 4	105 ± 3	97 ± 1	98 ± 3	93 ± 2	96 ± 3
E_R	(kJ mol^{-1})	22 ± 1	22 ± 1	20.5 ± 0.3	21 ± 1	23 ± 1	24 ± 1
r_{LnH}	(Å)	3.43 ± 0.6	3.41 ± 0.4	-	3.28 ± 0.1	3.12 ± 0.1	3.11 ± 0.3
T_e	(ps)	0.5 ± 0.2	0.6 ± 0.2	-	0.6 ± 0.1	0.4 ± 0.1	0.5 ± 0.3

[a] for a full list of parameters see Table VIII-23.

Table III-2. Parameters obtained from the nonlinear least squares fit of ^{1}H and ^{17}O NMR data for $[Ln(DTTA-Me)(H_2O)_2]^-$ complexes.[a] Reported errors correspond to one standard deviation obtained by statistical analysis

		Pr^{3+}	Nd^{3+}	Gd^{3+}	Dy^{3+}	Tm^{3+}	Yb^{3+}
$\Delta H^{\ddagger}$	(kJ mol^{-1})	26 ± 1	49 ± 1	40 ± 1	36 ± 1	13 ± 1	13 ± 1
k_{ex}^{298}	(10^6 s^{-1})	3.5 ± 0.1	5.8 ± 0.1	22.7 ± 0.7	40.6 ± 0.9	26.7 ± 0.8	13.9 ± 0.1
$\Delta S^{\ddagger}$	(J mol^{-1}K^{-1})	-31 ± 1	+49 ± 1	+29 ± 3	+21 ± 2	-60 ± 2	-64 ± 3
$\Delta V^{\ddagger}$	(cm^{3}mol^{-1})	+7.0 ± 0.2	+6.8 ± 0.2	+7.0 ± 2	+1.8 ± 0.2	+0.4 ± 0.4	-
$\tau_{R,O}^{298}$	(ps)	152 ± 4	156 ± 4	150 ± 1	149 ± 6	146 ± 3	133 ± 1
E_R	(kJ mol^{-1})	24 ± 1	21 ± 1	20 ± 1	26 ± 2	23 ± 1	23 ± 1
r_{LnH}	(Å)	3.37 ± 0.5	3.36 ± 0.7	-	3.28 ± 0.1	3.16 ± 0.1	3.12 ± 0.1
T_e	(ps)	0.5 ± 0.1	0.6 ± 0.1	-	0.7 ± 0.2	0.4 ± 0.1	0.5 ± 0.1

[a] for a full list of parameters see Table VIII-24.

Table III-3. Water exchange parameters obtained from fit of variable temperature ^{17}O NMR data for $[Gd(DTTA-Me)(H_2O)_2]^-$ complex

k_{ex}^{298}	(10^6 s^{-1})	22.7 ± 0.7
$\Delta H^{\ddagger}$	(kJ mol^{-1})	39.7 ± 0.7
$\tau_{R,O}^{298}$	(ps)	150 ± 1
E_R	(kJ mol^{-1})	20 ± 1
τ_v^{298}	(ps)	0.8 ± 0.1
Δ^2	(10^{20} s^{-2})	0.2 ± 0.02
$A/\hbar$	(10^6 rad s^{-1})	-3.5 ± 0.2

The following parameters were fixed: r_{GdO} = 2.5 Å, χ = 7.58 MHz and E_v = 1 kJ mol^{-1}.

III.3.1 Proton relaxivity

As it is shown in Figure III-2 and Figure III-3, the proton relaxivity of the lanthanide complexes (other than Gd^{3+}) is quite low, 0.013 to 0.18 mM^{-1} s^{-1} at 20 MHz and 25°C compared to that of the Gd^{3+} analogue $[Gd(DO3A)(H_2O)_2]$ (6.0 $mM^{-1}s^{-1}$ at 20 MHz and 25°C).[20] This has been already observed in the case of lanthanide aqua ions[7] where the relaxation rates decrease by two orders of magnitude from 10 $mM^{-1}s^{-1}$ for $[Gd(H_2O)_8]^{3+}$,[21] to 0.05 $mM^{-1}s^{-1}$ for $[Yb(H_2O)_8]^{3+}$, at 20 MHz and 25°C. In the case of Gd^{3+} electronic relaxation is several orders of magnitude slower compared to the other lanthanide ions, leading to high nuclear spin relaxation rates.

The relaxation increase measured on bulk water molecules is mostly due to the inner sphere contribution, the outer sphere contribution can go up to 25% at high magnetic fields. For proton frequencies lower than 200 MHz the NMRD profile is field independent indicating that the relaxation mechanism is dipolar and the short, field independent electronic relaxation time[22] is the dominating correlation time ($r_1 \cong c \left(\frac{\mu_{eff}^2}{r_{LnH}^6} \right) T_e$) allowing to calculate T_e. One should however keep in mind that the fitted T_e strongly depends on r_{LnH}. The values obtained for the lanthanides studied are of the same order, ranging from 0.4 to 0.7×10^{-12} s, and independent on the chelating ligand.

A magnetic field dependence of relaxivity is observed at proton frequencies of 200 MHz and higher, indicating that the Curie mechanism contributes significantly to the relaxation rates ($\frac{1}{T_{1,Cu}} \propto B_0^2$). As already mentioned for this mechanism, the rotational correlation time ($\tau_{R,H}$) is the characteristic time which allows in principle to calculate $\tau_{R,H}$. In the case of the light lanthanides, the Curie mechanism contributes only up to 20% to the overall relaxation so the rotational correlation times obtained are subject to large errors if determined by NMRD data alone.

III.3.2 Water exchange

Surprisingly water exchange reactions on lanthanide complexes other than Gd^{3+} have not been studied extensively. Besides some slow exchanging tetraamide complexes which are of interest as PARACEST agents for MRI[23] to our knowledge only $[Ln(PDTA)(H_2O)_2]^-$ [24] and $[Ln(DTPA-BMA)(H_2O)]$ [25] have been studied so far (Table III-4).

Water exchange on lanthanide aqua ions has been studied for the heavy Ln^{3+} from gadolinium to ytterbium[26] which are all eight coordinated. For those aqua ions a very fast water exchange has been found which decreases monotonically with the ionic radius (Table III-4). The lower limits detected for k_{ex}^{298} for the light lanthanide ions Pr^{3+} and Nd^{3+} [27] as well as rate constants from complex formation with SO_4^{2-} [28] suggest a maximum of k_{ex}^{298} for water exchange on $\left[Ln(H_2O)_q\right]^{3+}$ in the middle of the lanthanide series.[26] From negative activation volumes an associative interchange mechanism has been assigned to all measured exchange reactions on aqua ions of heavy lanthanides.

For lanthanide poly(aminocarboxylate) complexes, water exchange is in general notably slower compared to that of the aqua ions.[26] For gadolinium complexes with DTPA or DOTA water exchange rate constants are about two orders of magnitude slower compared to $[Gd(H_2O)_8]^{3+}$.[29,30] For water exchange on $[Ln(DTPA-BMA)(H_2O)]$ measured rate constants increase from neodymium to holmium which has been rationalised by an increase of steric compression on the bound water molecule leading to a decrease of the energy barrier in the dissociative reaction (Table III-4).[25] The very slow exchanging $[Ln(DOTA-4AmCe)(H_2O)]$ chelates have been studied in acetonitrile solution showing a minimum of k_{ex}^{298} at Eu^{3+}.[31] For $[Ln(PDTA)(H_2O)_2]^-$ with two water molecules in the first coordination sphere k_{ex}^{298} decreases toward the smaller Ln^{3+} ions.[24] This decrease is accompanied by a change in mechanism from associatively activated to dissociatively activated.[24]

Table III-4. Water exchange rate constants, k_{ex}^{298}, activation volumes, $\Delta V^{\ddagger}$, and exchange reaction mechanisms for different lanthanides complexes

	[Ln(H₂O)₈/₉]³⁺ ³²		[Ln(DTPA-BMA) (H₂O)] ²⁵		[Ln(L3) (H₂O)] ³¹,ᵃ	[Ln(PDTA)(H₂O)₂]⁻ ²⁴		[Ln(DTTA-Me) (H₂O)₂]⁻ ᵇ		[Ln(DO3A)(H₂O)₂] ᵇ	
	k_{ex}^{298}	$\Delta V^{\ddagger}$	k_{ex}^{298}	$\Delta V^{\ddagger}$	k_{ex}^{298}	k_{ex}^{298}	$\Delta V^{\ddagger}$	k_{ex}^{298}	$\Delta V^{\ddagger}$	k_{ex}^{298}	$\Delta V^{\ddagger}$
	(10^6 s⁻¹)	(cm³ mol⁻¹)	(10^6 s⁻¹)	(cm³ mol⁻¹)	(10^6 s⁻¹)	(10^6 s⁻¹)	(cm³ mol⁻¹)	(10^6 s⁻¹)	(cm³ mol⁻¹)	(10^6 s⁻¹)	(cm³ mol⁻¹)
Pr³⁺	> 400	-	-	-	0.022	-	-	3.5	+7.0 (D)	1.6	-0.4 (I)
Nd³⁺	> 500	-	0.53	-0.8 (Iₐ)	0.0059	-	-	5.8	+6.8 (D)	2.9	-0.5 (I)
Eu³⁺	-	-	0.66	+8.5 (D)	0.0013	-	-	-	-	-	-
Gd³⁺	804	-3.3 (Iₐ)	0.43	+7.3 (D)	-	102	-1.5 (Iₐ)	22.7	+7.0 (D)	11	-
Tb³⁺	496	-5.7 (Iₐ)	1.61	+9.8 (D)	-	24	-7.6 (Iₐ,A)	-	-	-	-
Dy³⁺	386	-6.0 (Iₐ)	3.53	+7.3 (D)	-	6.6	-5.5 (Iₐ,A)	40.6	+1.8 (I_d,I)	16.6	-0.5 (I)
Ho³⁺	191	-6.6 (Iₐ)	5.98	+9.4 (D)	-	-	-	-	-	-	-
Er³⁺	118	-6.9 (Iₐ)	-	-	0.057	0.56	-6.5 (Iₐ,A)	-	-	-	-
Tm³⁺	81	-6.0 (Iₐ)	-	-	-	0.35	-1.2 (Iₐ)	26.7	+0.4 (I)	3.2	-0.9 (I)
Yb³⁺	41	-	-	-	0.17	0.28	+7.4 (I_d,D)	13.9	-	2.2	-

ᵃ⁾ L3 = DOTA-4AmCe; studied in CD₃CN, ᵇ⁾ this work
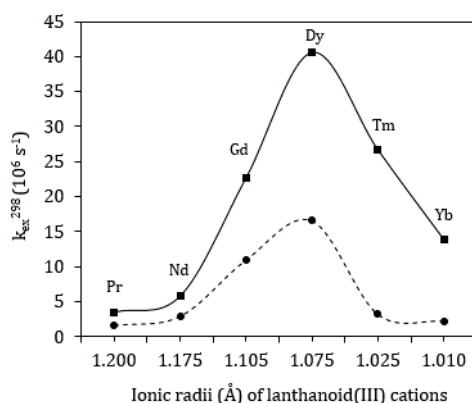
Figure III-7. Water exchange rate constants, k_{ex}^{298}, of $[Ln(DO3A)(H_2O)_2]^-$ (●, dashed line) and $[Ln(DTTA-Me)(H_2O)_2]$ (■, solid line) complexes, $[Ln^{3+}] \sim 100$ mM, T = 25°C.

Water exchange rate constants measured on DO3A and DTTA − Me complexes both show a maximum of k_{ex}^{298} around dysprosium (Figure III-7). Water exchange on complexes of the acyclic DTTA − Me ligand is much faster than on the macrocyclic DO3A. It was found earlier that in general, increasing the negative charge of the complex accelerates water exchange in a dissociative exchange reaction.[3] The higher negative charge weakens the electrostatic attraction between the 3+ lanthanide ions and the negatively charged oxygen atoms of the water molecules and favors dissociation.

Concerning $[Ln(DO3A)(H_2O)_2]$ small activation volumes $|\Delta V^{\ddagger}| < 1 \text{ cm}^3 \text{ mol}^{-1}$ indicate an interchange type of mechanism for all lanthanide complexes studied. It has been found earlier that DO3A complexes of lanthanides can form ternary complexes with bidentate anions in which the two inner sphere water molecules are replaced.[33-36] These formations of ternary complexes and recent results from DFT structure calculations[37] show that the two inner sphere water molecules are adjacent in $[Ln(DO3A)(H_2O)_2]$. One water molecule is farther from the negative carboxylate groups (Figure III-8), which perhaps allows the approach of the incoming water molecule in the interchange mechanism.
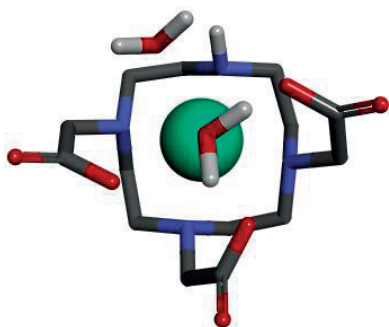
Figure III-8. DFT structure of $[Gd(DO3A)(H_2O)_2]$ drawn from the data in the Supporting Information of ref. 45.

The relatively constant $\Delta V^{\ddagger}$ measured for $[Ln(DO3A)(H_2O)_2]$ along the lanthanide series is a bit surprising in view of the 10-fold increase and decrease in k_{ex}^{298} from Pr^{3+} to Dy^{3+} to Yb^{3+}, respectively (Table III-1 and Figure III-7). A possible explanation could be found in a change of coordination geometry similar to that found for DOTA[4] and DOTMA[38] complexes. Nothing is known so far concerning geometrical isomers of lanthanide DO3A complexes in solution, probably due to fast interconversion rates compared to that of DOTA arising from a missing carboxylate arm.[4] For DOTA and DOTMA it is known that water exchange rate constants vary considerably between square-antiprism (SAP) or twisted square-antiprism (TSAP) structured complexes.[38,39] We also like to stress that pressure variation as used for the determination of $\Delta V^{\ddagger}$ could

displace the SAP/TSAP equilibrium and therefore lead to errors in activation volumes, even if no marked change was detected on chemical shifts measured.

Water exchange on $[\text{Ln}(\text{DTTA} - \text{Me})(\text{H}_2\text{O})_2]^-$ also varies by more than a factor of ten between Pr^{3+} complexes on one side and the Dy^{3+} chelate on the other side. In this case a change in mechanism is detected from dissociative for the larger ions (Pr^{3+} to Gd^{3+}, $\Delta V^\ddagger \sim +7$ cm^3 mol^{-1}) to interchange for the smaller ones (Dy^{3+}, Tm^{3+}, $\Delta V^\ddagger = +1.8$ to $+0.4$ cm^3 mol^{-1}). This seems contradictory because there should be less space for an incoming water molecule in case of the smaller ions. Two explanations are possible for this surprising result. The first is a change in coordination geometry. From the absence of formation of ternary complexes it had been concluded that the two water molecules in $[\text{Gd}(\text{DTTA} - \text{Me})(\text{H}_2\text{O})_2]^-$ are non-adjacent,[40] even if this structure has not been confirmed by the DFT calculations.[37] A non-adjacent arrangement could explain the dissociative character of the water exchange on $[\text{Ln}(\text{DTTA} - \text{Me})(\text{H}_2\text{O})_2]^-$. A water molecule has to leave the first coordination sphere at least to a considerable amount before it can be replaced by an incoming one. Chelates with smaller cations could favor a configuration with adjacent water molecules, which then exchange via an interchange mechanism. The second explanation takes into account that exchange of the two water molecules happens at different rates – one water molecule could exchange much faster than the other one. A decrease of the ionic radius of the Ln^{3+} could have an influence on the ratio of water exchange rates and lead to smaller apparent values of $\Delta V^\ddagger$. It should be noted that we measure changes in relaxation of bulk water induced by exchange with water bound to paramagnetic species by NMR and we cannot distinguish by this method different binding sites on the chelates.

III.4 Conclusions

A systematic study of water exchange kinetics of selected Ln^{3+} complexes with DO3A and DTTA $-$ Me as representatives for macrocyclic and acyclic ligands is reported. The number of inner sphere water molecules is found to be constant with $q = 2$ for all $[\text{Ln}(\text{L})(\text{H}_2\text{O})_q]^x$ complexes studied. Water exchange rate constants measured on DO3A

and DTTA-Me complexes both show a maximum around dysprosium. Moreover, a faster water exchange is observed on negatively charged complexes of the DTTA-Me ligand than on the complexes of DO3A. Variable pressure studies suggested an interchange type of mechanism for $[Ln(DO3A)(H_2O)_2]$ complexes since small activation volumes $|\Delta V^{\ddagger}| < 1\, cm^3\, mol^{-1}$ were obtained. In the case of $[Ln(DTTA-Me)(H_2O)_2]^-$ complexes for the larger ions (Pr^{3+} to Gd^{3+}) a dissociative activation mode has been found from the positive $\Delta V^{\ddagger}$ values; for the smaller ions (Dy^{3+}, Tm^{3+}) an interchange mechanism was assigned due to still positive but much smaller activation volumes.

III.5 Experimental procedures

III.5.1 Materials

$LnCl_3.xH_2O$ (99.9%) ($Ln = Pr^{3+}$, Nd^{3+}, Sm^{3+}, Gd^{3+}, Dy^{3+}, Tm^{3+}, Yb^{3+}) were obtained from Aldrich and were used without further purification. The DTTA-Me[4] (N,N'-[methylimino)bis(ethane-2,1-diyl)]bis[N-(carboxymethyl)glycine] was provided by EPFL through the synthetic platform; the synthesis of the ligand has been described in a previous communication.[40] DO3A (1,4,7,10-tetraazacyclododecane-*N,N',N''*-triacetate) was provided by CheMatech Co, Dijon, France. Other reagents were obtained from Sigma-Aldrich Chemical Co. commercial sources and used without further purification.

III.5.2 Preparation of [Ln(L)(H₂O)₂]ˣ Complexes

Ln^{3+} solutions (1 M) in water were prepared from $LnCl_3.xH_2O$. The exact concentration of the metal ion was measured by complexometric titration with Na_2H_2EDTA in urotropine/HCl buffer and xylenol orange as metal indicator. Solid ligands (L = DO3A, DTTA-Me) were dissolved in water in order to obtain 100 mM solutions. The exact concentration of the ligand was determined by back titration of Gd^{3+} excess with Na_2H_2EDTA solution. Samples were prepared by mixing adequate amount of solutions of $LnCl_3$ and of the ligand in a 1:1 molar ratio, allowing for 2-4% excess ligand and having final Ln^{3+} concentration of ~ 100 mM. The absence of free lanthanide in the solution was confirmed using xylenol orange indicator. The pH of the solution, measured

with a combined glass electrode calibrated with Metrohm buffer solutions, was maintained at 5.7 with 0.1 M NaOH solution. ^{17}O enriched water was added to have solutions with about 2% ^{17}O enrichment. The final Ln^{3+} concentration was measured by bulk magnetic susceptibility (BMS)[41] at 25°C on a Bruker DRX-400 (9.4 T, 400 MHz) spectrometer, by measuring the difference of the shift of the tert-butanol alkyl protons in the paramagnetic environment and in the diamagnetic reference, contained in a coaxial NMR tube. In order to eliminate susceptibility corrections to the chemical shift,[42] for ^{1}H and variable temperature ^{17}O NMR measurements the samples were sealed in glass spheres fitting into 10 mm NMR tubes.[42] For ^{17}O variable pressure measurements, the solution was placed inside a 5 mm NMR tube and closed with a movable MACOR piston.[43,44]

III.5.3 ^{1}H NMR relaxometry

Longitudinal relaxation rates ($1/T_1$) were measured by the inversion-recovery method[45] at 25°C and ^{1}H Larmor frequencies from 20 to 800 MHz using the following equipment: Bruker Minispec 20 MHz (0.47 T), Bruker Avance console connected to 100 MHz (2.35 T) and 200 MHz (4.7 T) cryomagnets, Bruker Avance-II 400 MHz (9.4 T) and Bruker Avance-II 800 MHz (18.8 T). The diamagnetic contributions to the ^{1}H NMR relaxation rates were determined with the acidified water reference (pH 3.0, 2% ^{17}O enrichment). In each case, the temperature was measured by the substitution technique.[46]

III.5.4 ^{17}O NMR measurements

Variable temperature ^{17}O NMR measurements were performed at two magnetic fields using Bruker Avance-II 400 (9.4 T, 54.2 MHz) and Bruker Avance-II 800 (18.8 T, 128.4 MHz) spectrometers in the temperature range of 5°C to 85°C. The temperature was controlled by Bruker B-VT 3000 temperature control units, and was measured by a substitution technique.[46] Variable-pressure NMR spectra were recorded up to a pressure of 160 MPa on a Bruker Avance-II 400 (9.4 T, 54.2 MHz) spectrometer equipped with a homebuilt high-pressure NMR probe.[47] The temperature was measured with a built-in Pt resistor. The longitudinal ($1/T_1$) and transverse ($1/T_2$) relaxation rates were measured

using the inversion recovery[45] and the Carr-Purcell-Meiboom-Gill spin-echo[48] methods, respectively. The chemical shift differences were determined in respect to an acidified water reference (pH 3.0, 2% ^{17}O enrichment). For all ^{17}O NMR measurements, the 90° pulse lengths have been determined at different temperatures and pressures for each sample.

III.6 Data fitting

All fittings have been performed using the Visualiseur/Optimiseur[49,50] 3.7.0 program running on a Matlab® 8 platform.

III.7 References

(1)   Laurent, S.; Elst, L. V.; Muller, R. N. *Contrast Media Mol. Imaging* **2006**, *1*, 128.
(2)   Geraldes, C. F.; Laurent, S. *Contrast Media Mol. Imaging* **2009**, *4*, 1.
(3)   Hermann, P.; Kotek, J.; Kubicek, V.; Lukes, I. *Dalton Trans.* **2008**, *0*, 3027.
(4)   Aime, S.; Botta, M.; Fasano, M.; Marques, M. P. M.; Geraldes, C. F. G. C.; Pubanz, D.; Merbach, A. E. *Inorg. Chem.* **1997**, *36*, 2059.
(5)   Choppin, G. R.; Wong, P. J. In *Coordination Chemistry*; American Chemical Society: 1994.
(6)   Caravan, P.; Greenfield, M. T.; Bulte, J. W. M. *Magn. Reson. Med.* **2001**, *46*, 917.
(7)   Bertini, I.; Capozzi, F.; Luchinat, C.; Nicastro, G.; Xia, Z. *J. Phys. Chem.* **1993**, *97*, 6351.
(8)   Peters, J. A.; Huskens, J.; Raber, D. J. *Prog. Nucl. Magn. Reson. Spectrosc.* **1996**, *28*, 283.
(9)   Alsaadi, B. M.; Rossotti, F. J. C.; Williams, R. J. P. *J. Chem. Soc., Dalton Trans.* **1980**, 2151.
(10)   Alsaadi, B. M.; Rossotti, F. J. C.; Williams, R. J. P. *J. Chem. Soc., Dalton Trans.* **1980**, 2147.
(11)   Burns, P. D.; La Mar, G. N. *J. Magn. Reson.* **1982**, *46*, 61.
(12)   Aime, S.; Barbero, L.; Botta, M.; Ermondi, G. *J. Chem. Soc., Dalton Trans.* **1992**, 225.
(13)   McLaughlin, A. C.; Leigh Jr, J. S. *J. Magn. Reson.* **1973**, *9*, 296.
(14)   Tóth, É.; Dhubhghaill, O. M. N.; Besson, G.; Helm, L.; Merbach, A. E. *Magn. Reson. Chem.* **1999**, *37*, 701.
(15)   Zhang, X.; Chang, C. A.; Brittain, H. G.; Garrison, J. M.; Telser, J.; Tweedle, M. F. *Inorg. Chem.* **1992**, *31*, 5597.
(16)   Djanashvili, K.; Platas-Iglesias, C.; Peters, J. A. *Dalton Trans.* **2008**, 602.
(17)   Halle, B.; Wennerström, H. k. *J. Magn. Reson.* **1981**, *44*, 89.
(18)   D'Angelo, P.; Zitolo, A.; Migliorati, V.; Chillemi, G.; Duvail, M.; Vitorge, P.; Abadie, S.; Spezia, R. *Inorg. Chem.* **2011**, *50*, 4572.
(19)   Dunand, F. A.; Borel, A.; Merbach, A. E. *J. Am. Chem. Soc.* **2002**, *124*, 710.
(20)   Aime, S.; Botta, M.; Crich, S. G.; Giovenzana, G.; Pagliarin, R.; Sisti, M.; Terreno, E. *Magn. Reson. Chem.* **1998**, *36*, S200.
(21)   O'Hara, P. B.; Koenig, S. H. *Biochem.* **1986**, *25*, 1445.
(22)   Fries, P. H.; Belorizky, E. *J. Chem. Phys.* **2012**, *136*.
(23)   Zhang, S.; Wu, K.; Sherry, A. D. *J. Am. Chem. Soc.* **2002**, *124*, 4226.
(24)   Graeppi, N.; Hugh Powell, D.; Laurenczy, G.; Zékány, L.; Merbach, A. *Inorg. Chim. Acta* **1995**, *235*, 311.
(25)   Pubanz, D.; Gonzalez, G.; Powell, D. H.; Merbach, A. E. *Inorg. Chem.* **1995**, *34*, 4447.
(26)   Helm, L.; Merbach, A. E. *Chem. Rev.* **2005**, *105*, 1923.
(27)   Powell, D. H.; Merbach, A. E. *Magn. Reson. Chem.* **1994**, *32*, 739.
(28)   Fay, D. P.; Litchinsky, D.; Purdie, N. *J. Phys. Chem.* **1969**, *73*, 544.
(29)   Powell, D. H.; Dhubhghaill, O. M. N.; Pubanz, D.; Helm, L.; Lebedev, Y. S.; Schlaepfer, W.; Merbach, A. E. *J. Am. Chem. Soc.* **1996**, *118*, 9333.
(30)   Micskei, K.; Powell, D. H.; Helm, L.; Brücher, E.; Merbach, A. E. *Magn. Reson. Chem.* **1993**, *31*, 1011.
(31)   Zhang, S.; Merritt, M.; Woessner, D. E.; Lenkinski, R. E.; Sherry, A. D. *Acc. Chem. Res.* **2003**, *36*, 783.

(32)   Cossy, C.; Helm, L.; Merbach, A. E. *Inorg. Chem.* **1988**, *27*, 1973.
(33)   Bruce, J. I.; Dickins, R. S.; Govenlock, L. J.; Gunnlaugsson, T.; Lopinski, S.; Lowe, M. P.; Parker, D.; Peacock, R. D.; Perry, J. J. B.; Aime, S.; Botta, M. *J. Am. Chem. Soc.* **2000**, *122*, 9674.
(34)   Dickins, R. S.; Aime, S.; Batsanov, A. S.; Beeby, A.; Botta, M.; Bruce, J. I.; Howard, J. A. K.; Love, C. S.; Parker, D.; Peacock, R. D.; Puschmann, H. *J. Am. Chem. Soc.* **2002**, *124*, 12697.
(35)   Botta, M.; Aime, S.; Barge, A.; Bobba, G.; Dickins, R. S.; Parker, D.; Terreno, E. *Chem. Eur. J.* **2003**, *9*, 2102.
(36)   Terreno, E.; Botta, M.; Boniforte, P.; Bracco, C.; Milone, L.; Mondino, B.; Uggeri, F.; Aime, S. *Chem. Eur. J.* **2005**, *11*, 5531.
(37)   Regueiro-Figueroa, M.; Platas-Iglesias, C. *J. Phys. Chem. A* **2015**, *119*, 6436.
(38)   Dunand, F. A.; Aime, S.; Merbach, A. E. *J. Am. Chem. Soc.* **2000**, *122*, 1506.
(39)   Aime, S.; Botta, M.; Garda, Z.; Kucera, B. E.; Tircso, G.; Young, V. G.; Woods, M. *Inorg. Chem.* **2011**, *50*, 7955.
(40)   Moriggi, L.; Cannizzo, C.; Prestinari, C.; Berrière, F.; Helm, L. *Inorg. Chem.* **2008**, *47*, 8357.
(41)   Corsi, D. M.; Platas-Iglesias, C.; Bekkum, H. v.; Peters, J. A. *Magn. Reson. Chem.* **2001**, *39*, 723.
(42)   Hugi, A. D.; Helm, L.; Merbach, A. E. *Helv. Chim. Acta* **1985**, *68*, 508.
(43)   Helm, L.; Merbach, A. E. *J. Chem. Soc., Dalton Trans.* **2002**, 633.
(44)   Frey, U.; Helm, L.; Merbach, A. E. *High Press. Res.* **1990**, *2*, 237.
(45)   Vold, R. L. *J. Chem. Phys* **1968**, *48*, 3831.
(46)   Ammann, C.; Meier, P.; Merbach, A. *J. Magn. Reson.* **1982**, *46*, 319.
(47)   Cusanelli, A.; Nicula-Dadci, L.; Frey, U.; Merbach, A. E. *Inorg. Chem.* **1997**, *36*, 2211.
(48)   Meiboom, S.; Gill, D. *Rev. Sci. Instrum.* **1958**, *29*, 688.
(49)   Yerly, F. *VISUALISEUR 2.3.6* **2004**.
(50)   Yerly, F. *OPTIMISEUR 3.0.0* **2002**.

Chapter IV

Complexation of $[\mathrm{Gd(DTTA-Me)(H_2O)_2}]^-$ by fluoride and its consequences to water exchange
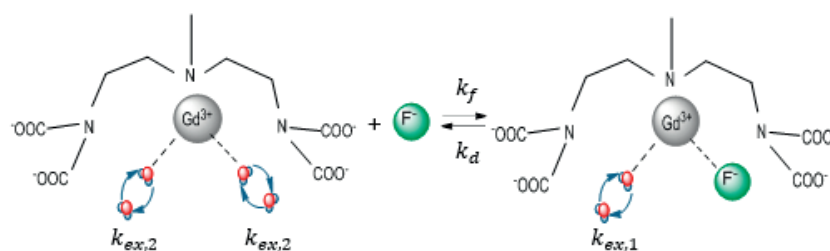
IV.1 Introduction

In chapter III, we studied the water exchange kinetics of selected lanthanide complexes of DO3A and DTTA − Me ligands. While analyzing the experimental data, we considered a unique rate constant for the exchange of the two coordinated water molecules in the first coordination sphere. However, one should keep in mind that what we observe is a mean rate constant for water exchange and the individual rate constants can be very similar or very different. In order to investigate the possible difference in the two exchange rates, one of the metal-bound water molecules can be replaced by an anion. In this regard, we studied the possible replacement of metal coordinated water molecule(s) in $[Gd(DTTA -$ $Me)(H_2O)_2]^-$ by fluoride anions. F^- binding to $[Gd(DTTA - Me)(H_2O)_2]^-$ allows to gain information on the kinetics of water exchange upon anion binding. On the other hand, F^- is a hard Lewis base that forms rather stable complexes with the Ln^{3+} ions, a property that has been used to design Ln^{3+} based fluoride sensors.[1]

The binding of F^- to $[Gd(DTTA - Me)(H_2O)_2]^-$ was investigated using proton relaxometric studies. Variable temperature ^{19}F NMR and ^{17}O NMR measurements were employed to determine the exchange rate constant of the bound fluoride and bound water molecule(s), respectively. Moreover, variable pressure ^{17}O NMR measurements were conducted for mechanistic assignment of the exchange reactions. Finally, the structures of the $[Gd(DTTA - Me)(H_2O)_2]^-$ and $[Gd(DTTA - Me)(H_2O)F]^{2-}$ complexes were investigated by using DFT calculations and wave function analysis based on the atoms-in-molecules theory of Bader.[2]

IV.2 Results and discussion

As we discussed in chapter III, the $DTTA^{4-}$ derivatives coordinate to Gd^{3+} leaving two water molecules coordinated in the first coordination sphere ($q = 2$).[3-6] Following the addition of fluoride to a solution of $[Gd(DTTA - Me)(H_2O)_2]^-$, one or both inner-sphere water molecules might be displaced by fluoride:

$$[Gd(DTTA-Me)(H_2O)_2]^- + F^- \rightleftharpoons [Gd(DTTA-Me)(H_2O)F]^{2-} + H_2O \quad (IV\text{-}1)$$

$$[Gd(DTTA-Me)(H_2O)F]^{2-} + F^- \rightleftharpoons [Gd(DTTA-Me)F_2]^{3-} \quad + H_2O \quad (IV\text{-}2)$$

Although the $[Gd(DTTA-Me)(H_2O)_2]^-$ complex is very stable ($log(K_f) = 18.6$) traces of free ions are present in Gd^{3+} solution (pGd = 15.8).[7] Therefore, insoluble GdF_3 might form due to fluoride binding to the free Gd^{3+} ions ($log(K_s) = 17.2$):[8]

$$Gd^{3+} + 3F^- \rightleftharpoons GdF_3 \quad\quad\quad\quad\quad\quad\quad\quad (IV\text{-}3)$$

To ensure a minimum of free Gd^{3+} an excess of free ligand can be added, as a high concentration ratio of $DTTA-Me^{4-}$ to Gd^{3+} will decrease the amount of free metal ion and avoid precipitation of GdF_3 at high fluoride concentrations. An excess of ligand can potentially affect the hydration number of the complex by coordination of a carboxylate group and thus replacing one or both coordinated water molecules. Thus, we measured ${}^1H$ relaxivity of a series of samples with an increasing $[DTTA-Me^{4-}]/[Gd^{3+}]$ ratio in order to detect a possible binding of the ligand used in excess.

Considering that inner-sphere longitudinal relaxivity is linearly proportional to the number of bound water molecules (q) (eq IV-4), possible variation in the hydration number can be studied by longitudinal relaxation rate measurements.

$$r_1^{IS} = \frac{1}{1000}\frac{q}{55.5}\frac{1}{T_{1m}+\tau_m} \quad\quad\quad\quad\quad\quad (IV\text{-}4)$$
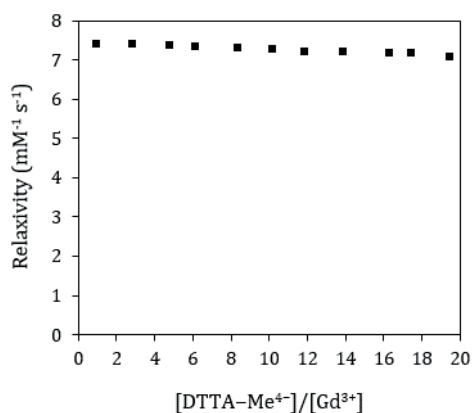
Figure IV-1. Proton relaxivity versus the concentration ratio of $[DTTA-Me^{4-}]/[Gd^{3+}]$ in aqueous solution, $[Gd^{3+}] = 0.16$ mM, $B_0 = 0.7$ T (30 MHz), T = 25°C, pH =7.4.

As shown in Figure IV-1, ^{1}H relaxivity remains nearly constant while increasing the concentration of free ligand, which confirms that the presence of an excess of ligand does not affect the hydration number of the complex; henceforth the highest $[\text{DTTA} - \text{Me}^{4-}]/$ $[\text{Gd}^{3+}]$ ratio of ~ 20 can be used for further studies. Moreover, simulations based on complex stability and GdF_3 solubility constants confirmed that even at the highest fluoride concentration, no GdF_3 precipitation is expected. These simulations have been performed based on the routines developed by Maeder[9] using a program running under Matlab® 8 platform.

Following a similar procedure, ternary complex formation of $[\text{Gd(DTTA} - \text{Me})(\text{H}_2\text{O})_2]^-$ with F^- was studied using ^{1}H relaxation enhancement measurements in a solution with a $[\text{DTTA} - \text{Me}^{4-}]/[\text{Gd}^{3+}]$ ratio of 20. Longitudinal water proton relaxation rate measurements were carried out at $[\text{F}^-]/[\text{Gd}^{3+}]$ ratios of up to ~ 4000 to investigate the number of inner-sphere water molecules displaced by fluoride (Figure IV-2).
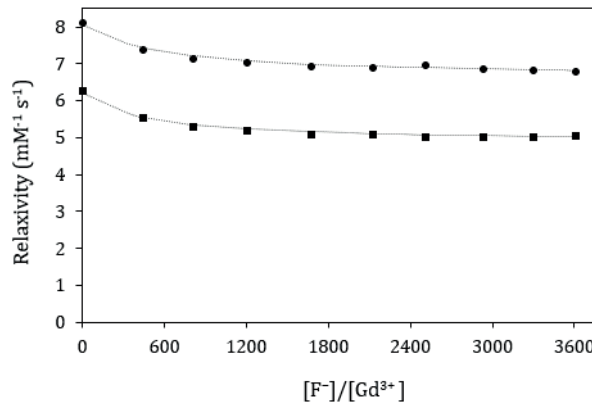
Figure IV-2. Proton relaxivity versus the concentration ratio of $[\text{F}^-]/[\text{Gd}^{3+}]$, $[\text{Gd}^{3+}]$ = 0.12 mM, B_0 = 0.7 T (30 MHz), T = 25°C (●) and 37°C (■), I = 1 M, pH = 7.4.

Upon increasing the fluoride concentration from 0 to ~ 0.5 M, the relaxivity decreases from 8.1 to 6.8 mM^{-1} s^{-1} at 30 MHz and 25°C. The degree of the relaxivity decrease indicates displacement of only one inner-sphere water molecule, as a relaxivity of 6.8 mM^{-1} s^{-1} (at 25°C) is aligned with what was previously observed for similar complexes with a hydration number of one.[10,11] A more important relaxivity decrease down to 2 - 3

$mM^{-1} s^{-1}$ is expected for a complex with a hydration number of zero, as it is the case of the structurally related $[Gd(TTHA)]^{3-}$ complex.[12] We therefore assert that fluoride can displace only one single water molecule in $[Gd(DTTA-Me)(H_2O)_2]^-$ solutions up to a $[F^-]/[Gd^{3+}]$ ratio of 4000. Relaxometric and luminescence emission studies[13-16] showed that lanthanide complexes with DO3A based ligands react with anions like carbonate, phosphate and lactate, which coordinate in a bidentate manner replacing both inner-sphere water molecules. In an earlier study it was shown that lactate does not bind to $[Gd(DTTA-Me)(H_2O)_2]^-$.[7] This might be a result of a difference in their inner-sphere water molecules arrangements or due to the negative charge of the $DTTA-Me^{4-}$ complex, which disfavors the interaction with anions. To understand the reasons for this different behavior, the structure of the $[Gd(DTTA-Me)(H_2O)_2]^-.4H_2O$ system was optimised using DFT calculations in aqueous solution. In these calculations we included explicitly four second-sphere water molecules, which were shown to be crucial to obtain accurate Gd-O$_{water}$ bond distances and ^{17}O hyperfine coupling constants of the coordinated water molecules.[17] Our results (Figure IV-3) provide a O1w-Gd-O2w angle of 72.1º, a value that is virtually identical to that obtained previously in a computational study for $[Gd(DO3A)(H_2O)_2].4H_2O$ (72.4º).[18] These results indicate that the two inner-sphere water molecules in these complexes are occupying adjacent positions in the Gd^{3+} coordination sphere. Thus, we conclude that the different anion binding ability of these bis-hydrated complexes is related to their overall charge, in which the higher negative charge of the $[Gd(DTTA-Me)(H_2O)F]^{2-}$ complex renders the formation of the bis-fluoride complex less favorable to occur.

An analysis of the metal coordination environment in $[Gd(DTTA-Me)(H_2O)_2]^-.4H_2O$ with the aid of SHAPE measures indicates that the best description of the coordination polyhedron is provided by a capped square antiprism, where N1, N2, N3 and O2 define one of the square faces of the polyhedron, the second square face is delineated by O1, O1w, O3 and O4, and O2w is at the capping position. We notice that the Gd-O2w distance (2.547 Å) is considerably longer than the Gd-O1w one (2.484 Å), which suggests that the water molecule occupying the capping position is considerably more labile.
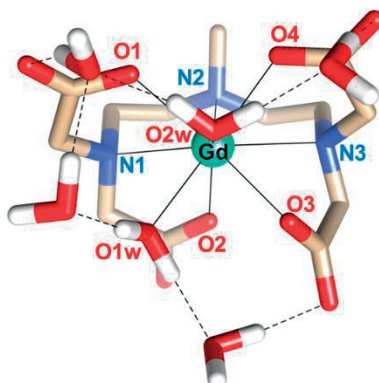
Figure IV-3. Optimised geometry of the $[Gd(DTTA-Me)(H_2O)_2]^-.4H_2O$ complex obtained with DFT calculations at the M06/LCRECP/TZVP level. Hydrogen atoms, except those of water molecules, are omitted for simplicity. Bond distances (Å) of the Gd^{3+} coordination environment: Gd-O1, 2.410; Gd-O2, 2.389; Gd-O3, 2.400; Gd-O4, 2.431; Gd-O1w, 2.484; Gd-O2w, 2.547; Gd-N1, 2.709; Gd-N2, 2.698; Gd-N3, 2.714.

IV.2.1 Thermodynamic stability of $[Gd(DTTA\text{-}Me)(H_2O)_xF_y]^z$

The observed bulk water proton longitudinal relaxation rates depend on the concentrations of the two complexes $[Gd(DTTA-Me)(H_2O)_2]^-$ and $[Gd(DTTA-Me)(H_2O)F]^{2-}$ and can therefore be used to determine the stoichiometric stability constant at the ionic strength I (K_{MLF}^I):

$$\frac{1}{T_{1,obs}} = \frac{1}{T_{1,d}} + r_{1,MLF}[MLF(H_2O)] + r_{1,ML}[ML(H_2O)_2] \qquad \text{(IV-5)}$$

$$K_{MLF}^I = \frac{[MLF(H_2O)]}{[ML(H_2O)_2]*[F]} \qquad \text{(IV-6)}$$

$$[M]_{tot} = [ML(H_2O)_2] + [MLF(H_2O)] \qquad \text{(IV-7)}$$

$$[F]_{tot} = [F] + [MLF(H_2O)] \qquad \text{(IV-8)}$$

where [M] and [F] are the metal ion and fluoride concentrations, $[ML(H_2O)_2]$ and $[MLF(H_2O)]$ are the equilibrium concentrations of $[Gd(DTTA-Me)(H_2O)_2]^-$ and $[Gd(DTTA-Me)(H_2O)F]^{2-}$ respectively and $r_{1,ML}$ and $r_{1,MLF}$ are their corresponding proton relaxivities. Solving eqs IV-5 to IV-8 for $[MLF(H_2O)]$ one finds:

$$[MLF(H_2O)] = \frac{[M]_{tot}+[F]_{tot}+\frac{1}{K^I_{MLF}}}{2} - \left[\left(\frac{[M]_{tot}+[F]_{tot}+\frac{1}{K^I_{MLF}}}{2}\right)^2 - [F]_{tot}*[M]_{tot}\right]^{1/2} \quad \text{(IV-9)}$$

Since the stoichiometric stability constant is ionic strength dependent, the thermodynamic stability constant corresponding to zero ionic strength (K^0_{MLF}) of a metal complex can be calculated using eq IV-10.

$$K^0_{MLF} = \frac{a_{MLF}}{a_{ML}*a_F} = K^I_{MLF}\frac{\gamma_{MLF}}{\gamma_{ML}*\gamma_F} \quad \text{(IV-10)}$$

where γ_i, the activity coefficients, are calculated using Davies' equation[19] where Z_i and I are the ion charge and the ionic strength, respectively:

$$\gamma_i = 10^{-0.509 \cdot Z_i^2\left(\frac{\sqrt{I}}{1+\sqrt{I}}-0.3 \cdot I\right)} \quad \text{(IV-11)}$$

From the thermodynamic stability constant, one can calculate ΔH^0, ΔS^0 and ΔV^0, the reaction enthalpy, entropy and volume from the variation of water proton relaxation rates with temperature and pressure:

$$K^0_{MLF} = exp\left[\frac{T\Delta S^0 - \Delta H^0}{RT}\right] \quad \text{(IV-12)}$$

$$\left(\frac{\partial ln(K^0_{MLF})}{\partial P}\right)_T = -\frac{\Delta V^0}{RT} \quad \text{(IV-13)}$$

The variation of water proton relaxation rates with temperature (20°C to 65°C) and pressure (up to ~160 MPa), has been studied at the magnetic field of 9.4 T. Performing a least squares fit of the experimental data (Figure IV-4 and Figure IV-5) using eqs IV-5 to IV-13, one can obtain the reaction enthalpy, entropy and volume values as well as the equilibrium constant (Table IV-1). It has to be noted that in the analysis of variable pressure data, the thermodynamic stability constant at zero pressure has been fixed to the value obtained by variable temperature studies, corrected for its corresponding temperature.
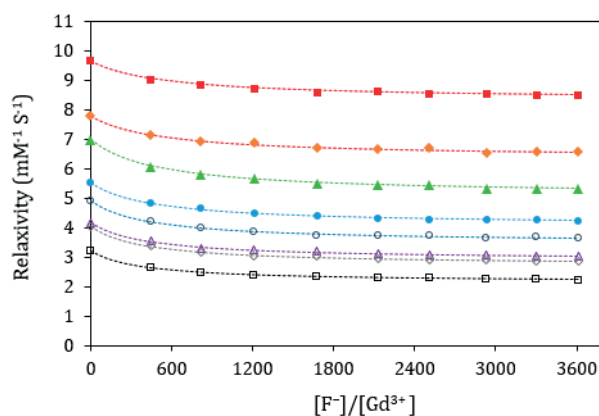
Figure IV-4. Proton relaxivity versus the concentration ratio of $[F^-]/[Gd^{3+}]$ for $\big[Gd(DTTA-Me)(H_2O)_xF_y\big]^z$, $[Gd^{3+}] = 0.12$ mM, $B_0 = 4.7$ T (200 MHz), T = 15°C ($\blacksquare$), 20°C ($\blacklozenge$), 30°C ($\blacktriangle$), 35°C ($\bullet$), 45°C ($\circ$), 50°C ($\triangle$), 55°C ($\lozenge$), 65°C ($\square$), I = 1 M, pH = 7.4. Dashed lines correspond to the best fitting of the experimental data.
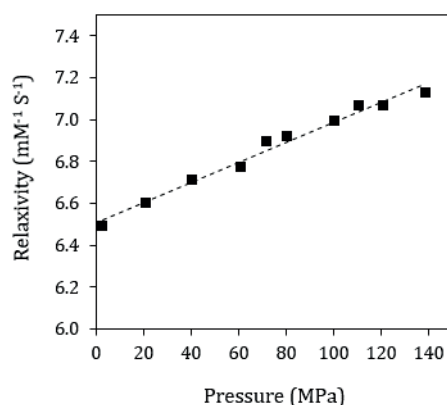
Figure IV-5. Pressure dependence of proton relaxivity for $\big[Gd(DTTA-Me)(H_2O)_xF_y\big]^z$, $[F^-] = 0.20$ M, $[F^-]/[Gd^{3+}] = 28$, $B_0 = 9.4$ T (400 MHz), T = 20°C, pH = 7.4. Dashed lines correspond to the best fitting of the experimental data.

Table IV-1. Stability constant and thermodynamic parameters for the formation of $[Gd(DTTA-Me)(H_2O)F]^{2-}$

$K_{MLF,298}^{I=1}$ (M^{-1})	$K_{MLF,298}^{0}$ (M^{-1})	ΔH^0 (kJ mol^{-1})	ΔS^0 (J K^{-1} mol^{-1})	ΔV^0 (cm^3 mol^{-1})
18.5 ± 0.3	11.6 ± 0.3	+6.3 ± 1.1	+41.5 ± 3.4	+4.5 ± 1.2

DFT calculations were carried out on the $[Gd(DTTA-Me)(H_2O)F]^{2-}.4H_2O$ system to gain insight into the binding of fluoride to the $[Gd(DTTA-Me)(H_2O)_2]^-$ complex. These calculations provided two energy minima that correspond to the replacement of a

coordinated water molecule either in the capping position (O2w) or at the upper square face of the square antiprism (Figure IV-6). The free energy difference of these two forms is only 1.9 kJ mol^{-1}, which suggests that both present significant populations in aqueous solution.
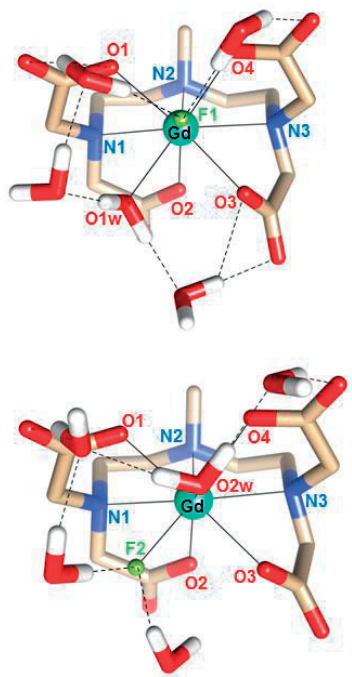
Figure IV-6. Optimised geometries of the $[Gd(DTTA - Me)(H_2O)F]^{2-}. 4H_2O$ complex obtained with DFT calculations. Hydrogen atoms, except those of water molecules, are omitted for simplicity.

IV.2.2 Fluoride complexation and water exchange on [Gd(DTTA-Me)(H₂O)ₓFᵧ]ᶻ

The fluoride complexation and water exchange dynamics on $[\mathrm{Gd(DTTA-Me)(H_2O)_2}]^-$ and $[\mathrm{Gd(DTTA-Me)(H_2O)F}]^{2-}$ is represented in Scheme IV-1. The fluoride complex formation and dissociation can be studied using $^{19}\mathrm{F}$ NMR relaxation and water exchange kinetics can be assessed by $^{17}\mathrm{O}$ NMR. Changing the fluoride to gadolinium ratio will allow to separate the water exchange reactions on $[\mathrm{ML(H_2O)_2}]$ and $[\mathrm{MLF(H_2O)}]$, which are characterised by the rate constants $k_{ex,2}$ and $k_{ex,1}$, respectively. It has to be highlighted that the direct exchange of water molecules between the two complexes was not considered in our treatment.
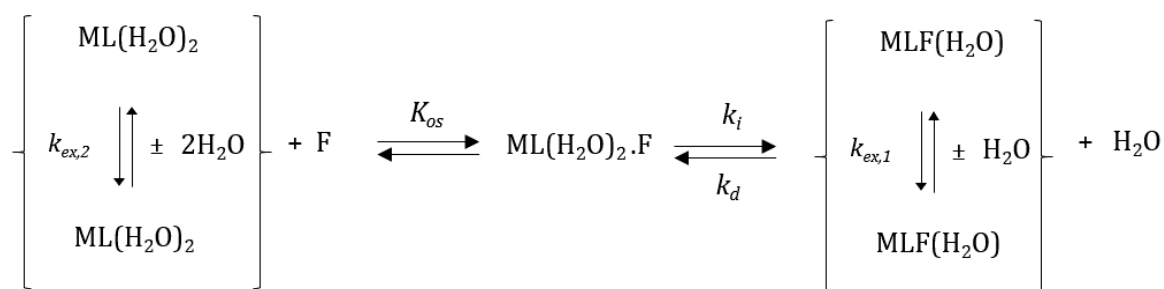
Scheme IV-1. Fluoride complexation and water exchange on Gd³⁺ complexes of $\mathrm{L = DTTA-Me}$.

IV.2.3 Variable temperature ¹⁹F NMR study

Since transverse relaxation of the observed $^{19}\mathrm{F}$ signal of free fluoride increases steadily with temperature (see Table VIII-29), the system is in the slow exchange regime. In this case the transverse relaxation of free fluoride is given by eq IV-14.[20] It has to be highlighted that due to strong interaction with the paramagnetic Gd³⁺ ion, the $^{19}\mathrm{F}$ spin of bound fluoride relaxes very fast and cannot be observed.

$$\frac{1}{T_{2,obs}} = \frac{1}{T_{2,d}} + \frac{1}{\tau} \tag{IV-14}$$

In eq IV-14, $1/T_{2,d}$, the relaxation rate of fluoride in the absence of the paramagnetic species, is small ($\sim$ 0.5 s^{-1} at fluoride concentrations less than 1 M[21]) and can be neglected, and τ is the lifetime of fluoride in the bulk. Thus eq IV-14 can be further simplified to:

$$\frac{1}{T_{2,obs}} = \frac{1}{\tau} = k_{obs} \tag{IV-15}$$

Moreover considering Eigen-Wilkins mechanism for complex formation, one can write:

$$k_{obs} = \frac{K_{os}\, k_i [ML]}{1 + K_{os}[F]} \tag{IV-16}$$

$$k_f = K_{os}\, k_i \tag{IV-17}$$

where k_f is the rate constant of fluoride complex formation and k_i is the interchange rate constant. [ML] is temperature dependent and can be calculated using the thermodynamic parameters in Table IV-1. K_{os} is the equilibrium constant for the formation of the outer sphere complex and can be estimated using the Fuoss-Eigen equation:[22]

$$K_{os} = \frac{4\pi a^3}{3000} N_A \exp\left(\frac{-V}{RT}\right) \tag{IV-18}$$

$$V = \frac{z_1 z_2 e^2}{4\pi a \varepsilon_0} \tag{IV-19}$$

with a representing the minimum distance of approach between complex and ligand in the outer sphere complex, N_A the Avogadro constant and R the gas constant. V is the Coulombic potential energy of the ions and is calculated by eq IV-19 where z_i is the charge number of each species and ε_0 is the vacuum permittivity. Assuming a minimum distance of approach of 4.5 Å, K_{os} will be *ca.* 0.05 M^{-1}. Hence, since $K_{os}[F] \ll 1$, one can write:

$$\frac{1}{T_{2,obs}} = k_{obs} = k_f\, [ML] \tag{IV-20}$$

The teperature dependence of k_f (Figure IV-7) is considered to follow Eyring's equation (eq II-28). Using eqs IV-14 to IV-20, one can calculate k_f and obtain activation parameters (Table IV-2).
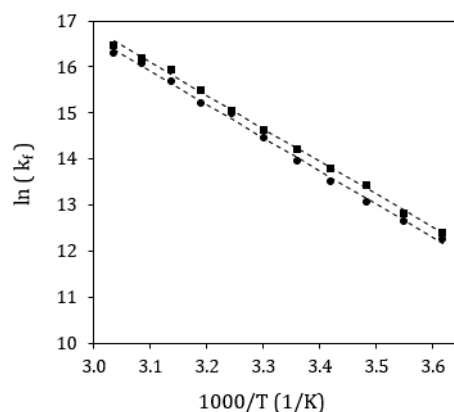
Figure IV-7. Temperature dependence of the formation rate constant k_f for $[Gd(DTTA - Me)(H_2O)_x F_y]^z$, $[F^-] = 0.210$ M ($\bullet$), $[F^-] = 0.313$ M ($\blacksquare$), $[Gd^{3+}] = 1$ mM, $B_0 = 9.4$ T (376.54 MHz). Dashed lines correspond to the best fitting of the experimental data.

Table IV-2. Parameters obtained from fits of ^{19}F NMR data for $[Gd(DTTA - Me)(H_2O)_x F_y]^z$

$[F]_{tot}$	(M)	0.210	0.313
k_f^{298}	(10^6 s^{-1} M^{-1})	1.3 ± 0.2	1.6 ± 0.2
$\Delta H^{\ddagger}$	(kJ mol^{-1})	58 ± 1	57 ± 1
$\Delta S^{\ddagger}$	(J mol^{-1})	$+66$	$+65$

The experimental formation rate constants calculated for the two fluoride concentrations are the same within experimental error. From the values in Table IV-2, we can calculate the interchange rate constant $k_i^{298} = k_f^{298}/K_{OS} \cong 28 \times 10^6$ s^{-1} and the dissociation rate constant $k_d^{298} = k_f^{298}/K_{298}^I \cong 0.08 \times 10^6$ s^{-1}.

IV.2.4 Variable temperature and pressure ^{17}O NMR study

In order to investigate the water exchange rate and mechanism on the mixture of $[Gd(DTTA-Me)(H_2O)_2]^-$ and $[Gd(DTTA-Me)(H_2O)F]^{2-}$, the variable temperature and pressure ^{17}O NMR transverse relaxation enhancements have been studied. The reduced relaxation rates can be calculated from the measured ^{17}O NMR relaxation rates of the paramagnetic solution and of the reference solution, a solution containing a diamagnetic analogue of the complex:

$$\frac{1}{T_{2r}} = \frac{1}{P_{m,tot}} \left(\frac{1}{T_{2,obs}} - \frac{1}{T_{2,d}} \right) \tag{IV-21}$$

where $P_{m,tot}$ is the partial molar fraction of water molecules bound to the metal. It has to be noted that $P_{m,tot}$ only changes if the number of inner sphere water molecules changes, otherwise it does not change with temperature and pressure. Since in the present study both mono- and bis-aqua compounds exist, their contribution to the final concentration of bound water molecules and also to the reduced relaxation rates has to be separated (eqs IV-22 and IV-24). [ML] and [MLF] can be calculated using the thermodynamic stability constant reported in Table IV-1, applying corrections due to temperature and ionic strenght difference.

$$P_{m,tot} = P_{m,ML} + P_{m,MLF} \tag{IV-22}$$

$$P_{m,X} = \frac{q\,[X]}{55.56}, X = ML, MLF \tag{IV-23}$$

$$\frac{1}{T_{2r}} = \frac{1}{P_{m,tot}} \left(\frac{P_{m,ML}}{T_{2r,ML}} + \frac{P_{m,MLF}}{T_{2r,MLF}} \right) \tag{IV-24}$$

$$\frac{1}{T_{2r,X}} = k_{ex,X} \frac{T_{2m,X}^{-2} + k_{ex,X} T_{2m,X}^{-2} + \Delta\omega_{m,X}^2}{\left(k_{ex,X} + T_{2m,X}^{-2} \right)^2 + \Delta\omega_{m,X}^2}, X = ML, MLF \tag{IV-25}$$

The temperature and pressure dependence of water exchange rate constants were calculated using eqs II-28 and II-35. ^{17}O NMR data have been fitted assuming that $1/T_{2m}$ is dominated by scalar relaxation[23], the scalar coupling constant and the electron spin relaxation (τ_v, Δ^2) are assumed to be pressure independent[24] and equal for both $[Gd(DTTA-Me)(H_2O)_2]^-$ and $[Gd(DTTA-Me)(H_2O)F]^{2-}$ complexes. Water

exchange rate constants at zero pressure were fixed to the values obtained from variable temperature studies, corrected for the corresponding temperature. The experimental data and the corresponding fitted curves are presented in Figure IV-8 and Figure IV-9, while the obtained water exchange parameters are compiled in Table IV-3.
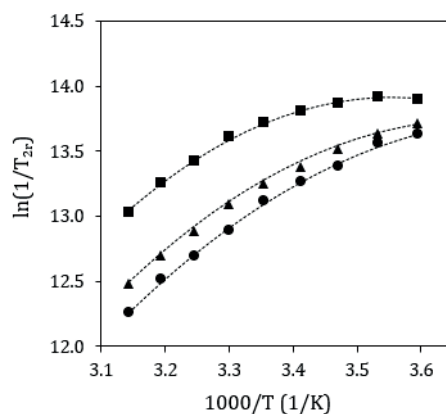
Figure IV-8. Temperature dependence of the reduced transverse ^{17}O relaxation rates, $[F^-] = 0$ M (■), $[F^-] = 0.1$ M (▲), $[F^-] = 0.2$ M (●), $[Gd^{3+}] = 10$ mM, $B_0 = 9.4$ T (400 MHz). The lines show the best simultaneous fits according to all data using the parameters listed in Table IV-3.
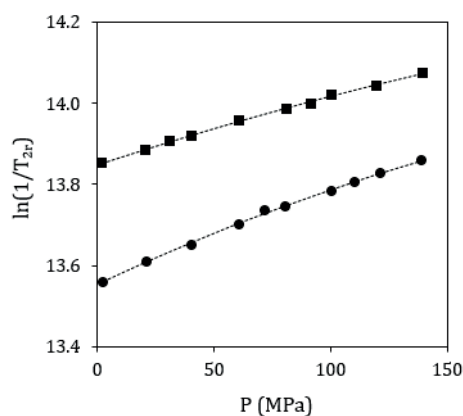
Figure IV-9. Pressure dependence of the reduced transverse ^{17}O relaxation rates, $[F^-] = 0$ M (■), $[F^-] = 0.20$ M (●), $[Gd^{3+}] \sim 10$ mM, T = 295 K, $B_0 = 9.4$ T (400 MHz). Dashed lines correspond to the best fitting of the experimental data

Table IV-3. Activation parameters for the water exchange reaction obtained from variable temperature and pressure ^{17}O NMR data[a]

		$[Gd(DTTA-Me)(H_2O)_2]^-$	$[Gd(DTTA-Me)(H_2O)F]^{2-}$
k_{ex}^{298}	$(10^6\,s^{-1})$	24.6 ± 1.2	177 ± 6
$\Delta H^{\ddagger}$	$(kJ\,mol^{-1})$	50 ± 2	42 ± 2
$\Delta S^{\ddagger}$	$(J\,mol^{-1})$	$+64 \pm 2$	$+53 \pm 2$
$\Delta V^{\ddagger,b}$	$(cm^3\,mol^{-1})$	$+8 \pm 2$	$+15 \pm 4$

[a] for a full list of parameters see Table VIII-33 [b] activation volume determined at 295 K

The water exchange rate constant of the mono fluorinated complex $[Gd(DTTA-Me)(H_2O)F]^{2-}$ $(k_{ex,1}^{298} = 177 \times 10^6\,s^{-1})$ is seven times faster than on the bis-aqua complex without fluoride $(k_{ex,2}^{298} = 24.6 \times 10^6\,s^{-1})$. Previous studies on Gd^{3+} complexes of DTPA[10,23] and DOTA-like ligands[25,26] and their amides demonstrated that the negatively charged species show much higher k_{ex} values than the corresponding electroneutral or positively charged ones.[27] Furthermore, complexes with negatively charged side chains generally have shown faster water exchange rates than their neutral counterparts. The rate constant for water exchange on $[Gd(DTTA-Me)(H_2O)_2]^-$ $(k_{ex,2}^{298} = 24.6 \times 10^6\,s^{-1})$ is close to the interchange rate constant calculated for complex formation with fluoride $(k_i^{298} = 28 \times 10^6\,s^{-1})$. This allows to conclude that the dissociation of a bound water molecule is the rate determining step in the complex formation of $[Gd(DTTA-Me)(H_2O)F]^{2-}$. The number of fluoride dissociation and complexation events $k_d^{298} = 0.08 \times 10^6\,s^{-1}$ is however much lower than that of water exchange either on $[Gd(DTTA-Me)(H_2O)_2]^-$ $(k_{ex,2}^{298} = 24.6 \times 10^6\,s^{-1})$ or on $[Gd(DTTA-Me)(H_2O)F]^{2-}$ $(k_{ex,1}^{298} = 177 \times 10^6\,s^{-1})$.

The positive values of $\Delta S^{\ddagger}$ and $\Delta V^{\ddagger}$ suggest a dissociative activation mode for the exchange of a water molecule on both complexes. The activation volume of $+15\,cm^3\,mol^{-1}$ measured on $[Gd(DTTA-Me)(H_2O)F]^{2-}$ is the most positive value measured so far for water exchange on gadolinium poly(aminocarboxylate) complexes, and approaches the molecular volume estimated for a water molecule at the M06/TZVP level ($17.2\,cm^3\,mol^{-1}$), calculated as the volume inside a contour of 0.001 electrons/Bohr^3 following the suggestion of Bader.[28] Thus, it appears that the negative fluoride ion assists in the dissociation of the water molecule from the inner coordination sphere of Gd^{3+}, so that a

limiting dissociative mechanism **D** can be assigned to that exchange reaction. The activation volume for water exchange on $[Gd(DTTA - Me)(H_2O)_2]^-$ (+7 cm^3 mol^{-1}) is smaller but still clearly positive. Water exchange reactions on other gadolinium poly(aminocarboxylate) complexes have been assigned to proceed via dissociative mechanisms, **D**, on the bases of similar activation volumes.[23]

The DFT calculations performed on $[Gd(DTTA - Me)(H_2O)_2]^-.4H_2O$ and $[Gd(DTTA - Me)(H_2O)F]^{2-}.4H_2O$ and wave function analysis provide some insight into the nature of the Gd-O$_{water}$ and Gd-F bonds and the kinetics of water and fluoride exchange. Indeed, the nature of the bonding between the Gd^{3+} ion and the water molecule can be characterised by the values of electron density at the bond critical point, ρ_{BCP}, and its Laplacian ($\nabla^2\rho_{BCP}$).[2] Generally ρ_{BCP} values above 0.20 a. u. and negative $\nabla^2\rho_{BCP}$ values are characteristic of covalent bonds, while ρ_{BCP} < 0.10 a. u. and positive $\nabla^2\rho_{BCP}$ values are indicative of ionic bonds.[29] The data shown in Table IV-4 indicate that the Gd-O$_{water}$ and Gd-F bonds are characterised by small ρ_{BCP} values (ca. 0.03-0.05 a.u.) with the Laplacian being small and positive. Thus, this points to a predominantly electrostatic nature of the Gd-O$_{water}$ and Gd-F interactions, as would be expected. Our DFT calculations show that F$^-$ binding at either the capping position or the upper square face of the coordination polyhedron provokes a significant lengthening of the Gd-O$_{water}$ distance of the remaining coordinated water molecule. This effect is accompanied by a decrease of the ρ_{BCP} values and the electron localisation function (ELF) at the concerned bond critical points (Table IV-4). Since lower values of ρ_{BCP} and ELF indicate weaker bonds,[30,31] these results indicate that F$^-$ binding weakens the Gd-O$_{water}$ bond involving the remaining inner-sphere water molecule. Water exchange proceeds through a dissociative mechanism that requires the rupture of the Gd-O$_{water}$ bond to reach an eight-coordinated transition state, and therefore weaker Ln-Ow bonds are expected to provide faster water exchange rates.

Table IV-4. Calculated Gd-Ow and Gd-F bond distances (Å), electron density (ρ, a.u.), electron localisation function (ELF) and Laplacian of the electron density ($\nabla^2\rho_{BCP}$) at the bond critical points (BCP) of $[Gd(DTTA - Me)(H_2O)_2]^-\cdot 4H_2O$ and $[Gd(DTTA - Me)(H_2O)F]^{2-}\cdot 4H_2O$

$[Gd(DTTA - Me)(H_2O)_2]^-$	Bond	ρ_{BCP}	ELF	$\nabla^2\rho_{BCP}$
$Gd - O1w$	2.484	0.0379	0.0866	0.168
$Gd - O2w$	2.547	0.0331	0.0782	0.144
$[Gd(DTTA - Me)(H_2O)F]^{2-}$ [a]				
$Gd - O1w$	2.504	0.0361	0.0819	0.161
$Gd - F1$	2.325	0.0482	0.0861	0.250
$[Gd(DTTA - Me)(H_2O)F]^{2-}$ [b]				
$Gd - O2w$	2.588	0.0302	0.0740	0.131
$Gd - F2$	2.297	0.0516	0.0903	0.270

[a] fluoride in capping position [b] water molecule in capping position

IV.3 Conclusions

The ternary complex formation of $[Gd(DTTA - Me)(H_2O)_2]^-$ with fluoride ions has been studied with multinuclear NMR spectroscopy and DFT calculations. From ^{1}H NMR measurements, it was concluded that the fluoride addition forms a complex where only one inner-sphere water molecule is displaced by a fluoride ion. Fluoride addition causes a decrease in relaxivity of the complex, associated with the drop in hydration number. The water exchange rate constant of 177×10^6 s^{-1} at 298 K measured by variable temperature NMR on $[Gd(DTTA - Me)(H_2O)F]^{2-}$ is more than 7 times faster than that on $[Gd(DTTA - Me)(H_2O)_2]^-$ ($k_{ex,2}^{298} = 24.6 \times 10^6$ s[-1]). Both exchange reactions follow a dissociative mechanism with a very positive activation volume of $\Delta V^{\ddagger} = + 15$ cm[3] mol^{-1} for water exchange on $[Gd(DTTA - Me)(H_2O)F]^{2-}$. Water exchange on both compounds is faster than formation of the fluoride complex. DFT calculations revealed that F[-] can replace any of the two bound water molecules. The binding of the negatively charged fluoride weakens the Gd-O$_{water}$ bond of the remaining water molecules. The dissociative character of the reaction is fortified and the departure of the coordinated water molecule facilitated.

IV.4 Experimental and computational procedures

IV.4.1 Materials

The ligand, $DTTA - Me^{4-}$, was provided by EPFL through the synthetic platform. The synthesis of the ligand has been described in a previous communication.[7] [17]O-enriched water (19.2%) was purchased from D-Chem LTD. Other reagents were obtained from Sigma-Aldrich Chemical Co. commercial sources and used without further purification.

IV.4.2 Preparation of [Gd(DTTA-Me)(H₂O)₂]⁻ samples

The solid salt $GdCl_3 \cdot xH_2O$ was dissolved in water to prepare the Gd^{3+} stock solution. The exact ion concentration was measured by complexometric titration using a Na_2H_2EDTA solution in an urotropine buffer at pH 5.8 and xylenol orange as the indicator. The ligand $DTTA - Me^{4-}$ stock solution was prepared in water and its exact concentration was determined by back titration of the Gd^{3+} excess with a Na_2H_2EDTA solution. Tris buffer (2 M) at pH 7.4 and NaCl (5 M) solutions were prepared dissolving the solid salt in water. The complex $[Gd(DTTA - Me)(H_2O)_2]^-$ was prepared by mixing appropriate amounts of $GdCl_3$, ligand, Tris buffer and NaCl solutions to have ligand to gadolinium concentration ratios $[DTTA - Me^{4-}]/[Gd^{3+}]$ ranging from 1 to 20 while keeping the final concentration of Gd^{3+}, Tris buffer and ionic strength constant at 160 µM, 0.5 M and 1 M, respectively. The absence of free gadolinium was checked with xylenol orange test.[32]

IV.4.3 Equilibrium constants measurement by a variable temperature ¹H NMR study

$[Gd(DTTA - Me)(H_2O)_xF_y]^z$ samples were prepared by mixing $[Gd(DTTA - Me)(H_2O)_2]^-$, $[DTTA - Me^{4-}]/[Gd^{3+}] = 20$, and NaF solutions (0.9 M) with an increasing concentration ratio of $[F^-]/[Gd^{3+}]$ from 0 to ~ 4000 maintaining the final concentration of Gd^{3+}, Tris buffer and ionic strength constant at 120 µM , 0.5 M and 1 M, respectively. The solutions were placed into 5 millimeter NMR tubes and ¹H NMR

longitudinal relaxation rates $(1/T_1)$ were measured on a Bruker Minispec at the proton Larmor frequency of 30 MHz (0.71 T) at 25°C and 37°C and on a Bruker Avance-200 (4.7 T, 200 MHz) spectrometer in a temperature range from 15°C to 65°C. The diamagnetic contribution to the ^{1}H longitudinal relaxation rates were 0.42 s^{-1} (25°C) and 0.33 s^{-1} (37°C) as measured on the Bruker Minispec.

IV.4.4 Equilibrium constants measurement by a variable pressure ^{1}H NMR study

$[\text{Gd(DTTA} - \text{Me)(H}_2\text{O)}_x\text{F}_y]^z$ samples were prepared by mixing $[\text{Gd(DTTA} - \text{Me)(H}_2\text{O)}_2]^-$, $[\text{DTTA} - \text{Me}^{4-}]/[\text{Gd}^{3+}] = 20$, and NaF solutions (0.9 M) with different $[\text{F}^-]/[\text{Gd}^{3+}]$ concentration ratios of 0 and 20 maintaining the final concentration of Gd^{3+}, Tris buffer and ionic strength constant at 10 mM, 0.5 M and 1 M, respectively. The solutions were placed in a 5 millimeter NMR tube and closed with a movable MACOR piston. ^{1}H NMR longitudinal relaxation rates were measured up to a pressure of 160 MPa at 22°C on a Bruker Avance-II 400 (9.4 T) spectrometer equipped with a homebuilt high-pressure probe.[33,34] The temperature was measured with a built-in Pt resistor. The diamagnetic contribution to the ^{1}H longitudinal relaxation rates were ~ 0.5 s^{-1}.

IV.4.5 Fluoride complexation on DTTA-Me complexes of Gd^{3+}·by ^{19}F NMR

$[\text{Gd(DTTA} - \text{Me)(H}_2\text{O)}_x\text{F}_y]^z$ samples were prepared as previously described keeping the $[\text{DTTA} - \text{Me}^{4-}]/[\text{Gd}^{3+}]$ concentration ratio of 20 constant while changing the $[\text{F}^-]/[\text{Gd}^{3+}]$ concentration ratios to 200 and 300 having a final Gd^{3+} concentration of 1 mm. ^{19}F NMR experiments were carried out on a Bruker Avance-II 400 spectrometer, where the ^{19}F resonance frequency is 376.48 MHz. The transverse relaxation rates $(1/T_2)$ were obtained with the Carr-Purcell-Meiboom-Gill spin-echo technique.[35]

IV.4.6 Variable temperature and pressure ^{17}O NMR

$[\text{Gd(DTTA} - \text{Me)(H}_2\text{O)}_x\text{F}_y]^z$ samples with different $[\text{F}^-]/[\text{Gd}^{3+}]$ concentration ratios of 0, 10, 20 were prepared, as previously described $([\text{DTTA} - \text{Me}^{4-}]/[\text{Gd}^{3+}] = 20)$,

having final concentrations of Gd^{3+}, Tris buffer and ionic strength constant at 10 mm , 0.5 M and 1 M, respectively. ^{17}O enriched water was added to have solutions with ~ 2% ^{17}O enrichment. The final concentration of Gd^{3+} was measured by bulk magnetic susceptibility (BMS)[36] at 25°C on a Bruker DRX-400 (9.4 T, 400 MHz) spectrometer. For variable temperature measurements, in order to eliminate susceptibility corrections to the chemical shift,[37] samples were sealed in glass spheres fitting into 10 millimeter NMR tubes. Measurements were performed on a Bruker Avance-II 400 (9.4 T, 54.2 MHz) spectrometer using a BVT-3000 temperature control unit to stabilise the temperature. For variable pressure measurements, since the high pressure probe does not allow the use of spherical samples, the solution was placed inside a 5 millimeter NMR tube closed with a movable MACOR piston.[33,38] Variable pressure ^{17}O NMR spectra were recorded up to a pressure of 160 MPa at 22°C on a Bruker Avance-II 400 (9.4T, 54.2 MHz) spectrometer equipped with a homebuilt high-pressure probe.[34] The temperature was measured with a built-in Pt resistor. In all cases the transverse relaxation rates $(1/T_2)$ were obtained using the Carr-Purcell-Meiboom-Gill spin-echo technique.[35] The diamagnetic contributions to the ^{17}O NMR relaxation rates were determined with reference samples containing comparable concentrations of diamagnetic components: NaF, NaCl, and Tris buffer. For all ^{17}O NMR measurements, the 90° pulse lengths have been determined at different temperatures and pressures for each sample.

IV.5 Data fitting

Least squares fitting of the ^1H NMR, ^{17}O NMR and ^{19}F NMR data were performed using the Visualiseur/Optimiseur 3.7.0 program running on a Matlab® 8 platform.

IV.6 Computational Methods

DFT calculations have been performed by Carlos Platas-Iglesias at the Universidade da Coruña.

IV.7 References

(1) Liu, T.; Nonat, A.; Beyler, M.; Regueiro-Figueroa, M.; Nchimi Nono, K.; Jeannin, O.; Camerel, F.; Debaene, F.; Cianférani-Sanglier, S.; Tripier, R.; Platas-Iglesias, C.; Charbonnière, L. J. *Angew. Chem. Int. Ed.* **2014**, *53*, 7259.

(2) Bader, R. F. W. In *Atoms in Molecules: A Quantum Theory*; Oxford University Press: Oxford, 1990.

(3) Livramento, J. B.; Sour, A.; Borel, A.; Merbach, A. E.; Tóth, É. *Chem. Eur. J.* **2006**, *12*, 989.

(4) Livramento, J. B.; Toth, E.; Sour, A.; Borel, A.; Merbach, A. E.; Ruloff, R. *Angew. Chem. Int. Ed. Engl.* **2005**, *44*, 1480.

(5) Costa, J.; Tóth, É.; Helm, L.; Merbach, A. E. *Inorg. Chem.* **2005**, *44*, 4747.

(6) Costa, J.; Ruloff, R.; Burai, L.; Helm, L.; Merbach, A. E. *J. Am. Chem. Soc.* **2005**, *127*, 5147.

(7) Moriggi, L.; Cannizzo, C.; Prestinari, C.; Berrière, F.; Helm, L. *Inorg. Chem.* **2008**, *47*, 8357.

(8) Menon, M. P.; James, J.; Hill, T. L. *Int. J. Radiat. Appl. Instrum. Appl. Radiat. Isot.* **1988**, *39*, 949.

(9) Maeder, M.; Neuhold, Y.-M. In *Practical Data Analysis in Chemistry* ; Elsevier: 2007.

(10) Caravan, P.; Ellison, J. J.; McMurry, T. J.; Lauffer, R. B. *Chem. Rev.* **1999**, *99*, 2293.

(11) Aime, S.; Fasano, M.; Terreno, E. *Chem. Soc. Rev.* **1998**, *27*, 19.

(12) Chang, C. A.; Brittain, H. G.; Telser, J.; Tweedle, M. F. *Inorg. Chem.* **1990**, *29*, 4468.

(13) Dickins, R. S.; Aime, S.; Batsanov, A. S.; Beeby, A.; Botta, M.; Bruce, J. I.; Howard, J. A. K.; Love, C. S.; Parker, D.; Peacock, R. D.; Puschmann, H. *J. Am. Chem. Soc.* **2002**, *124*, 12697.

(14) Terreno, E.; Botta, M.; Boniforte, P.; Bracco, C.; Milone, L.; Mondino, B.; Uggeri, F.; Aime, S. *Chem. Eur. J.* **2005**, *11*, 5531.

(15) Botta, M.; Aime, S.; Barge, A.; Bobba, G.; Dickins, R. S.; Parker, D.; Terreno, E. *Chem. Eur. J.* **2003**, *9*, 2102.

(16) Bruce, J. I.; Dickins, R. S.; Govenlock, L. J.; Gunnlaugsson, T.; Lopinski, S.; Lowe, M. P.; Parker, D.; Peacock, R. D.; Perry, J. J. B.; Aime, S.; Botta, M. *J. Am. Chem. Soc.* **2000**, *122*, 9674.

(17) Esteban-Gómez, D.; de Blas, A.; Rodríguez-Blas, T.; Helm, L.; Platas-Iglesias, C. *ChemPhysChem.* **2012**, *13*, 3640.

(18) Regueiro-Figueroa, M.; Platas-Iglesias, C. *J. Phys. Chem. A* **2015**, *119*, 6436.

(19) Davies, C. W. *J. Chem. Soc.* **1938**, 2093.

(20) McLaughlin, A. C.; Leigh Jr, J. S. *J. Magn. Reson.* **1973**, *9*, 296.

(21) Hertz, H. G.; Keller, G.; Versmold, H. *Ber. Bunsenges. Phys. Chem.* **1969**, *73*, 549.

(22) Fuoss, R. M. *J. Am. Chem. Soc.* **1958**, *80*, 5059.

(23) Tóth, é.; Helm, L.; Merbach, A. In *The Chemistry of Contrast Agents in Medical Magnetic Resonance Imaging*; John Wiley & Sons, Ltd: Chichester, U.K., 2013.

(24) Cossy, C.; Helm, L.; Merbach, A. E. *Inorg. Chem.* **1989**, *28*, 2699.

(25) Zhang, S.; Jiang, X.; Sherry, A. D. *Helv. Chim. Acta* **2005**, *88*, 923.

(26) Ratnakar, S. J.; Woods, M.; Lubag, A. J. M.; Kovács, Z.; Sherry, A. D. *J. Am. Chem. Soc.* **2008**, *130*, 6.

(27) Hermann, P.; Kotek, J.; Kubicek, V.; Lukes, I. *Dalton Trans.* **2008**, *0*, 3027.

(28)   Bader, R. F. W.; Carroll, M. T.; Cheeseman, J. R.; Chang, C. *J. Am. Chem. Soc.* **1987**, *109*, 7968.
(29)   Kerridge, A. *RSC Advances* **2014**, *4*, 12078.
(30)   Zhang, J.; Heinz, N.; Dolg, M. *Inorg. Chem.* **2014**, *53*, 7700.
(31)   Zhang, J.; Dolg, M. *J. Phys. Chem. A* **2015**, *119*, 774.
(32)   Brunisholz, G.; Randin, M. *Helv. Chim. Acta.* **1959**, *42*, 1927.
(33)   Frey, U.; Helm, L.; Merbach, A. E. *High Press. Res.* **1990**, *2*, 237.
(34)   Cusanelli, A.; Nicula-Dadci, L.; Frey, U.; Merbach, A. E. *Inorg. Chem.* **1997**, *36*, 2211.
(35)   Meiboom, S.; Gill, D. *Rev. Sci. Instrum.* **1958**, *29*, 688.
(36)   Corsi, D. M.; Platas-Iglesias, C.; Bekkum, H. v.; Peters, J. A. *Magn. Reson. Chem.* **2001**, *39*, 723.
(37)   Hugi, A. D.; Helm, L.; Merbach, A. E. *Helv. Chim. Acta* **1985**, *68*, 508.
(38)   Helm, L.; Merbach, A. E. *J. Chem. Soc., Dalton Trans.* **2002**, 633.

Chapter V

Evaluation of water exchange kinetics on $\left[\text{Ln(AAZTAPh} - \text{NO}_2\text{)(H}_2\text{O)}_q\right]^{-}$ complexes using proton NMR
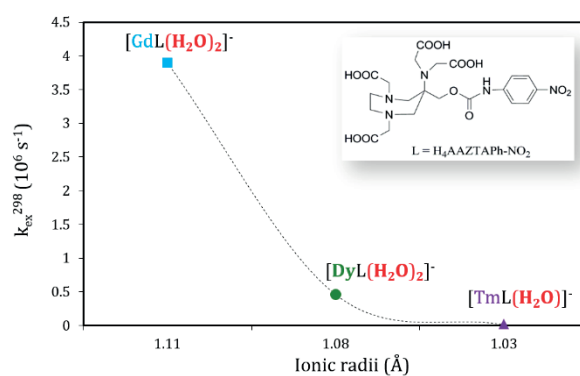
V.1 Introduction

The heptadentate polyaminocarboxylate ligand AAZTA (AAZTA = 6-amino-6-methylperhydro-1,4-diazepine tetraacetic acid) was studied extensively as a potential MRI probe. The Gd^{3+} complex of AAZTA, having two inner-sphere water molecules, has shown excellent relaxation enhancement properties with high thermodynamic stability in aqueous solution and a nearly complete inertness toward the influence of bidentate endogenous anions (r_1 = 7.1 mM^{-1} s^{-1} at 20 MHz and 298 K; τ_m = 90 ns).[1,2] In the present study, the water exchange properties of lanthanide complexes of an AAZTA-derivative, $AAZTAPh-NO_2$, (Scheme V-1) $\left[Ln(AAZTAPh-NO_2)(H_2O)_q\right]^-$, (Ln = Gd^{3+}, Dy^{3+} and Tm^{3+}) have been determined. Possible variation of the number of coordinated water molecules with different lanthanide complexes of $AAZTAPh-NO_2$ is also discussed. Water exchange rate and its activation parameters can be extracted experimentally by either measuring the temperature dependence of ^{17}O NMR or ^1H NMR relaxation rates of bulk water induced by the presence of a paramagnetic solution. The advantages of ^{17}O NMR measurements is that the outer-sphere contribution to both transverse and longitudinal ^{17}O relaxation rates can be neglected.[3] However, this technique requires relatively high concentrations of Ln^{3+} (> 5 mM),[4] sometimes much higher than the limits of the solubility of complexes. The solubility of the lanthanide complexes of $AAZTAPh-NO_2$ (L$_1$) in water at 25°C is at most 6 mM due to the nitrophenyl moiety, which greatly reduces the solubility. Such low values preclude accurate ^{17}O NMR measurements for lanthanides other than Gd^{3+}. In this regard, the water exchange rates can be extracted by measuring the temperature dependence of the ^1H NMR transverse relaxation rates of bulk water. It has to be noted that the measurement has to be done at physiological pH, where the proton exchange rate is assumed to be equal to the water exchange rate since by increasing the acidity or basicity of the solution, the proton exchange may become faster than the water exchange due to acid- or base-catalysed pathway.[5] Moreover, the outer-sphere relaxation contribution cannot be neglected while analyzing the ^1H NMR data.

In order to assess the accuracy of the water exchange values obtained by proton NMR, water exchange rates of dysprosium(III) complexes of ligands DTTA $-$ Me (L$_2$) and DO3A (L$_3$) (Scheme V-1) have been studied. The results were compared with the values obtained by ^{17}O NMR measurements as reported in chapter III.[6] Moreover, dysprosium(III) complexes of the three ligands (L$_{1-3}$) are compared and discussed as potential negative contrast agents for very high field MRI.

H$_4$AAZTAPh-NO$_2$ (L$_1$)

H$_4$DTTA-Me (L$_2$)
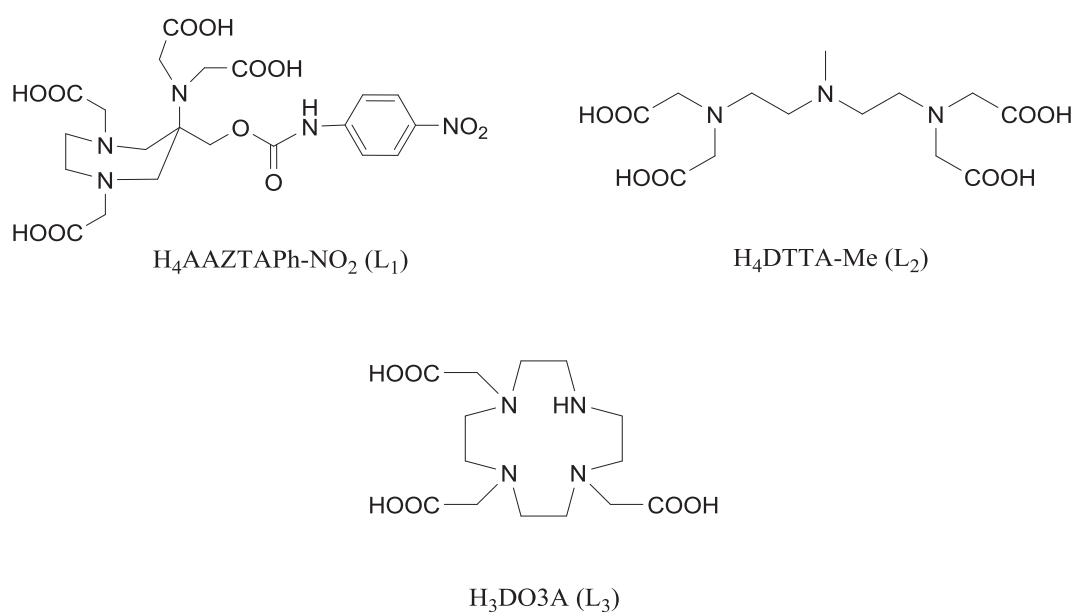
H$_3$DO3A (L$_3$)

Scheme V-1. Schematic drawing of the ligands H$_4$AAZTAPh $-$ NO$_2$, H$_4$DTTA $-$ Me and H$_3$DO3A.

Furthermore, variable pressure measurements have been carried out and used to assign the reaction mechanisms by the determination of the activation volume, $\Delta V^{\ddagger}$, as a direct measure of the degree of associativity or dissociativity at the transition state. Again, due to the low solubility of the compounds, proton NMR method is used. The results were compared with the values obtained by ^{17}O NMR when applicable.

V.2 Data treatment

V.2.1 ^{1}H NMR relaxation

The measured transverse proton relaxation rate is calculated using eq II-1 and II-2. The inner-sphere transverse proton relaxation rate of the bound water is considered to be the sum of dipolar (II-10), scalar (eq II-11), and Curie relaxation (II-12) contributions. For all Ln^{3+} except Gd^{3+}, a single electronic relaxation time T_e may be introduced as the values of T_{2e} are reported[7] to be near to those of T_{1e} and very small. Moreover, since $T_e(\sim 10^{-13} \text{ s}) \ll \tau_R(\sim 10^{-10} \text{ s})$, τ_c in eq II-10 are dominated by the values of T_e. In the case of Gd^{3+} the electron spin relaxation rates were calculated by the Bloembergen-Morgan theory of paramagnetic electron spin relaxation (eqs II-17 and II-18).[8,9] At high magnetic field (7 T and above), the Curie spin relaxation becomes the dominant contribution to the water ^{1}H relaxation and the scalar contribution can be neglected.

V.3 Results and discussions

V.3.1 Water exchange on $[DyL_{2,3}(H_2O)_2]^x$ by ^{1}H NMR relaxation

To verify that water exchange on polyaminocarboxylate complexes of lanthanide(III) ions can be studied quantitatively by ^{1}H NMR relaxation, proton transverse relaxation rates and chemical shifts of $[Dy(DTTA-Me)(H_2O)_2]^-$ and $[Dy(DO3A)(H_2O)_2]$ were measured. Experimental data has been fitted using the full Swift and Connick equation (eq II-4) for inner-sphere relaxation contribution. The following parameters have been fixed: $q = 2$, $a_{LnH} = 3.6 \times 10^{-10}$ m and $D_{LnH}^{298} = 25 \times 10^{-10}$ m^{2}s^{-1}. The diffusion constant is assumed to obey Arrhenius law. The electronic relaxation time (T_e) and rotational correlation time ($\tau_{R,H}$), were fixed to the values obtained from ^{17}O NMR measurements reported in Table III-1 and Table III-2.[6] Moreover, since the C_{OS}, indicating the outer-sphere contribution to the chemical shift is ill defined, we have fitted the data two times, fixing C_{OS} to the two limiting values of 0 and 0.25. In this regard, the errors reported in Table V-1 represent the effect of C_{OS} variation on the water exchange parameters. The experimental and calculated results are shown in Figure V-1 and Figure V-2 and the corresponding parameters are given in Table V-1.
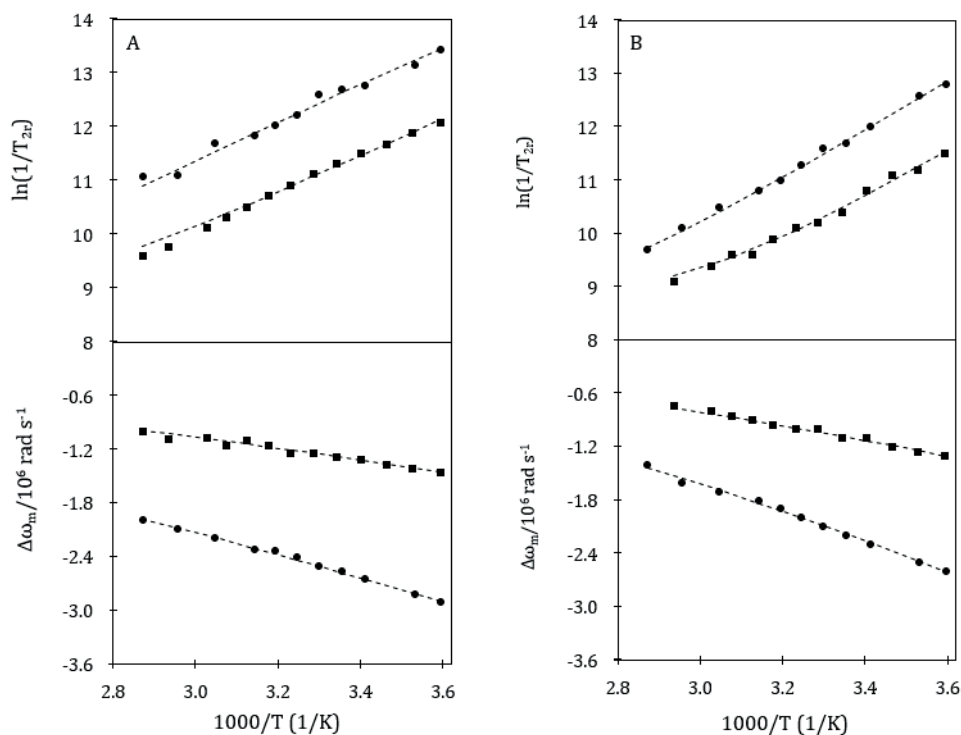
Figure V-1. ^{1}H NMR temperature dependence of $\ln(1/T_{2r})$ of $[Dy(DO3A)(H_2O)_2]$ (A) and $[Dy(DTTA-Me)(H_2O)_2]^-$ (B), $[Ln^{3+}] \sim 100$ mM, $B_0 = 9.4$ T (■) and 18.8 T (●), pH = 5.7. Dashed lines correspond to the best fitting of the experimental data.
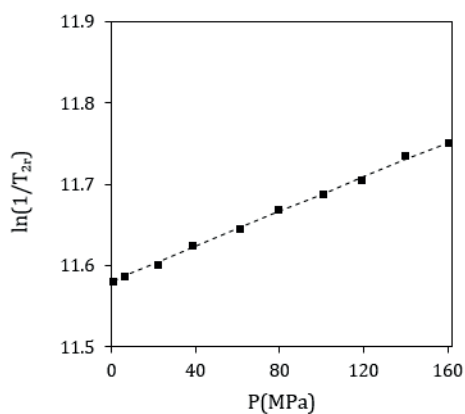
Figure V-2. ^{1}H NMR pressure dependence of $\ln(1/T_{2r})$ of $[Dy(DO3A)(H_2O)_2]$, $[Dy^{3+}] = 86.32$ mM, $B_0 = 9.4$ T, T = 20°C, pH = 5.7. Dashed lines correspond to the best fitting of the experimental data.

Table V-1. Water exchange properties[a] of $\left[Dy(L_{2,3})(H_2O)_2\right]^x$ obtained by ^{1}H and ^{17}O NMR

		[Dy(DO3A)(H₂O)₂]		[Dy(DTTA − Me)(H₂O)₂]⁻	
		[17]O[b]	[1]H	[17]O[b]	[1]H
k_{ex}^{298}	(10^6 s⁻¹)	16.6 ± 0.3	19 ± 4	40.6 ± 0.9	45 ± 10
$\Delta H^{\ddagger}$	(kJ mol⁻¹)	29 ± 1	20 ± 1	36 ± 1	29 ± 1
$\Delta S^{\ddagger}$	(J mol⁻¹)	-9 ± 3	-38 ± 2	$+21 \pm 2$	0 ± 2
$\Delta V^{\ddagger}$	(cm³mol⁻¹)	$- 0.5 \pm 0.3$	-0.2 ± 0.1[c]	$+1.8 \pm 0.2$	-

a) for full list of parameters see Table VIII-37, b) from Table III-1 and Table III-2, c) no outer-sphere contribution for chemical shift is considered

It is apparent from Figure V-1 that both $\left[DyL_{2,3}(H_2O)_2\right]^x$ compounds are in the fast exchange region as defined by $k_{ex} \gg 1/T_{2m}$, $\Delta\omega_m$ over the whole temperature range studied. The obtained exchange rate constants and activation parameters including $\Delta V^{\ddagger}$ are close to the values previously reported from ^{17}O NMR measurements (Table III-1 and Table III-2),[6] supporting the hypothesis that reliable k_{ex} values can be obtained by proton NMR measurements. It has to be noted that the outer-sphere contribution to the total proton relaxation rates goes up to 3% and 9% at 18.8 T for Dy^{3+} complexes of DO3A and DTTA − Me, respectively. Although ^{1}H NMR measurements provide reliable results, due to uncertainties in outer-sphere contributions to the chemical shifts, ^{17}O NMR measurements should be considered as the first choice for the assessment of water exchange rate constants if the solubility limits of the samples permit.

V.3.2 Inner-sphere water molecules on [Ln(AAZTAPh-NO₂)(H₂O)q]⁻

The Gd^{3+} complex of $AAZTAPh − NO_2$ was considered to have two water molecules in the first coordination sphere, as found for the parent Gd − AAZTA complex.[1] However, the number of water molecules coordinated to the other lanthanide complexes of $AAZTAPh − NO_2$ can possibly change when moving from Gd^{3+} to Tm^{3+}. The hydration state of lanthanide chelates can be assessed by different techniques such as luminescence lifetime measurements for Eu^{3+} and Tb^{3+} chelates or analysis of the ^{17}O NMR lanthanide chemical shifts data.[10] As mentioned before, the latter cannot be used in this study due to low concentrations of the chelates. However, since inner-sphere proton relaxivity is linearly proportional to the number of coordinated water molecules, ^{1}H nuclear magnetic relaxation dispersion (NMRD) profiles can be used for the assessment of hydration

number variation. In this regard, longitudinal water proton relaxation rate measurements were carried out for both Dy^{3+} and Tm^{3+} complexes. The results are compared with the previously reported NMRD profiles[6] for the $q = 2$ chelates $[LnDO3A(H_2O)_2]$ and $[Ln(DTTA - Me)(H_2O)_2]^-$, $Ln = Dy^{3+}$, Tm^{3+} (Figure V-3).
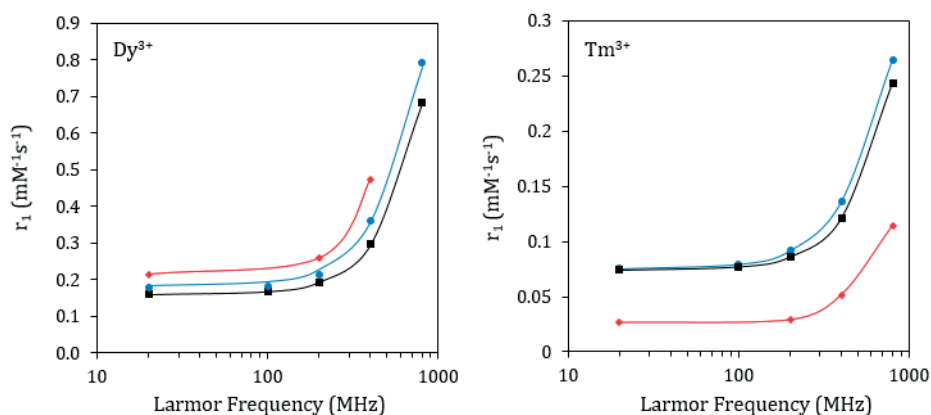
Figure V-3. ^{1}H NMRD profiles of $[Ln(AAZTAPh - NO_2)(H_2O)_q]^-$ (♦), $[Ln^{3+}] \sim 5$ mM and of $[Ln(DO3A)(H_2O)_2]$ (●) and $[Ln(DTTA - Me)(H_2O)_2]^-$ (■), $[Ln^{3+}] \sim 100$ mM reported in chapter III, $Ln = Dy^{3+}$ and Tm^{3+}, $T = 25°C$.

As shown in Figure V-3, the decrease in the relaxivity of $[Tm(AAZTAPh - NO_2)(H_2O)_q]^-$ compared to the other $[TmL_{2,3}(H_2O)_2]^x$ complexes indicates a change in the number q of inner-sphere water molecules. However, the relaxivity of $[Dy(AAZTAPh - NO_2)(H_2O)_q]^-$ is in good agreement with those observed previously for $[DyL_{2,3}(H_2O)_2]^x$ complexes. In this regard, a hydration number of 2 and 1 for dysprosium(III) and thulium(III) complexes of $AAZTAPh - NO_2$, respectively, was assumed for the further studies.

V.3.3 Water exchange on [Ln(AAZTAPh-NO₂)(H₂O)$_q$]⁻

Water exchange on $\left[\text{Ln(AAZTAPh} - \text{NO}_2)(\text{H}_2\text{O})_q\right]^-$ has been studied by ^{1}H NMR relaxation for Ln = Gd^{3+}, Dy^{3+} and Tm^{3+}. Due to the low lanthanide concentration ($\sim$ 5 mM), very small chemical shift differences $\left(\Delta\omega_p/2\pi < 40 \text{ Hz}\right)$ were observed for Dy^{3+} and Tm^{3+} chelates. However, as mentioned above, in the slow exchange regime, the inner-sphere transverse relaxation rate will be independent of $\Delta\omega_m$ and no chemical shift data will be necessary for the assessment of the water exchange rate constants. In the case of $[\text{Gd(AAZTAPh} - \text{NO}_2)(\text{H}_2\text{O})_2]^-$, since a concentration of $\sim$ 5 mM is sufficient for accurate ^{17}O NMR measurements, variable temperature and pressure ^{17}O NMR relaxation rates and chemical shift measurements were performed. Hence, a simultaneous fit of ^{17}O and ^{1}H NMR relaxation rates and chemical shifts were performed to assess the water exchange kinetic parameters. Again, the following parameters were fixed: $a_{\text{LnH}} = 3.6 \times 10^{-10}$ m, $D_{\text{LnH}}^{298} = 25 \times 10^{-10}$ m^{2}s^{-1} and the diffusion constant was assumed to obey Arrhenius law. $\tau_{R,O}$ was calculated from the ^{17}O NMR longitudinal relaxation rates as the quadrupolar contribution to the longitudinal relaxation is dominant. $\tau_{R,H}$ was assumed to be equal to $\tau_{R,O}$. When Ln = Dy^{3+} and Tm^{3+}, since $\tau_m\Delta\omega_m^2 \gg 1/T_{2,m}$ the simplified Swift and Connick equation (eq II-46) was used, hence no further information on rotational correlation time was needed. Moreover, chemical shift at zero pressure $(\Delta\omega_m^0)_T$ in eq II-36, was fixed to the value obtained from the fit of ^{1}H NMR variable temperature transverse relaxation rates. The experimental data and calculated curves are shown in Figure V-4 to Figure V-7 and the corresponding fitted parameters are given in Table V-2.
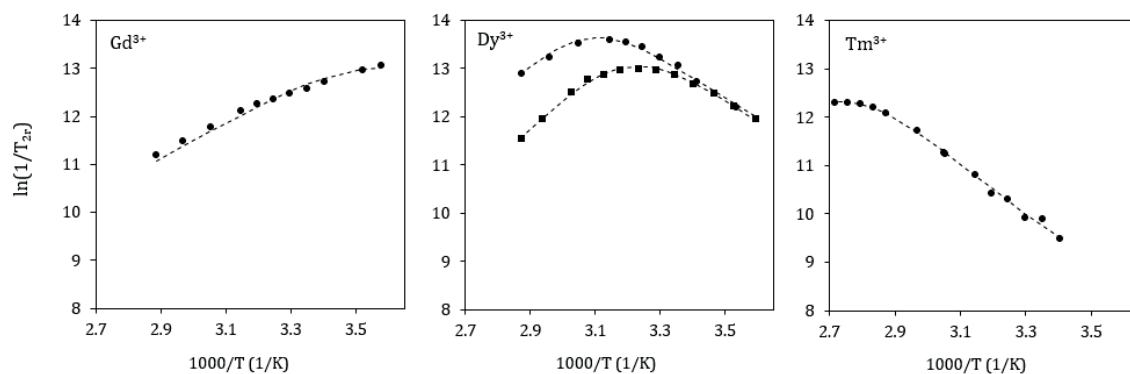
Figure V-4. ^{1}H NMR temperature dependence of $\ln(1/T_{2r})$ of $\left[\text{Ln}(\text{AAZTAPh} - \text{NO}_2)(\text{H}_2\text{O})_q\right]^-$, Ln = Gd^{3+}, Dy^{3+} and Tm^{3+}, $[\text{Ln}^{3+}] \sim 5$ mM, $B_0 = 9.4$ T (■) and 18.8 T (●), pH = 5.7. Dashed lines correspond to the best fitting of the experimental data.
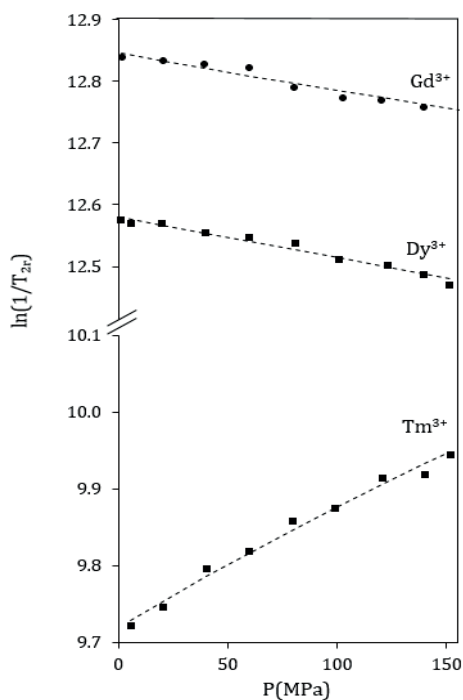
Figure V-5. ^{1}H NMR pressure dependence of $\ln(1/T_{2r})$ of $\left[\text{Ln}(\text{AAZTAPh} - \text{NO}_2)(\text{H}_2\text{O})_2\right]^-$, Ln = Gd^{3+}, Dy^{3+} and Tm^{3+}, $B_0 = 9.4$ T, T = 20°C, pH = 5.7. Dashed lines correspond to the best fitting of the experimental data.
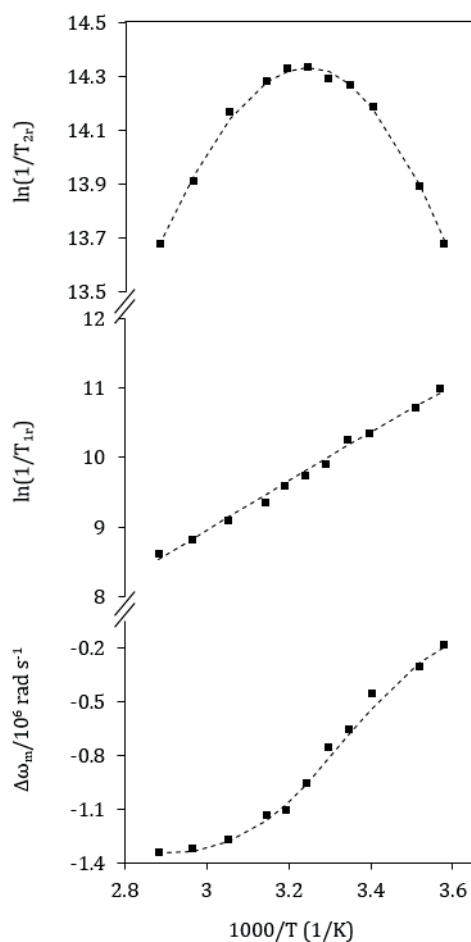
Figure V-6. ^{17}O NMR temperature dependence of $\ln(1/T_{2r})$ (top), $\ln(1/T_{1r})$ (middle) and $\Delta\omega_m$ (bottom) of $[Gd(AAZTAPh-NO_2)(H_2O)_2]^-$, $[Gd^{3+}]$ = 4.32 mM, B_0 = 9.4 T, pH = 5.7. Dashed lines correspond to the best fitting of the experimental data.
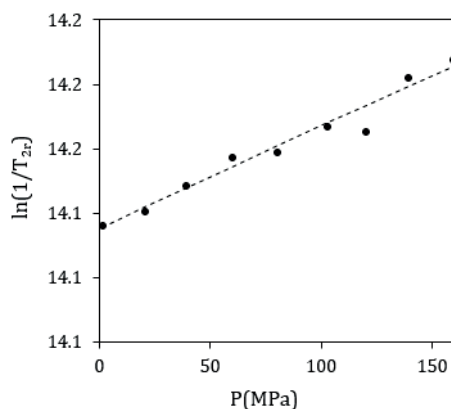
Figure V-7. ^{17}O NMR pressure dependence of $\ln(1/T_{2r})$ of $[Gd(AAZTAPh-NO_2)(H_2O)_2]^-$, $[Gd^{3+}]$ = 4.32 mM, B_0 = 9.4 T, T = 20°C, pH = 5.7. Dashed lines correspond to the best fitting of the experimental data.

Table V-2. Water exchange properties of $\left[\text{Ln}(\text{AAZTAPh} - \text{NO}_2)(\text{H}_2\text{O})_q\right]^-$

		$[\text{Gd}(\text{AAZTAPh} - \text{NO}_2)(\text{H}_2\text{O})_2]^{-\ a,b}$	$[\text{Dy}(\text{AAZTAPh} - \text{NO}_2)(\text{H}_2\text{O})_2]^{-\ b}$	$[\text{Tm}(\text{AAZTAPh} - \text{NO}_2)(\text{H}_2\text{O})_2]^{-\ b}$
q		2	2	1
k_{ex}^{298}	$(10^6\ \text{s}^{-1})$	3.9 ± 0.1	0.46 ± 0.01	0.014 ± 0.0007
$\Delta H^{\ddagger}$	(kJ mol^{-1})	42 ± 1	36 ± 0.9	46 ± 1
$\Delta S^{\ddagger}$	(J mol^{-1})	21 ± 2	-15.5 ± 1	-9.8 ± 2
$\Delta V^{\ddagger}$	$(\text{cm}^3\text{mol}^{-1})$	$-1.4 \pm 0.8\ (\text{I}_a)$	$+ 1.9 \pm 0.1\ (\text{I}_d)$	$-5.6 \pm 0.2\ (\text{I}_a/\text{A})$

a) from simultaneous fit of ^{17}O and ^{1}H NMR data b) for a full list of parameters see Table VIII-44 and Table VIII-47

As it is shown in Figure V-4, $\text{AAZTAPh} - \text{NO}_2$ complexes with the three lanthanides studied appear to be in different NMR exchange regimes in the temperature range studied: fast exchange is found for Gd^{3+}, intermediate for Dy^{3+} and slow for Tm^{3+} complexes. The results show a two orders of magnitude decrease of the exchange rate constant on going from Gd^{3+} to Tm^{3+} complexes. A similar strong decrease of k_{ex}^{298} was previously reported by Graeppi et al[11] for PDTA complexes. The very slow exchange rates observed for $[\text{Tm}(\text{AAZTAPh} - \text{NO}_2)(\text{H}_2\text{O})]^-$ reduce the inner-sphere contribution to proton relaxivity by inefficient transfer of the bound water relaxation to the bulk.[12] The outer-sphere relaxivity of this complex at 20°C is about 30% of the total proton relaxivity. In the case of $[\text{Dy}(\text{AAZTAPh} - \text{NO}_2)(\text{H}_2\text{O})_2]^-$, outer-sphere contributions goes only up to 8% (Figure VIII-2). Furthermore, k_{ex}^{298} on $[\text{Gd}(\text{AAZTAPh} - \text{NO}_2)(\text{H}_2\text{O})_2]^-$ is 2.8 times slower compared to $[\text{Gd}(\text{AAZTA})(\text{H}_2\text{O})_2]^-$ $(k_{ex}^{298} \sim 11 \times 10^6)$.[1] The remarkable decrease of k_{ex} may find its explanation in structural differences between the $\text{AAZTAPh} - \text{NO}_2$ and the AAZTA complexes or in the occurrence of a different population of diastereoisomers.[13]

The activation volumes $\Delta V^{\ddagger}$ measured for the $q = 2$ chelates $[\text{Gd}(\text{AAZTAPh} - \text{NO}_2)(\text{H}_2\text{O})_2]^-$ and $[\text{Dy}(\text{AAZTAPh} - \text{NO}_2)(\text{H}_2\text{O})_2]^-$ are slightly negative for the first one (-1.4 cm^3 mol^{-1}) and slightly positive (+1.9 cm^3 mol^{-1}) for the second (Table V-2). Interchange type mechanisms for the water exchange reactions can therefore be assigned to both of them, an associatively activated **I$_a$** mechanism to the exchange on the Gd^{3+} chelate and a dissociatively activated **I$_d$** mechanism to the exchange on the Dy^{3+} chelate. The change in activation mode is probably due to the decrease of the ionic radius from

1.107 Å for nine-coordinated Gd^{3+} to 1.083 Å for nine-coordinated Dy^{3+}.[14] The activation volume measured for the $q = 1$ chelate $[Tm(AAZTAPh - NO_2)(H_2O)]^-$ is clearly negative (-5.6 cm^3 mol^{-1}) which is indicative for an associative mode of activation (I_a or **A**). The decrease of the coordination number from nine to eight from Dy^{3+} to Tm^{3+} is responsible for the change in mechanism. In the eight-coordinated chelate, there is enough space for an incoming water molecule and therefore for an increase of the coordination number to nine in the transition state or an intermediate in the case of a limiting associative mechanism **A**.

V.3.4 [Dy(AAZTAPh-NO₂)(H₂O)₂]⁻ complexes as a potential negative contrast agent

Dysprosium complexes have been proposed as T_2 relaxation agent in MRI mainly due to the high magnetic moment of Dy^{3+}.[15-18] To be considered as a good T_2 agent, the compounds should have one or more inner-sphere water molecules and a water exchange rate falling within a narrow range of values:[16] the maximum transverse relaxivity, r_2, is reached for $\tau_m = \Delta\omega_m^{-1}$ or $k_{ex} = \Delta\omega_m$ and its value is $r_2 = 1.8 \times 10^{-5} q \Delta\omega_m/2$.
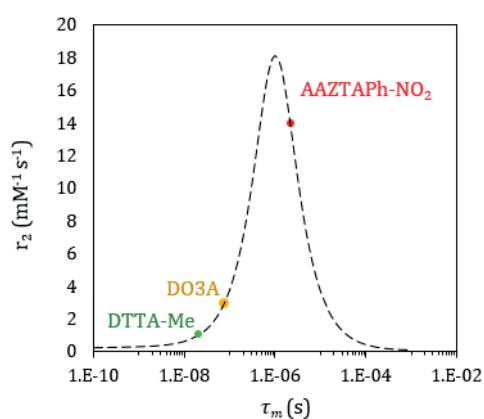
Figure V-8. Effect of water residency time on the proton transverse relaxivity (r_2) of bis-aqua $[DyL(H_2O)_2]^x$ complexes, as calculated with eqs 1 to 15 for $\Delta\omega_m = 1 \times 10^6$ rad s^{-1}, $B_0 = 9.4$ T, T = 25°C.

If we assume that the paramagnetic chemical shift $\Delta\omega_m$ is about the same (1×10^6 rad s$^-$^{1}) for the three bis-aqua dysprosium complexes with $\mathrm{L} = \mathrm{DO3A}$, $\mathrm{DTTA-Me}$ and $\mathrm{AAZTAPh-NO_2}$, we can calculate r_2 at 9.4 T and 25°C (Figure V-8). Transverse relaxivity of $[\mathrm{Dy(AAZTAPh-NO_2)(H_2O)_2}]^-$ is close to the optimal value with a water residence time of 2.2 μs, much longer than for the other two compounds (52 ns and 22 ns for DO3A and DTTA$-$Me, respectively). The relatively high r_2 value indicates that the slow exchanging $[\mathrm{Dy(AZZTAPh-NO_2)(H_2O)_2}]^-$ complex might be of interest as 'negative' contrast agents for high field imaging applications.

V.4 Conclusions

Water exchange kinetics on $[\mathrm{Ln(AAZTAPh-NO_2)(H_2O)_q}]^-$ with $\mathrm{Ln} = \mathrm{Gd^{3+}}$, $\mathrm{Dy^{3+}}$ and $\mathrm{Tm^{3+}}$ have been studied using proton nuclear magnetic relaxation. ^{1}H NMR has been found to represent a valuable and reliable method to assess the exchange rate constant of metal coordinated water molecules when ^{17}O NMR is not applicable due to low chelate concentration. A change in the number of inner-sphere water molecules from two to one was observed replacing $\mathrm{Dy^{3+}}$ by the smaller $\mathrm{Tm^{3+}}$. Moreover, water exchange rate constants were found to decrease more than two orders of magnitude from $[\mathrm{Gd(AAZTAPh-NO_2)(H_2O)_2}]^-$ to $[\mathrm{Tm(AAZTAPh-NO_2)H_2O}]^-$. Water exchange reactions on bis-aqua $\mathrm{Gd^{3+}}$ and $\mathrm{Dy^{3+}}$ complexes follow an associative respectively dissociative interchange mechanism as evinced by the activation volumes of -1.4 and +1.9 cm^3 mol^{-1}. The water exchange on the *mono*-aqua complex $[\mathrm{Tm(AAZTAPh-NO_2)H_2O}]^-$ follows an associative activation mode ($\mathbf{I_a}$ or $\mathbf{A}$ mechanism) with $\Delta V^{\neq} = -5.6$ cm^3 mol^{-1}. Moreover, $[\mathrm{Dy(AAZTAPh-NO_2)(H_2O)_2}]^-$ is characterised by a nearly optimal rate of water exchange and such as to maximise its transverse relaxivity. These properties make this complex a potentially very effective negative contrast agent for high magnetic fields imaging applications.

V.5 Experimental procedures

V.5.1 Materials

LnCl$_3$.xH$_2$O, Ln = Gd^{3+}, Dy^{3+} and Tm^{3+} (99.9%) were obtained from Aldrich and were used without further purification. The H$_4$DTTA − Me was provided by EPFL through the synthetic platform, H$_3$DO3A was provided by CheMatech Co, Dijon, France and H$_4$AAZTAPh − NO$_2$ was synthesised by Dr. Lorenzo Tei at the Università del Piemonte Orientale "A. Avogadro". Other reagents were obtained from Sigma-Aldrich Chemical Co. commercial sources and used without further purification.

V.5.2 Preparation of [Ln(L)(H$_2$O)$_q$]^x complexes

Ln^{3+} solutions (1 M, pH < 3) in water were prepared from LnCl$_3$.xH$_2$O. The exact concentration of Ln^{3+} was measured by complexometric titration with Na$_2$H$_2$EDTA in urotropine/HCl buffer and xylenol orange as metal indicator. Solid ligands were dissolved in water in order to obtain 6 mM (L$_1$) and 100 mM (L$_2$ and L$_3$) solutions. The exact concentration of the ligand was determined by back titration of Gd^{3+} excess with Na$_2$H$_2$EDTA solution. $\left[\text{Ln(L}_1\text{)(H}_2\text{O)}_q\right]^-$ solutions were prepared by gradual addition of the stoichiometric amount of Ln^{3+} while controlling the pH by adding 0.1 M NaOH solution. Mixing LnCl$_3$ and the ligand solutions at once leads to precipitation due to low solubility of the ligand at low pH. $\left[\text{Ln(L}_{2,3}\text{)(H}_2\text{O)}_2\right]^x$ samples were prepared by mixing adequate amount of solution of LnCl$_3$ and the ligand in a 1:1 molar ratio, allowing for 2-4 % excess of the ligand while having a final Ln^{3+} concentration of ~ 100 mM. The absence of free Ln^{3+} was verified by xylenol orange indicator. The final pH was maintained at 5.7. ^{17}O enriched water was added to have solutions with about 2% ^{17}O enrichment. The final Ln^{3+} concentration was measured by bulk magnetic susceptibility (BMS)[19] at 25°C on a Bruker DRX-400 (9.4 T, 400 MHz) spectrometer. For variable temperature measurements, the samples were sealed in glass spheres fitting into 10 mm NMR tubes, in order to eliminate susceptibility corrections to the chemical shift.[20] For variable pressure measurements, since the high-pressure probe does not allow the use of spherical samples,

the solution was placed inside a 5 mm NMR tube closed with a movable MACOR piston.[21,22]

V.5.3 NMR measurements

Variable temperature ^{1}H and ^{17}O NMR measurements were performed using Bruker Avance-II 400 (9.4 T, 54.2 MHz) and Bruker Avance-II 800 (18.8 T, 108.4 MHz) spectrometers in the temperature range of 5°C to 85°C. The temperature was controlled by a Bruker B-VT 3000 temperature control unit, and was measured using a substitution technique.[23] Variable pressure ^{1}H and ^{17}O NMR spectra were recorded up to a pressure of ~160 MPa at 20°C on a Bruker Avance-II 400 (9.4 T, 54.2 MHz) spectrometer equipped with a homebuilt high-pressure probe.[24] The temperature was measured with a built-in Pt resistor. In all cases the longitudinal ($1/T_1$) and transverse ($1/T_2$) relaxation rates were obtained using the inversion recovery[25] and the Carr-Purcell-Meiboom-Gill spin-echo[26] methods respectively, and the chemical shift differences in comparison to the acidified water reference (pH 3.0, 2% ^{17}O enrichment) were measured. For all measurements, the 90° pulse lengths have been determined at different temperatures and pressures for each sample.

V.6 Data fitting

All fittings have been performed using the Visualiseur/Optimiseur[27,28] 3.7.0 program running on a Matlab® 8 platform.

V.7 References

(1)   Aime, S.; Calabi, L.; Cavallotti, C.; Gianolio, E.; Giovenzana, G. B.; Losi, P.; Maiocchi, A.; Palmisano, G.; Sisti, M. *Inorg. Chem.* **2004**, *43*, 7588.

(2)   Gugliotta, G.; Botta, M.; Tei, L. *Org. Biomol. Chem.* **2010**, *8*, 4569.

(3)   Micskei, K.; Helm, L.; Brucher, E.; Merbach, A. E. *Inorg. Chem.* **1993**, *32*, 3844.

(4)   Helm, L.; Nicolle, G. M.; Merbach, R. E. In *Adv. Inorg. Chem.*; 2005.

(5)   Tóth, é.; Helm, L.; Merbach, A. In *The Chemistry of Contrast Agents in Medical Magnetic Resonance Imaging*; John Wiley & Sons, Ltd: Chichester, U.K., 2013.

(6)   Karimi, S.; Helm, L. *Inorg. Chem.* **2016**, *55*, 4555.

(7)   Fries, P. H.; Belorizky, E. *J. Chem. Phys.* **2012**, *136*.

(8)   McLachlan, A. D. *Proc. R. Soc. Lond. A* **1964**, *280*, 271.

(9)   Powell, D. H.; Merbach, A. E.; González, G.; Brücher, E.; Micskei, K.; Ottaviani, M. F.; Köhler, K.; Von Zelewsky, A.; Grinberg, O. Y.; Lebedev, Y. S. *Helv. Chim. Acta.* **1993**, *76*, 2129.

(10)   Djanashvili, K.; Platas-Iglesias, C.; Peters, J. A. *Dalton Trans.* **2008**, 602.

(11)   Graeppi, N.; Hugh Powell, D.; Laurenczy, G.; Zékány, L.; Merbach, A. *Inorg. Chim. Acta* **1995**, *235*, 311.

(12)   Hugh Powell, D.; Favre, M.; Graeppi, N.; Ni Dhubhghaill, O. M.; Pubanz, D.; Merbach, A. *J. Alloys Compd.* **1995**, *225*, 246.

(13)   Elemento, E. M.; Parker, D.; Aime, S.; Gianolio, E.; Lattuada, L. *Org. Biomol. Chem.* **2009**, *7*, 1120.

(14)   Shannon, R. D. *Acta Cryst.* **1976**, *32*, 751.

(15)   Caravan, P.; Greenfield, M. T.; Bulte, J. W. M. *Magn. Reson. Med.* **2001**, *46*, 917.

(16)   Soesbe, T. C.; Ratnakar, S. J.; Milne, M.; Zhang, S.; Do, Q. N.; Kovacs, Z.; Sherry, A. D. *Magn. Reson. Med.* **2014**, *71*, 1179.

(17)   Vander Elst, L.; Roch, A.; Gillis, P.; Laurent, S.; Botteman, F.; Bulte, J. W. M.; Muller, R. N. *Magn. Reson. Med.* **2002**, *47*, 1121.

(18)   Vander Elst, L.; Zhang, S.; Sherry, A.; Laurent, S.; Botteman, F.; Muller, R. *Acad Radiol* **2002**, *9*, S297.

(19)   Corsi, D. M.; Platas-Iglesias, C.; Bekkum, H. v.; Peters, J. A. *Magn. Reson. Chem.* **2001**, *39*, 723.

(20)   Hugi, A. D.; Helm, L.; Merbach, A. E. *Helv. Chim. Acta* **1985**, *68*, 508.

(21)   Helm, L.; Merbach, A. E. *J. Chem. Soc., Dalton Trans.* **2002**, 633.

(22)   Frey, U.; Helm, L.; Merbach, A. E. *High Press Res.* **1990**, *2*, 237.

(23)   Ammann, C.; Meier, P.; Merbach, A. *J. Magn. Reson.* **1982**, *46*, 319.

(24)   Cusanelli, A.; Nicula-Dadci, L.; Frey, U.; Merbach, A. E. *Inorg. Chem.* **1997**, *36*, 2211.

(25)   Vold, R. L. *J. Chem. Phys* **1968**, *48*, 3831.

(26)   Meiboom, S.; Gill, D. *Rev. Sci. Instrum.* **1958**, *29*, 688.

(27)   Yerly, F. *VISUALISEUR 2.3.6* **2004**.

(28)   Yerly, F. *OPTIMISEUR 3.0.0* **2002**.

Chapter VI

Evaluation of water exchange kinetics of concentrated lanthanide perchlorate and chloride aqueous solutions
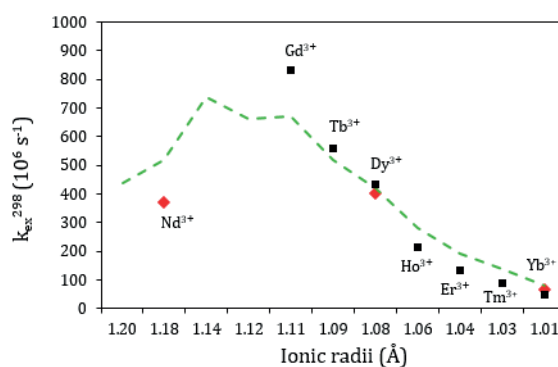
VI.1 Introduction

It is fifty years since Spedding and coworkers for a first time in 1966 postulated a change in preferred coordination number of hydrate complexes of rare earth ions in aqueous solution from their measurements of apparent molal volumes.[1] The first direct measurements by X-ray diffraction[2-4] and by neutron scattering[5-8] confirmed the change in coordination number along the series. In the following, these first results have been confirmed by further neutron scattering,[9,10] EXAFS[11-13] and XANES[13,14] spectroscopy measurements as well as computational methods.[15-21] The general result of these studies is the change of the coordination number (CN) from nine at the beginning of the series to eight at the end.[22] The reason for the decrease of CN is founded in the lanthanide contraction, the steady decrease of the ionic radius from La^{3+} to Lu^{3+}.[23,24] The difficulty is in determining at what lanthanide ion the change will occur. From Swaddles interpretation of the partial molar volumes[25] and from neutron scattering,[10] the changeover occurs around Sm^{3+}. EXAFS and XANES show a larger range of lanthanide ions from Nd^{3+} to Gd^{3+} for the transition of CN.[12,13,22]

Closely related to the question of the coordination number and the structure of the first hydration sphere of lanthanide ions (Ln^{3+}) are the questions on the rate of water exchange from the first sphere and the mechanism of the exchange reaction. After first results obtained in the sixties,[26] Merbach and his co-workers performed more systematic studies.[27-31] Exchange rate constants, k_{ex}, for water exchange could only be measured for lanthanide ions of the second half of the series (from Gd^{3+} to Yb^{3+}), all having CN = 8. This is a consequence of the very fast exchange reactions together with the magnetic properties of the lanthanides defining the NMR chemical shift difference between water in the first coordination sphere and the bulk.[28] For Pr^{3+} and Nd^{3+}, both having CN = 9, only lower limits of k_{ex} have been found so far.[31] Moreover, from the negative activation volumes ($\Delta V^{\ddagger}$) measured for all eight-coordinated lanthanides, $[Ln(H_2O)_8]^{3+}$, an associative interchange mechanism $\mathbf{I_a}$ has been assigned for water exchange.[29,32] The very fast water exchange on the trivalent lanthanides was concluded to be the result of the small difference in energy between the eight and the nine coordinated forms.[32] From this model it has been predicted that the rate constants on the light, nine-coordinated Ln^{3+}

should decrease from the middle towards the beginning of the lanthanide series and the water exchange should follow a dissociative mechanism.

From what precedes, a direct measurement of the water exchange rate constant and the assignment of the reaction mechanisms are fundamental for the validation of the proposed model. To be able to measure k_{ex} on the most favorable light lanthanide ions, Pr^{3+} and Nd^{3+}, ^{17}O NMR relaxation has to be measured at the highest magnetic field available which is 18.8 T in our laboratory. A second possibility to extend the range of observable k_{ex} towards faster reactions is increasing the concentration of lanthanide ions to concentrations well above 1 m. However, by working at such high concentrations, one has to ensure first that anions do not enter the first coordination sphere of Ln^{3+} and second that the exchange rate constant does not change at such high concentrations.

Herein, we report a variable temperature and pressure ^{17}O NMR study of water exchange on aqueous solutions of $Ln(ClO_4)_3$, Ln = Nd^{3+}, Dy^{3+}, Yb^{3+} and $LnCl_3$, Ln = Nd^{3+}, Dy^{3+}, performed at different concentrations and two magnetic field strengths.

VI.2 Procedures and data treatment

Water exchange rate constants and mechanisms on hydrated lanthanide ions as discussed in chapter II can be determined from variable temperature and pressure ^{17}O NMR relaxation and chemical shifts measurements.[28,30,33] It has been shown that for dilute Ln^{3+} other than Gd^{3+}, the exchange rate constant can be obtained from eq II-39. This method works well as long as the difference between measured relaxation rates is large compared to the uncertainty of the individual rates. The only way to increase this difference for a given lanthanide at constant magnetic field, temperature and pressure is increasing the concentration of the lanthanide ions and therefore increasing P_m. In the case of concentrated Ln^{3+} ions, one has to take into account that the mole fraction of bulk water (P_A) is < 1 and therefore eq II-39 is no longer valid, hence one should use eq II-45 for non-dilute and fast exchanging lanthanide systems. The temperature and pressure variation of k_{ex} and that of $\Delta\omega_m$ can be calculated using eqs II-28, II-29, II-35 and II-36.

VI.3 Results and discussions

VI.3.1 $^{35/37}$Cl NMR studies

Several luminescence lifetime measurements in concentrated $Ln(ClO_4)_3$ and $LnCl_3$ aqueous solutions showed that ClO_4^- and Cl^- do not enter into the first coordination shell of the lanthanide ions.[34,35,36] Similar results have been obtained from UV-vis spectroscopy,[37,38] X-ray diffraction,[19,48-50] EXAFS,[11] and neutron diffraction.[7,9] An EXAFS,[39] and a computational study[40] conclude that at 1 m solution, one Cl^- is present in the first coordination shell of La^{3+} but not for other lanthanide ions.[40,41] A study using THz spectroscopy[42] performed at $LaCl_3$ solutions up to 3.3 M showed an increasing formation of solvent shared ion pairs with increasing salt concentration but no inner shell complexation.

To assess eventual entering of Cl^- or ClO_4^- into the first coordination sphere of Ln^{3+}, $1/T_1$ and $1/T_2$ of ^{35}Cl and ^{37}Cl NMR in 2 m DyX_3, $X = Cl^-, ClO_4^-$ solutions (Figure VI-1) have been measured. Chlorine has two useful NMR active nuclei ^{35}Cl and ^{37}Cl with respectively 75.78% and 24.22% abundance both with a spin 3/2 and therefore an electric quadrupole moment. Since the quadrupolar relaxation mechanism is expected to be dominant for the nuclei of chloride ions, the relaxation rates in extreme narrowing condition are related to the nuclear quardupolar moment (eQ) by:

$$\frac{1}{T_{i,q}} = \frac{3\pi^2}{10}\left(\frac{2I+3}{I^2(2I-1)}\right)(1+\eta^2/3)\left(\frac{e^2qQ}{\hbar}\right)^2 \tau_R \quad \text{with } i = 1, 2 \qquad \text{(VI-1)}$$

where eq is the principle component of the electric field gradient tensor, η is an asymmetry parameter and τ_R is the correlation time for the quadrupole interaction. As the ratios of the quadroplar moments for ^{35}Cl and ^{37}Cl are known, one can prove the relaxation rates only depended on quadrupolar relaxation if they follow eq VI-2:

$$\left(\left(\frac{1}{T_{i,obs}}\right)/(eQ)^2\right)^{37} = \left(\left(\frac{1}{T_{i,obs}}\right)/(eQ)^2\right)^{35} \quad \text{with } i = 1,2 \qquad \text{(VI-2)}$$
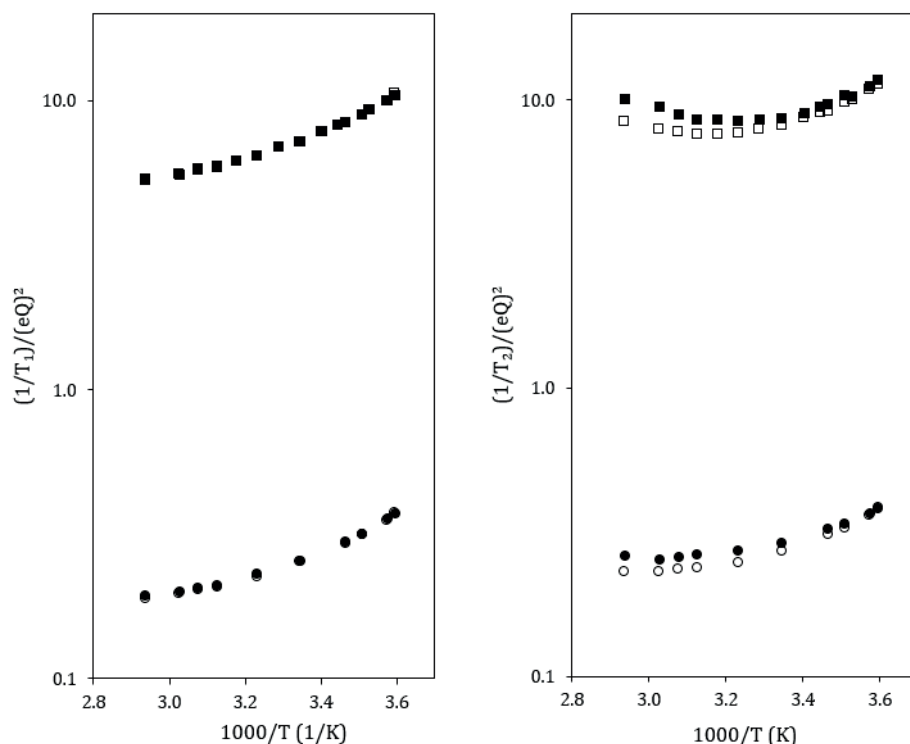
Figure VI-1. Variable temperature ^{35}Cl (empty symbols) and ^{37}Cl NMR (filled symbols) longitudinal and transverse relaxation rates of 2 m solutions of $Dy(ClO_4)_3$ ($\bullet$), $DyCl_3$ ($\blacksquare$), $B_0 = 9.4$ T.

As it is shown in (Figure VI-1), longitudinal relaxation rates for both isomers are equal, if normalised by the square of the electric quadrupole moment, $(eQ)^2$, showing the absence of paramagnetic contributions to T_1 relaxation. Scaled transverse relaxation rates show a difference at high temperature, which can be attributed to the interaction with the paramagnetic Dy^{3+} probably due to second sphere effects. One should keep in mind that at 2 m LnX_3, there are only seven water molecules per ion and necessarily there have to be anions in the second coordination shell of the lanthanide ion. Similar measurements performed on 0.1 m $GdCl_3$ solutions lead to similar results (Figure VI-2). We therefore conclude that Cl^- and ClO_4^- anions do not enter the first coordination shell of lanthanide ions even at the highest concentrations used in this study.
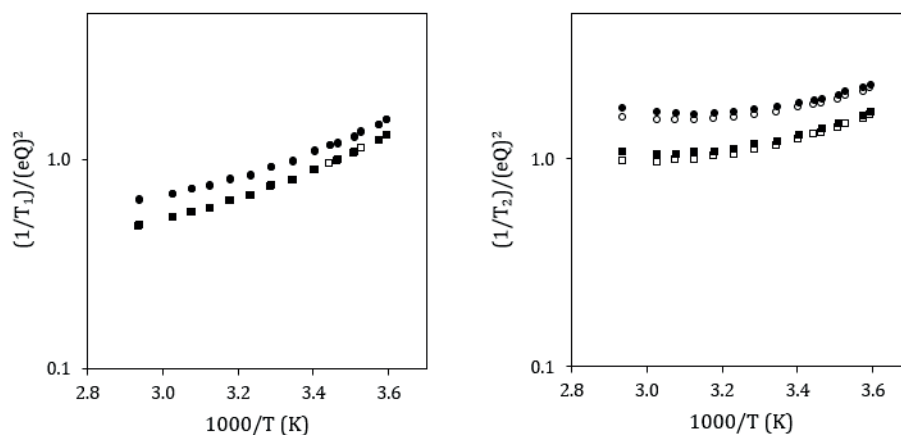
Figure VI-2. Variable temperature ^{35}Cl (empty symbols) and ^{37}Cl NMR (filled symbols) longitudinal and transverse relaxation rates of $GdCl_3$, $[Gd^{3+}] = 0.10$ m (■, □), 0.21 m (●, ○), $B_0 = 9.4$ T.

VI.3.2 Water exchange studies by ^{17}O NMR

Variable temperature ^{17}O relaxation rates and chemical shift differences have been measured at 9.4 T and 18.8 T for four concentrations (0.5 m, 1 m, 1.5 m and 2 m) of $Ln(ClO_4)_3$ (Ln = Nd^{3+}, Dy^{3+}, Yb^{3+}) and $LnCl_3$ (Ln = Nd^{3+}, Dy^{3+}). The relaxation differences and the chemical shifts both normalised to the mole fraction of first shell water, are reported in Figure VI-3 and Figure VI-4. The fitting of the data with eq II-45 has been performed by including scalar, dipolar and Curie relaxation to $1/T_{2m} - 1/T_{1m}$. The Ln-O distances were fixed to the values reported by D'Angelo and co-workers.[24] Water coordination numbers, were taken as nine for the light lanthanide (Nd^{3+}) and eight for the heavy ones (Dy^{3+}, Yb^{3+}). Electronic relaxation times were fixed to the calculated values reported by Alsaadi.[43] The obtained parameters concerning water exchange rate constants are summarised in Table VI-1 and Table VI-2 and the corresponding fitted curves are shown in Figure VI-3 and Figure VI-4.
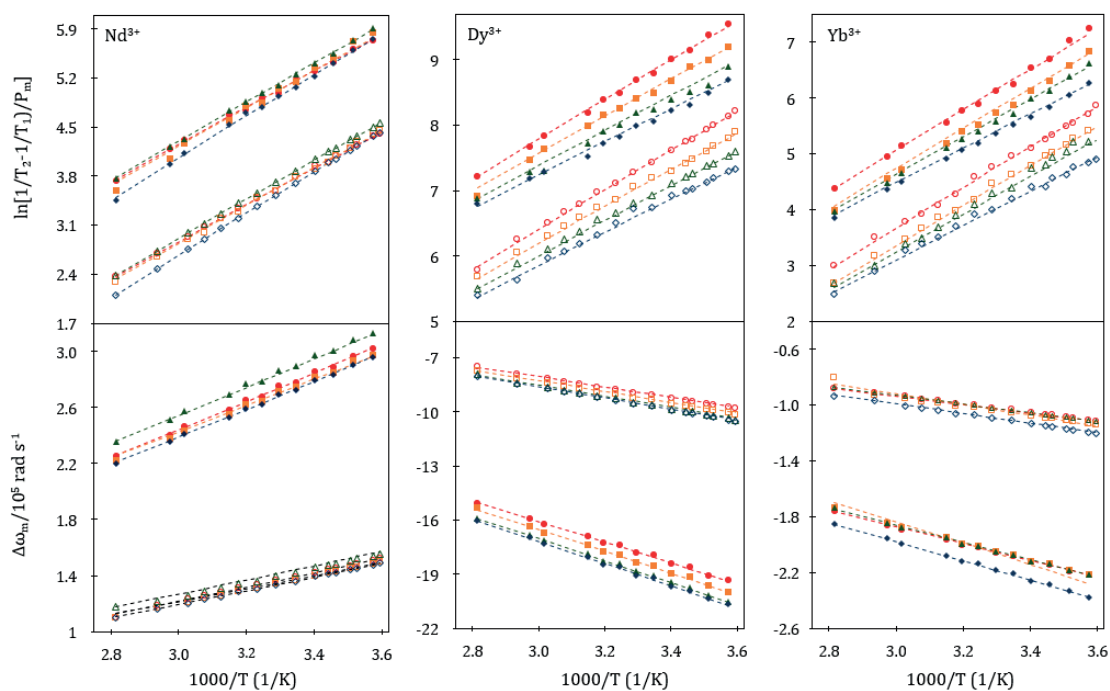
Figure VI-3. Variable temperature ^{17}O NMR data of $Ln(ClO_4)_3$, $Ln = Nd^{3+}$, Dy^{3+}, Yb^{3+}, at four different concentrations, 0.5 m (●, ○), 1.0 m (■, □), 1.5 m (▲, △), 2 m (◆, ◊), $B_0 = 9.4$ T (empty symbols) and 18.8 T (filled symbols). Dashed lines correspond to the best fitting of the experimental data using parameters listed in Table VI-1.
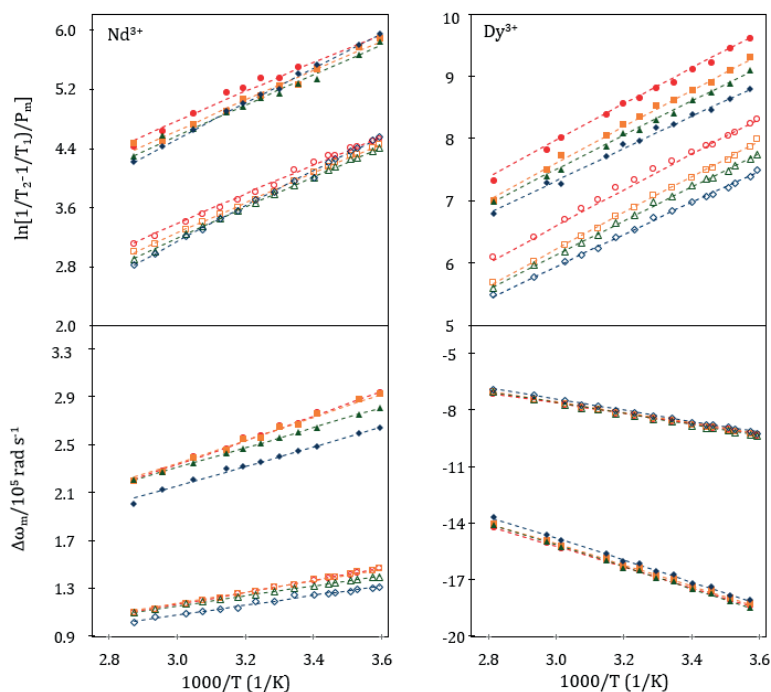
Figure VI-4. Variable temperature ^{17}O NMR data of $LnCl_3$, $Ln = Nd^{3+}$, Dy^{3+}, at four different concentrations, 0.5 m (●, ○), 1.0 m (■, □), 1.5 m (▲, △), 2 m (◆, ◊), $B_0 = 9.4$ T (empty symbols) and 18.8 T (filled symbols). Dashed lines correspond to the best fitting of the experimental data using parameters listed in Table VI-2.

Variable pressure transverse and longitudinal relaxation difference as well as the chemical shift difference have been studied on ~ 2 m solutions at 9.4 T and 295 K (Figure VI-5 and Figure VI-6). Eqs II-35 and II-36 have been fitted to the experimental data leading to activation volumes given in Table VI-1 and Table VI-2.
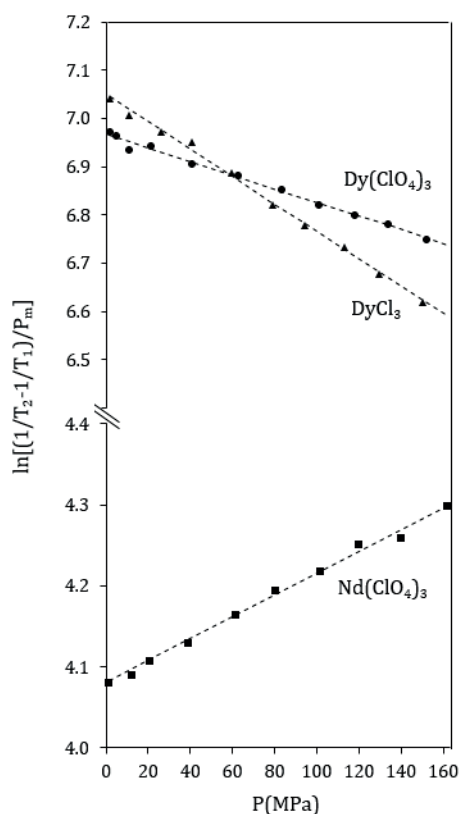
Figure VI-5. ^{17}O NMR pressure dependence of $\ln[(1/T_2 - 1/T_1)/P_B]$ of $Ln(ClO_4)_3$, $Ln = Nd^{3+}$, Dy^{3+} and $LnCl_3$, $Ln = Dy^{3+}$, $[Ln^{3+}] \sim 2$ m, $B_0 = 9.4$ T, $T = 25°C$. Dashed lines correspond to the best fitting of the experimental data using parameters listed in Table VI-1 and Table VI-2.
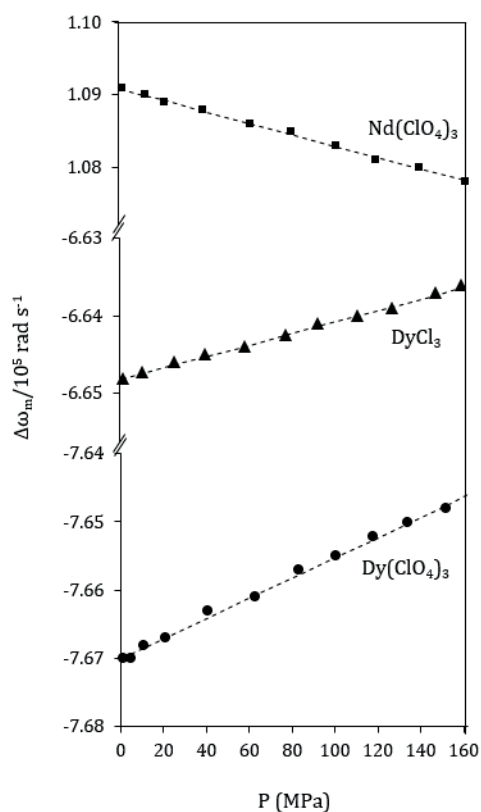
Figure VI-6. ^{17}O NMR pressure dependence of chemical shift of $Ln(ClO_4)_3$, $Ln = Nd^{3+}$, Dy^{3+} and $LnCl_3$, $Ln = Dy^{3+}$, $[Ln^{3+}] \sim 2$ m, $B_0 = 9.4$ T, T = 25°C. Dashed lines correspond to the best fitting of the experimental data using parameters listed in Table VI-1 and Table VI-2.

Table VI-1. Parameters obtained from the least squares fit of ^{17}O NMR data for $Ln(ClO_4)_3$

		Nd^{3+}				Dy^{3+}				Yb^{3+}			
$[Ln^{3+}]$	(m)	0.50	1.05	1.48	2.05	0.49	1.05	1.48	2.01	0.50	1.08	1.50	2.05
k_{ex}^{298}	(10^6 s^{-1})	371 ± 1	291 ± 1	245 ± 2	201 ± 2	400 ± 4	474 ± 7	550 ± 8	562 ± 8	65.1 ± 0.8	77.5 ± 0.9	78.2 ± 0.9	92.7 ± 1
$\Delta H^{\ddagger}$	(kJ mol^{-1})	12.8 ± 0.1	13.6 ± 0.1	14.5 ± 0.3	15.8 ± 0.3	17.3 ± 0.4	15.5 ± 0.5	14.5 ± 0.6	13.2 ± 0.6	22.6 ± 0.4	21.7 ± 0.4	20.5 ± 0.4	17.9 ± 0.4
$\Delta S^{\ddagger}$	(J mol^{-1}K^{-1})	-37.8 ± 1.0	-37.1 ± 0.8	-35.7 ± 0.8	-33.1 ± 0.7	-22.2 ± 0.7	-26.8 ± 0.6	-29.1 ± 0.6	-33.2 ± 0.5	-19.5 ± 0.5	-21.2 ± 0.5	-24.9 ± 0.6	-32.4 ± 0.5
$\Delta V^{\ddagger}$	(cm^{3}mol^{-1})	-	-	-	+3.7 ± 0.1	-	-	-	-3.4 ± 0.2	-	-	-	-

Table VI-2. Parameters obtained from the least squares fit of ^{17}O NMR data for $LnCl_3$

		Nd^{3+}				Dy^{3+}			
$[Ln^{3+}]$	(m)	0.50	1.02	1.45	1.80	0.52	1.03	1.49	1.99
k_{ex}^{298}	(10^6 s^{-1})	259 ± 3	237 ± 4	199 ± 1	163 ± 1	311 ± 3	377 ± 5	380 ± 4	386 ± 4
$\Delta H^{\ddagger}$	(kJ mol^{-1})	7.2 ± 0.5	8.1 ± 0.5	9.0 ± 0.2	11.5 ± 0.2	16.0 ± 0.4	15.4 ± 0.5	14.5 ± 0.5	13.0 ± 0.5
$\Delta S^{\ddagger}$	(J mol^{-1}K^{-1})	-59.8 ± 0.4	-57.3 ± 0.4	-55.8 ± 0.5	-49.3 ± 0.4	-28.8 ± 0.4	-29.1 ± 0.6	-32.1 ± 0.6	-37.0 ± 0.5
$\Delta V^{\ddagger}$	(cm^{3}mol^{-1})	-	-	-	-	-	-	-	-7.0 ±0 .2

So far, directly measured water exchange rate constants have been reported for 0.3 m perchlorate salt solutions of heavy lanthanides (Gd^{3+} to Yb^{3+}).[28,29] It has been found that k_{ex} decreases by about two orders of magnitude from the larger gadolinium ion to the smaller ytterbium ion and for the light lanthanides Pr^{3+} and Nd^{3+}, only lower limits of water exchange is reported.[31] Moreover, from the similarity of the water exchange rate constants and the interchange rate constants k_i measured for complex formation with SO_4^{2-} a maximum of lability has been predicted for the lanthanide hydrate complexes (Figure VI-7).[44]

Our results measured on the neodymium ion are the first direct experimental proof for the maximum of water exchange rate constant occurring in the middle of the lanthanide series. At the lowest concentration used in the study (0.5 m), we found $k_{ex}^{298} = 3.7 \times 10^8$ s^{-1} for perchlorate and 2.6×10^8 s^{-1} for chloride solutions. The activation volume measured on $Nd(ClO_4)_3$ is clearly positive (Table VI-1) indicating a dissociative mechanism for water exchange. Water exchange rate constants obtained for the heavier lanthanides (Dy^{3+} and Yb^{3+}) at 0.5 m are close to the values reported by Cossy et al.[28] Negative activation volumes, $\Delta V^{\ddagger} = $ -3.4 and -7.0 cm^3 mol^{-1}, respectively for $DyCl_3$ and $Dy(ClO_4)_3$ indicate an associative mechanism.[33] The change of mechanism should occur at Eu^{3+} or Sm^{3+}. Both have such small chemical shifts of bound water molecules ($\Delta\omega_m$) that a direct measurement of k_{ex} will not be possible at magnetic fields available today.
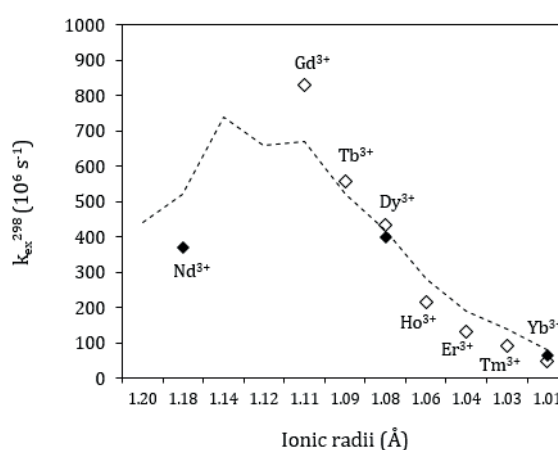
Figure VI-7. Water exchange rate constant of $Ln(ClO_4)_3$ from this work (filled symbols, $[Ln^{3+}] \sim 0.5$ m) and from references 28,33 (empty symbols, $[Ln^{3+}] \sim 0.3$ m). Interchange rate constants, k_i, for the SO_4^{2-} substitution are shown as dotted line.[44]

From the data in Table VI-1 and Table VI-2, it can be seen that a concentration dependence of k_{ex} is found for all the three lanthanides as well as for both anions studied. Surprisingly, an opposite dependence of k_{ex} on the concentration, independent on the nature of the anion (Figure VI-9) is observed: whereas water exchange on Nd^{3+} slows down with increasing concentration, it becomes faster for Dy^{3+} and Yb^3. It has to be noted that as mentioned before at high concentrations highly charged lanthanides form weak outer-sphere complexes with anions (eq VI-3) in which the lanthanide and the anion remain separated by at least one water molecule and the complexation with ions adds and does not replace the water molecule (Figure VI-8):

$$\left[Ln(H_2O)_q\right]^{3+} + X^{n-} \rightleftarrows \left[Ln(H_2O)_qX\right]^{(3-n)+} \tag{VI-3}$$
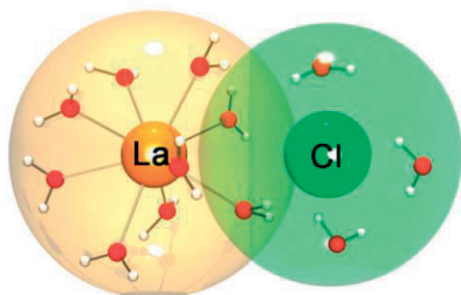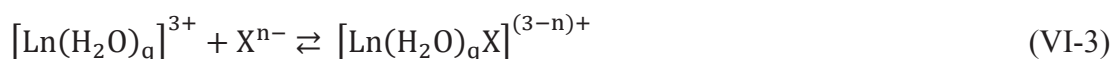
Figure VI-8. Sketches of solvent separated ion pair.[42]

In this case, the exchanging water molecules can come from or go to the first coordination shell of anions and not from or to the bulk (considering that Cl^- and ClO_4^- are surrounded by 6[45-47] and 8-12[48] water molecules respectively). Hence, in the case of an associative mechanism, the probability that an incoming water molecule comes from the first sphere of an anion will increase with the concentration. Similarly for a dissociative mechanism the probability that a leaving water molecule will end in the first sphere of anion will increase with concentration.

From our exchange rate constants measured on solutions containing Cl^- and ClO_4^- anions we find at all concentrations studied a small difference of k_{ex} for both lanthanides studied, Nd^{3+} and Dy^{3+}. The exchange rate constant is about 20% smaller on $LnCl_3$ as compared with that found on $Ln(ClO_4)_3$ at $[Ln^{3+}] = 0.5$ m.
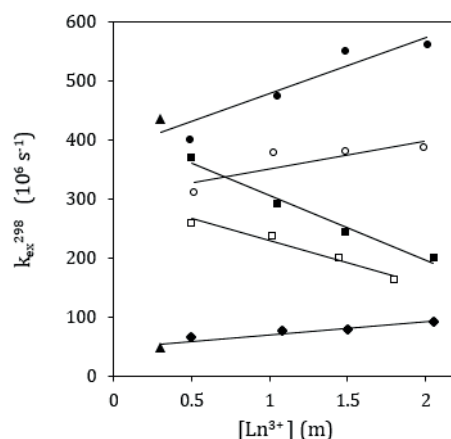
Figure VI-9. Water exchange rate constant as a function of concentration for Nd^{3+} (■, □), Dy^{3+} (●, ○), and Yb^{3+} (♦), ClO_4^- (filled symbols) and Cl^- (empty symbols), triangle symbols are from reference 28,33 (▲, $[Ln^{3+}] \sim 0.3$ m).

VI.4 Conclusions

Water exchange kinetics and mechanisms on concentrated $Ln(ClO_4)_3$ and $LnCl_3$ aqueous solutions were studied by variable temperature and pressure ^{17}O NMR spectroscopy. Water exchange rate constant of neodymium aqua ions was obtained experimentally for the first time confirming that k_{ex} reaches its maximum in the middle of the lanthanide series. A change in the mechanism of water exchange from a dissociative mechanism for neodymium aqua ions to an associative mechanism for dysprosium aqua ions was obtained. Moreover, a different variation of k_{ex} with concentration was found for the light and the heavy lanthanides. k_{ex} was found to decrease by increasing Nd^{3+} concentration however on the heavier lanthanides k_{ex} increased as the Ln^{3+} concentration increased. Difference in the k_{ex} variation can be linked to the different exchange mechanism obtained for the light and the heavy lanthanides.

VI.5 Experimental procedures

VI.5.1 Materials

$Ln(ClO_4)_3$ (50% solution, 99.9%) (Ln = La^{3+}, Nd^{3+}, Dy^{3+}, Yb^{3+}) and $LnCl_3$ (powder, 99.9%) (Ln = La^{3+}, Nd^{3+}, Gd^{3+}, Dy^{3+}) were obtained from Sigma-Aldrich Chemical Co. and used as received.

VI.5.2 Preparation of LnCl₃ and Ln(ClO₄)₃ samples

$Ln(ClO_4)_3$, Ln = La^{3+}, Nd^{3+}, Dy^{3+}, Yb^{3+} solutions (~ 50% in water, pH ≤ 3) were evaporated at reduced pressure to have stock solutions of ~ 2.5 m. $LnCl_3$, Ln = La^{3+}, Nd^{3+}, Gd^{3+}, Dy^{3+} solutions, $[Ln^{3+}]$ ~ 2 m, were prepared by dissolving the weighted amounts of $LnCl_3$ in distilled, deionised water. The pH of the solution was adjusted to 2 to prevent hydrolysis by adding 0.1 m HCl solution. In this range, pH does not affect the relaxation rate of the lanthanide ions.[43] The resulting solutions were filtered through a Milipore filter (pore size 40 μm). The exact concentration of the metal content in all lanthanide salts was determined by complexometric titration with Na_2H_2EDTA in urotropine/HCl buffer and xylenol orange as metal indicator. Dilutions (1.5 m, 1 m and 0.5 m) were prepared by weight using distilled, deionised water from lanthanide salts stock solutions (~ 2.5 m). In order to improve sensitivity for ^{17}O NMR measurements, providing a signal to noise ratio large enough for accurate shift measurements, ^{17}O enriched water (Yeda R&D Co., Rehovot, Israel) was added to the solutions (final enrichment of 2%). For variable temperature ^{17}O NMR measurements in order to eliminate susceptibility corrections to the chemical shift,[49] the samples were sealed in glass spheres fitting into 10 millimeter NMR tubes. For ^{17}O variable pressure measurements, the solution was placed inside a 5 millimeter NMR tube and closed with a movable MACOR piston.[50,51]

VI.5.3 ¹⁷O NMR measurements

Variable temperature ^{17}O NMR measurements were performed at two magnetic fields using Bruker Avance-II 400 (9.4 T, 54.2 MHz) and Bruker Avance-II 800 (18.8 T, 128.4 MHz) spectrometers in the temperature range of 5°C to 80°C. The temperature was

controlled by Bruker B-VT 3000 temperature control units, and was measured by a substitution technique.[52] Variable pressure NMR spectra were recorded up to a pressure of 160 MPa at 22°C on a Bruker Avance-II 400 (9.4 T, 54.2 MHz) spectrometer equipped with a homebuilt high-pressure NMR probe.[53] The temperature was measured with a built-in Pt resistor. The longitudinal ($1/T_1$) and transverse ($1/T_2$) relaxation rates were measured using the inversion recovery[54] and the Carr-Purcell-Meiboom-Gill spin-echo[55] methods, respectively. An analog complex of $LaCl_3$ and $La(ClO_4)_3$ with the exact concentration and pH were used to determine the diamagnetic contributions to the ^{17}O NMR shifts and relaxation rates in the absence of a paramagnetic solute. For all ^{17}O NMR measurements, the 90° pulse lengths have been determined at different temperatures and pressures for each sample.

VI.5.4 $^{35/37}Cl$ NMR measurements

The $^{35/37}Cl$ NMR measurements, $1/T_1$ by the inversion-recovery method,[54] $1/T_2$ by the Carr-Purcell-Meiboom-Gill method[55] were performed using Bruker Avance II-400 (9.4 T, 39.245 MHz) for $DyCl_3$ and $Dy(ClO_4)_3$ samples at ~ 2 m concentration and for $GdCl_3$ at 0.1 m and 0.2 m.

VI.6 Data fitting

All fittings have been performed using the Visualiseur/Optimiseur 3.7.0 program running on a Matlab® 8 platform.[56,57]

VI.7 References

(1)   Spedding, F. H.; Pikal, M. J.; Ayers, B. O. *J. Phys. Chem* **1966**, *70*, 2440.

(2)   Habenschuss, A.; Spedding, F. H. *J. Chem. Phys* **1979**, *70*, 2797.

(3)   Habenschuss, A.; Spedding, F. H. *J. Chem. Phys* **1979**, *70*, 3758.

(4)   Habenschuss, A.; Spedding, F. H. *J. Chem. Phys* **1980**, *73*, 442.

(5)   Narten, A. H.; Hahn, R. L. *Science* **1982**, *217*, 1249.

(6)   Narten, A. H.; Hahn, R. L. *J. Phys. Chem.* **1983**, *87*, 3193.

(7)   Annis, B. K.; Hahn, R. L.; Narten, A. H. *J. Chem. Phys.* **1985**, *82*, 2086.

(8)   Hahn, R. L.; Narten, A. H.; Annis, B. K. *J Less Common. Met.* **1986**, *122*, 233.

(9)   Cossy, C. d.; Barnes, A. C.; Enderby, J. E.; Merbach, A. E. *J. Chem. Phys.* **1989**, *90*, 3254.

(10)   Cossy, C.; Helm, L.; Powell, D. H.; Merbach, A. E. *New J. Chem.* **1995**, *19*, 27.

(11)   Yamaguchi, T.; Nomura, M.; Wakita, H.; Ohtaki, H. *J. Chem. Phys.* **1988**, *89*, 5153.

(12)   Persson, I.; D'Angelo, P.; De Panfilis, S.; Sandström, M.; Eriksson, L. *Chem. Eur. J.* **2008**, *14*, 3056.

(13)   D'Angelo, P.; Zitolo, A.; Migliorati, V.; Persson, I. *Chem. Eur. J.* **2010**, *16*, 684.

(14)   D'Angelo, P.; Zitolo, A.; Migliorati, V.; Mancini, G.; Persson, I.; Chillemi, G. *Inorg. Chem.* **2009**, *48*, 10239.

(15)   Kowall, T.; Foglia, F.; Helm, L.; Merbach, A. E. *J. Am. Chem. Soc.* **1995**, *117*, 3790.

(16)   Kowall, T.; Foglia, F.; Helm, L.; Merbach, A. E. *J. Phys. Chem.* **1995**, *99*, 13078.

(17)   Clavaguéra, C.; Pollet, R.; Soudan, J. M.; Brenner, V.; Dognon, J. P. *J. Phys. Chem. B* **2005**, *109*, 7614.

(18)   Duvail, M.; Vitorge, P.; Spezia, R. *J. Chem. Phys.* **2009**, *130*, 104501.

(19)   Hofer, T. S.; Tran, H. T.; Schwenk, C. F.; Rode, B. M. *J. Comput. Chem.* **2004**, *25*, 211.

(20)   Duvail, M.; Vitorge, P.; Spezia, R. *Chem. Phys. Lett.* **2010**, *498*, 90.

(21)   Zhang, J.; Heinz, N.; Dolg, M. *Inorg. Chem.* **2014**, *53*, 7700.

(22)   D'Angelo, P.; Spezia, R. *Chem. Eur. J.* **2012**, *18*, 11162.

(23)   Seitz, M.; Oliver, A. G.; Raymond, K. N. *J. Am. Chem. Soc.* **2007**, *129*, 11153.

(24)   D'Angelo, P.; Zitolo, A.; Migliorati, V.; Chillemi, G.; Duvail, M.; Vitorge, P.; Abadie, S.; Spezia, R. *Inorg. Chem.* **2011**, *50*, 4572.

(25)   Swaddle, T. W.; Mak, M. K. S. *Can. J. Chem.* **1983**, *61*, 473.

(26)   Reuben, J.; Fiat, D. *J. Chem. Phys* **1969**, *51*, 4918.

(27)   Southwood-Jones, R. V.; Earl, W. L.; Newman, K. E.; Merbach, A. E. *J. Chem. Phys.* **1980**, *73*, 5909.

(28)   Cossy, C.; Helm, L.; Merbach, A. E. *Inorg. Chem.* **1988**, *27*, 1973.

(29)   Cossy, C.; Helm, L.; Merbach, A. E. *Inorg. Chem.* **1989**, *28*, 2699.

(30)   Micskei, K.; Powell, D. H.; Helm, L.; Brücher, E.; Merbach, A. E. *Magn. Reson. Chem.* **1993**, *31*, 1011.

(31)   Powell, D. H.; Merbach, A. E. *Magn. Reson. Chem.* **1994**, *32*, 739.

(32)   Helm, L.; Merbach, A. E. *Chem. Rev.* **2005**, *105*, 1923.

(33)   Cossy, C.; Helm, L.; Merbach, A. E. *Inorg. Chim. Acta.* **1987**, *139*, 147.

(34)   Buenzli, J. C. G.; Yersin, J. R. *Inorg. Chem.* **1979**, *18*, 605.

(35)   Breen, P. J.; Horrocks, W. D. *Inorg. Chem.* **1983**, *22*, 536.

(36)   Kimura, T.; Kato, Y. *J. Alloys Compd.* **1998**, *278*, 92.

(37)   Silber, H. B.; Bakhshandehfar, R.; Contreras, L. A.; Gaizer, F.; Gonsalves, M.; Ismail, S. *Inorg. Chem.* **1990**, *29*, 4473.

(38)   Ruas, A.; Guilbaud, P.; Auwer, C. D.; Moulin, C.; Simonin, J.-P.; Turq, P.; Moisy, P. *J. Phys. Chem. A* **2006**, *110*, 11770.
(39)   Díaz-Moreno, S.; Ramos, S.; Bowron, D. T. *J. Phys. Chem. A* **2011**, *115*, 6575.
(40)   Molina, J. J.; Duvail, M.; Dufrêche, J.-F.; Guilbaud, P. *J. Phys. Chem. B* **2011**, *115*, 4329.
(41)   Bowron, D. T.; Diaz Moreno, S. *Coord. Chem. Rev.* **2014**, *277–278*, 2.
(42)   Sharma, V.; Bohm, F.; Seitz, M.; Schwaab, G.; Havenith, M. *Phys. Chem. Chem. Phys.* **2013**, *15*, 8383.
(43)   Alsaadi, B. M.; Rossotti, F. J. C.; Williams, R. J. P. *J. Chem. Soc., Dalton Trans.* **1980**, 2151.
(44)   Fay, D. P.; Litchinsky, D.; Purdie, N. *J. Phys. Chem.* **1969**, *73*, 544.
(45)   Ohtomo, N.; Arakawa, K. *Bull. Chem. Soc. Jpn.* **1979**, *52*, 2755.
(46)   Cummings, S.; Enderby, J. E.; Neilson, G. W.; Newsome, J. R.; Howe, R. A.; Howells, W. S.; Soper, A. K. *Nature* **1980**, *287*, 714.
(47)   Ohtomo, N.; Arakawa, K. *Bull. Chem. Soc. Jpn.* **1980**, *53*, 1789.
(48)   Ohtaki, H.; Radnai, T. *Chem. Rev.* **1993**, *93*, 1157.
(49)   Hugi, A. D.; Helm, L.; Merbach, A. E. *Helv. Chim. Acta.* **1985**, *68*, 508.
(50)   Helm, L.; Merbach, A. E. *J. Chem. Soc., Dalton Trans.* **2002**, 633.
(51)   Frey, U.; Helm, L.; Merbach, A. E. *High Press. Res.* **1990**, *2*, 237.
(52)   Ammann, C.; Meier, P.; Merbach, A. *J. Magn. Reson.* **1982**, *46*, 319.
(53)   Cusanelli, A.; Nicula-Dadci, L.; Frey, U.; Merbach, A. E. *Inorg. Chem.* **1997**, *36*, 2211.
(54)   Vold, R. L. *J. Chem. Phys* **1968**, *48*, 3831.
(55)   Meiboom, S.; Gill, D. *Rev. Sci. Instrum.* **1958**, *29*, 688.
(56)   Yerly, F. *OPTIMISEUR 3.0.0* **2002**.
(57)   Yerly, F. *VISUALISEUR 2.3.6* **2004**.

Chapter VII

General conclusions

VII.1 General conclusions

In the present work, water exchange kinetics of lanthanide(III) complexes and aqua ions were studied by multinuclear NMR spectroscopy. Chapter III to V dealt with the water exchange on lanthanide complexes having two water molecules in their first coordination sphere. Aiming to understand whether either the number of inner-sphere water molecules (q) and/or the mechanism of the water exchange varies along the lanthanide series, a comprehensive study on selected Ln^{3+} complexes with three different ligands (DO3A, DTTA-Me, AAZTAPh-NO2), was conducted. It was found that a change in q or water exchange mechanism is ligand dependent. For lanthanide complexes of both DO3A and $DTTA - Me$, the number of inner sphere water molecules was found to be constant with $q = 2$ along the series, however, for $AAZTAPh - NO_2$, a change in q from two to one when going from Dy^{3+} to Tm^{3+} was observed. Moreover, an interchange type of mechanism was indicated for all lanthanide complexes of DO3A. However, a change from a dissociative (Ln = Pr^{3+} to Gd^{3+}) to interchange (Ln = Dy^{3+}, Tm^{3+}) was obtained for $[Ln(DTTA - Me)(H_2O)_2]^-$. In the case of $[Ln(AAZTAPh - NO_2)(H_2O)_q]^-$, the results indicated an associative and dissociative interchange mechanism for Gd^{3+} and Dy^{3+} complexes and an associative activation mode for Tm^{3+} complex.

In order to understand whether the observed rate constant for the exchange of the two metal coordinated water molecules is the same or different for both sites, in chapter IV, water exchange kinetics of a fluoride complex of $[Gd(DTTA - Me)(H_2O)_2]^-$ was studied. It was found that fluoride binding facilitate the departure of the coordinated water molecule as it weakens the Gd-O$_{water}$ bonds. A seven times accelerated water exchange for $[Gd(DTTA - Me)(H_2O)F]^{2-}$ than for $[Gd(DTTA - Me)(H_2O)_2]^-$ was obtained. Hence, F$^-$ complex formation could not lead us to a final conclusion regarding the possible difference in the rate constants because of the potential influence of the more negative charge and/or structural changes.

In chapter VI, in order to get more insight on the water exchange kinetics and mechanisms on lanthanide aqua ions, concentrated perchlorates and chlorate aqueous lanthanides solutions were studied. The obtained results expand the general understanding of water exchange on the lanthanide aqua ions. Reporting the first direct experimental water exchange rate constants on neodymium(III) ion verifies the existence of a maximum of the water exchange rate constant along the lanthanide series. Furthermore, a change in the water exchange mechanism from a dissociative mechanism for light lanthanides (Ln = Nd^{3+}) to an associative mechanism for heavy lanthanides (Ln = Dy^{3+}) was observed as it has been predicted. In addition, water exchange rate constants were found to change by concentration; k_{ex} decreased by increasing neodymium(III) concentration whereas on the heavier lanthanides k_{ex} increased as the lanthanide(III) concentration increased.

Chapter VIII

Appendix

VIII.1 General Appendix

VIII.1.1   Symbols

$\Delta H^{\ddagger}$	activation enthalpy for the water exchange
$\Delta S^{\ddagger}$	activation entropy for the water exchange
$\Delta V^{\ddagger}$	activation volume for the water exchange
$\Delta \beta^{\ddagger}$	compressibility of activation
$\Delta \omega_m$	chemical shift difference in paramagnetic environment (rad s^{-1})
$\Delta \omega_r$	reduced chemical shift difference (rad s^{-1})
$\Delta \omega_{OS}$	chemical shift difference due to outer-sphere contribution (rad s^{-1})
Δ^2	mean square zero-filed-splitting energy
δ	chemical shift (ppm)
η	asymmetry parameter of the electric field gradient
μ	magnetic moment
ν_0	nuclear Larmor frequency (s^{-1})
τ	variable delay
τ_c	correlation time
τ_d	correlation time for translational diffusion
τ_m	mean residence time of the bound water molecule
τ_R	rotational correlation time
τ_R^{298}	rotational correlation time at 298 K
$\tau_{R,H}$	rotational correlation time for the Ln-H$_{water}$ vector
$\tau_{R,O}$	rotational correlation time for the Ln-O$_{water}$ vector
τ_v	correlation time for the modulation of the ZFS
χ	quadrupolar coupling constant
ω	angular frequency (rad s^{-1})
ω_0	angular Larmor frequency (rad s^{-1})
ω_I	nucleus Larmor frequency (rad s^{-1})
ω_{obs}	observed chemical shift difference (rad s^{-1})
ω_S	electron Larmor frequency (rad s^{-1})
A	associative water exchange mechanism
$A/\hbar$	hyperfine or scalar coupling constant
a_{LnH}	distance of closest approach of a second coordination sphere water proton to the metal center
B	magnetic field
B_0	static magnetic field
B_1	contact contribution to chemical shift constant
B_2	pseudocontact contribution to chemical shift constant
c	paramagnetic solute concentration
C_{Os}	outer sphere empirical constant
D	dissociative water exchange mechanism
D_{LnH}	relative translational diffution coeaficient of Ln and water proton
E_{LnH}	translational diffusion activation energy for mutual diffusion of Ln and water proton
E_R	activation energy for the rotational correlation time
E_v	activation energy for the modulation of the ZFS
g_e	Landé g-factor

$\boldsymbol{I}$	interchange water exchange mechanism
$\boldsymbol{I_a}$	associative-like interchange water exchange mechanism
$\boldsymbol{I_d}$	dissociative-like interchange water exchange mechanism
$J(\omega, \tau)$	spectral density function
M	magnetisation
M_0	equilibrium magnetisation along the z-axis
M_{xy}	magnetisation component in the xy-plane
M_z	magnetisation component along the z-axis
P_m	mole fraction of bound water
P	pressure
q	hydration number (number of water molecules in the inner sphere of a complex)
r	radius
r_1	relaxivity
r_{LnH}	water proton-lanthanide distance in the inner sphere of the complex
r_{LnO}	water oxygen-lanthanide distance in the inner sphere of the complex
S	spin of the particle S
T	temperature
T_1	longitudinal relaxation time
T_2	transverse relaxation time
$T_{1,d}$	longitudinal relaxation time of the diamagnetic reference
$T_{2,d}$	transverse relaxation time of the diamagnetic reference
T_{1e}	electron spin longitudinal relaxation time
T_{2e}	electron spin transverse relaxation time
T_{1m}	longitudinal relaxation time of the bound water molecule
T_{2m}	transverse relaxation time of the bound water molecule
$T_{i,Cu}$	nuclear relaxation time due to Curie relaxation
$T_{i,dd}$	nuclear relaxation time due to dipolar relaxation
$T_{i,obs}$	observed nuclear relaxation time
$T_{i,p}$	nuclear relaxation time in paramagnetic environment
$T_{i,q}$	nuclear relaxation time due to quadrupolar relaxation
$T_{i,Sc}$	nuclear relaxation time due to scalar relaxation

VIII.1.2 Abbreviations

BMS	bulk magnetic susceptibility
CA	contrast agent
CPMG	Carr-Purcell-Meiboom-Gill
DFT	density functional theory
FID	free induction decay
IR	inversion recovery pulse sequence
IS	inner-sphere
Me	methyl
MRI	magnetic resonance imaging
NMR	nuclear magnetic resonance
NMRD	nuclear magnetic resonance dispersion
OS	outer-sphere
PET	positron emission tomography
PRE	paramagnetic relaxation enhancement
RF	radiofrequency
SBM	Solomon–Bloembergen–Morgan
SPECT	single-photon emission computed tomography
TFA	trifluoroacetic acid
ZFS	zero-field-splitting

VIII.1.3 Constants and numbers

γ_e	gyromagnetic ratio of electron	$-1.7609 \cdot 10^{11}$	rad T^{-1} s^{-1}
γ_H	gyromagnetic ratio of proton	$2.6751 \cdot 10^{8}$	rad T^{-1} s^{-1}
γ_O	gyromagnetic ratio of oxygen	$-3.626 \cdot 10^{7}$	rad T^{-1} s^{-1}
μ_0	vacuum permeability	$4\pi\ 10^{-7}$	N A^{-2}
μ_B	Bohr magneton	$9.274\ 10^{-24}$	J T^{-1}
h	Planck constant	$6.6261\ 10^{-34}$	J s
$\hbar$	reduced Planck constant ($= h/2\pi$)	$1.0545\ 10^{-34}$	J s
k_B	Boltzmann constant	$1.3807\ 10^{-34}$	J K^{-1}
N_A	Avogadro constant	$6.022\ 10^{-23}$	mol^{-1}
R	perfect gas constant	8.3145	J K^{-1} mol^{-1}

VIII.2   Appendix to chapter I

Table VIII-1. NMR properties of some elements

Isotope	Natural abundance (%)	Nuclear spin (*I*)	Magnetogyric ratio (γ) ($\times 10^7$ rad T^{-1} s^{-1})	Quadrupole moment (*eQ*) ($\times 10^{28}$ C m^{-2})
^{17}O	3.7×10^{-2}	5/2	-3.6279	-0.02578
^{1}H	99.98	1/2	26.7519	-
^{19}F	100	1/2	25.181	-
^{35}Cl	75.53	3/2	2.624	-0.08249
^{37}Cl	24.47	3/2	2.1842	-0.06493

VIII.3   Appendix to chapter III

VIII.3.1   Lanthanide properties

Table VIII-2. Values of $\langle S_z \rangle$ and C^D for the selected lanthanides at room temperature[1,2]

Ln	$\langle S_z \rangle$	C^D
Pr	-2.956	-11
Nd	-4.452	-4.2
Sm	0.224	-0.7
Gd	31.5	0
Dy	28.565	-100
Tm	8.21	53
Yb	2.589	22

VIII.3.2 ^{17}O NMR experimental data of [Ln(DO3A)(H$_2$O)$_2$]

Table VIII-3. Variable temperature ^{17}O longitudinal (1/T$_1$) and transverse (1/T$_2$) relaxation rates and chemical shifts (δ) of [Pr(DO3A)(H$_2$O)$_2$] and the chemical shifts of acidified water as the reference (δ_d), B$_0$ = 9.4 T and 18.8 T, pH = 5.7, [Pr^{3+}] = 115.1 mM

B$_0$ = 9.4 T

T (K)	δ (ppm)	δ_d (ppm)	1/T$_1$ (s^{-1})	1/T$_2$ (s^{-1})
278	8.7	7.6	434	482
283	8.5	7.4	369	411
288	8.2	7.1	305	336
293	8.1	6.9	271	300
298	7.8	6.6	228	249
303	7.6	6.5	206	226
308	7.3	6.1	176	192
313	7.1	6.0	161	176
318	6.9	5.7	140	153
323	6.7	5.5	129	141
328	6.4	5.2	114	124
338	6.0	4.8	95	103
358	5.3	4.0	67	72

B$_0$ = 18.8 T

T (K)	δ (ppm)	δ_d (ppm)	1/T$_1$ (s^{-1})	1/T$_2$ (s^{-1})
278	5.2	4.0	615	793
283	5.0	3.8	483	637
288	4.7	3.5	403	530
293	4.5	3.3	351	469
298	4.2	3.1	300	399
303	4.0	2.9	271	354
308	3.8	2.6	230	303
313	3.6	2.4	218	281
318	3.4	2.2	181	239
333	2.8	1.6	137	172
338	2.6	1.3	114	145
358	1.8	0.5	77	96

Table VIII-4. Variable temperature ^{17}O longitudinal ($1/T_1$) and transverse ($1/T_2$) relaxation rates and chemical shifts (δ) of $[Nd(DO3A)(H_2O)_2]$ and the chemical shifts of acidified water as the reference (δ_d), $B_0 = 9.4$ T and 18.8 T, pH = 5.7, $[Nd^{3+}] = 85.4$ mM

$B_0 = 9.4$ T

T (K)	δ (ppm)	δ_d (ppm)	$1/T_1$ (s^{-1})	$1/T_2$ (s^{-1})
278	9.0	7.6	282	373
283	8.8	7.4	235	301
288	8.5	7.1	202	250
293	8.3	6.9	180	215
298	8.0	6.6	153	179
303	7.8	6.5	139	158
308	7.5	6.1	120	135
313	7.4	6.0	110	121
318	7.0	5.7	97	106
323	6.9	5.5	89	96
328	6.6	5.2	80	85
338	6.1	4.8	67	70
358	5.3	4.0	55	56

$B_0 = 18.8$ T

T (K)	δ (ppm)	δ_d (ppm)	$1/T_1$ (s^{-1})	$1/T_2$ (s^{-1})
278	5.5	4.0	316	627
283	5.2	3.8	265	533
288	4.9	3.5	218	417
293	4.7	3.3	197	359
298	4.5	3.1	162	267
303	4.2	2.9	150	238
308	4.0	2.6	126	182
313	3.8	2.4	118	166
318	3.6	2.2	101	133
333	2.9	1.6	78	94
338	2.6	1.3	69	80
358	1.8	0.5	50	55

Table VIII-5. Variable temperature ^{17}O longitudinal ($1/T_1$) and transverse ($1/T_2$) relaxation rates and chemical shifts (δ) of $[Sm(DO3A)(H_2O)_2]$ and the chemical shifts of acidified water as the reference (δ_d), $B_0 = 9.4$ T and 18.8 T, pH = 5.7, $[Sm^{3+}] = 101.6$ mM

$B_0 = 9.4$ T

T (K)	δ (ppm)	δ_d (ppm)	$1/T_1$ (s^{-1})	$1/T_2$ (s^{-1})
278	7.6	7.7	292	314
283	7.5	7.5	251	269
288	7.1	7.2	209	224
293	7.0	7.0	186	198
298	6.7	6.7	158	169
303	6.4	6.5	143	152
308	6.2	6.3	124	132
313	5.9	6.0	113	121
318	5.8	5.8	100	106
323	5.6	5.6	92	98
328	5.3	5.4	82	88
338	4.8	4.9	69	73

$B_0 = 18.8$ T

T (K)	δ (ppm)	δ_d (ppm)	$1/T_1$ (s^{-1})	$1/T_2$ (s^{-1})
278	4.0	4.0	317	340
283	3.6	3.8	270	290
288	3.5	3.5	222	250
293	3.2	3.3	205	219
298	3.0	3.1	166	177
303	2.8	2.8	156	166
308	2.6	2.6	129	137
313	2.4	2.3	122	128
318	2.2	2.2	104	109
333	1.6	1.5	80	85
338	1.4	1.3	71	75
358	0.8	0.5	52	54

Table VIII-6. Variable temperature ^{17}O longitudinal ($1/T_1$) and transverse ($1/T_2$) relaxation rates and chemical shifts (δ) of $[Dy(DO3A)(H_2O)_2]$ and the chemical shifts of acidified water as the reference (δ_d), $B_0 = 9.4$ T and 18.8 T, pH = 5.7, $[Dy^{3+}] = 114.7$ mM

$B_0 = 9.4$ T

T (K)	δ (ppm)	δ_d (ppm)	$1/T_1$ (s^{-1})	$1/T_2$ (s^{-1})
278	-5.5	7.7	293	943
283	-5.4	7.4	249	761
288	-5.3	7.1	210	605
293	-5.2	6.8	185	501
298	-5.0	6.6	158	401
303	-4.9	6.4	143	334
308	-4.8	6.1	124	267
313	-4.7	5.9	113	226
318	-4.5	5.7	100	184
323	-4.5	5.5	92	158
328	-4.4	5.2	83	133
338	-4.2	4.9	69	100
358	-3.7	4.4	50	62

$B_0 = 18.8$ T

T (K)	δ (ppm)	δ_d (ppm)	$1/T_1$ (s^{-1})	$1/T_2$ (s^{-1})
278	-9.1	4.1	290	3015
283	-9.0	3.8	236	2500
288	-8.9	3.5	195	1767
293	-8.8	3.2	176	1299
298	-8.7	2.9	147	963
303	-8.5	2.6	136	846
308	-8.5	2.6	115	627
313	-8.3	2.2	108	554
318	-8.2	2.2	94	408
333	-7.9	1.4	73	231
338	-7.9	1.3	65	178
358	-7.5	0.5	50	96

Table VIII-7. Variable temperature ^{17}O longitudinal ($1/T_1$) and transverse ($1/T_2$) relaxation rates and chemical shifts (δ) of $[Tm(DO3A)(H_2O)_2]$ and the chemical shifts of acidified water as the reference (δ_d), $B_0 = 9.4$ T and 18.8 T, pH = 5.7, $[Tm^{3+}] = 114.7$ mM

$B_0 = 9.4$ T

T (K)	δ (ppm)	δ_d (ppm)	$1/T_1$ (s^{-1})	$1/T_2$ (s^{-1})
278	4.7	6.0	308	333
283	4.5	5.9	254	276
289	4.2	5.5	217	235
294	4.1	5.4	188	207
299	3.8	5.1	162	177
304	3.7	5.0	145	158
309	3.4	4.6	126	136
315	3.3	4.5	114	124
320	3.0	4.2	101	110
325	2.8	4.0	93	102
330	2.6	3.7	83	89
341	2.2	3.3	69	76
358	1.4	2.5	55	59

$B_0 = 18.8$ T

T (K)	δ (ppm)	δ_d (ppm)	$1/T_1$ (s^{-1})	$1/T_2$ (s^{-1})
278	4.8	6.2	307	418
283	4.7	6.0	263	359
293	4.3	5.6	196	264
298	4.0	5.3	164	220
303	3.9	5.3	153	203
308	3.6	4.9	129	169
313	3.6	4.9	123	163
318	3.3	4.5	104	134
328	3.1	4.3	90	117
338	2.6	3.8	71	91
348	2.3	3.4	63	81
358	2.0	3.1	53	69

Table VIII-8. Variable temperature ^{17}O longitudinal ($1/T_1$) and transverse ($1/T_2$) relaxation rates and chemical shifts (δ) of $[Yb(DO3A)(H_2O)_2]$ and the chemical shift of acidified water as the reference (δ_d), $B_0 = 9.4$ T and 18.8 T, pH = 5.7, $[Yb^{3+}] = 123.8$ mM

$B_0 = 9.4$ T

T (K)	δ (ppm)	δ_d (ppm)	$1/T_1$ (s^{-1})	$1/T_2$ (s^{-1})
278	5.1	6.0	294	307
283	5.0	5.8	250	262
288	4.9	5.7	209	219
293	4.6	5.5	185	194
298	4.5	5.4	156	165
303	4.3	5.1	142	149
308	4.1	4.9	122	129
313	3.9	4.7	112	118
318	3.7	4.5	99	104
323	3.5	4.3	91	96
328	3.3	4.0	81	85
338	2.9	3.7	68	72
358	2.5	3.2	48	50

$B_0 = 18.8$ T

T (K)	δ (ppm)	δ_d (ppm)	$1/T_1$ (s^{-1})	$1/T_2$ (s^{-1})
278	5.8	6.7	311	365
283	5.8	6.7	275	322
288	5.5	6.3	219	261
293	5.5	6.4	201	238
298	5.1	5.9	164	196
303	5.2	6.0	152	180
308	4.8	5.6	127	153
313	4.9	5.6	120	143
318	4.4	5.2	102	123
333	4.1	4.8	78	93
338	3.7	4.4	69	83
358	3.0	3.8	50	60

Table VIII-9. Variable pressure ^{17}O longitudinal ($1/T_1$) and transverse ($1/T_2$) relaxation rates of $[Pr(DO3A)(H_2O)_2]$, $B_0 = 9.4$ T, pH = 5.7, $[Pr^{3+}] = 96.3$ mM

P (MPa)	$1/T_1$ (s^{-1})	$1/T_2$ (s^{-1})
2.3	184.8	221.7
21	182.2	219.4
34	181.0	218.4
41	180.5	217.8
51	179.9	217.5
61	178.8	216.5
78	177.1	215.0
91	176.2	214.3
103	174.9	213.2
118	174.4	213.0
130	173.9	212.6
160	172.0	211.1

Table VIII-10. Variable pressure ^{17}O longitudinal ($1/T_1$) and transverse ($1/T_2$) relaxation rates of $[Nd(DO3A)(H_2O)_2]$, $B_0 = 9.4$ T, pH = 5.7, $[Nd^{3+}] = 60.2$ mM

P (MPa)	$1/T_1 (s^{-1})$	$1/T_2 (s^{-1})$
0.6	171.5	204.2
2.3	171.8	204.5
15	171.5	204.3
20	169.2	202.0
32	169.3	202.2
40	167.2	200.2
50	166.5	199.6
60	164.7	197.9
71	164.7	197.9
76	164.0	197.0
81	163.5	196.7
90	163.3	196.7
100	161.8	195.1
118	160.0	193.6
125	159.8	193.3
135	159.3	193.0
140	158.6	192.1
148	157.5	191.1
160	156.0	189.8

Table VIII-11. Variable pressure ^{17}O longitudinal ($1/T_1$) and transverse ($1/T_2$) relaxation rates of $[Dy(DO3A)(H_2O)_2]$, $B_0 = 9.4$ T, pH = 5.7, $[Dy^{3+}] = 86.3$ mM

P (MPa)	$1/T_1 (s^{-1})$	$1/T_2 (s^{-1})$
0.8	179.0	445.7
1.2	178.3	446.9
6	177.9	446.6
22	175.1	452.3
39	173.4	456.6
62	169.5	461.3
79	166.9	467.9
101	164.7	472.8
119	163.3	479.2
140	161.8	485.0
161	160.1	492.4

Table VIII-12. Variable pressure ^{17}O longitudinal ($1/T_1$) and transverse ($1/T_2$) relaxation rates of $[Tm(DO3A)(H_2O)_2]$, $B_0 = 9.4$ T, pH = 5.7, $[Tm^{3+}] = 114.7$ mM

P (MPa)	$1/T_1 (s^{-1})$	$1/T_2 (s^{-1})$
0.7	174.9	230.6
3.8	174.5	230.4
6	174.1	230.0
22	171.2	227.4
39	169.5	225.8
61	166.8	223.4
80	165.0	221.8
102	163.0	219.9
122	160.8	218.3
141	159.9	217.5
162	158.8	216.4

VIII.3.3 ^{17}O NMR experimental data of [Ln(DTTA-Me)(H$_2$O)$_2$]$^-$

Table VIII-13. Variable temperature ^{17}O longitudinal (1/T$_1$) and transverse (1/T$_2$) relaxation rates and chemical shifts (δ) of [Pr(DTTA $-$ Me)(H$_2$O)$_2$]$^{-1}$ and the chemical shift of acidified water as the reference (δ_d), B$_0$ = 9.4 T and 18.8 T, pH = 5.7, [Pr^{3+}] =114.8 mM

B$_0$ = 9.4 T

T (K)	δ (ppm)	δ_d (ppm)	1/T$_1$ (s^{-1})	1/T$_2$ (s^{-1})
278	9.2	7.6	387	434
283	8.9	7.4	331	369
288	8.8	7.1	274	305
293	8.6	6.9	245	271
298	8.3	6.6	205	228
303	8.1	6.5	187	206
308	7.9	6.1	160	176
313	7.7	6.0	147	161
318	7.5	5.7	128	140
323	7.3	5.5	118	129
328	7.1	5.2	105	114
338	6.8	4.9	87	95
358	6.2	4.2	62	67

B$_0$ = 18.8 T

T (K)	δ (ppm)	δ_d (ppm)	1/T$_1$ (s^{-1})	1/T$_2$ (s^{-1})
278	5.6	4.0	430	615
283	5.4	3.8	340	483
288	5.1	3.5	291	403
293	4.9	3.3	250	351
298	4.7	3.1	214	300
303	4.5	2.8	198	271
308	4.4	2.6	165	230
313	4.1	2.4	153	218
318	4.0	2.2	131	181
333	3.3	1.5	99	137
338	3.2	1.3	87	114
358	2.4	0.5	62	79

Table VIII-14. Variable temperature ^{17}O longitudinal ($1/T_1$) and transverse ($1/T_2$) relaxation rates and chemical shifts (δ) of $[Nd(DTTA - Me)(H_2O)_2]^{-1}$ and the chemical shift of acidified water as the reference (δ_d), $B_0 = 9.4$ T and 18.8 T, pH = 5.7, $[Nd^{3+}] = 86.1$ mM

$B_0 = 9.4$ T

T (K)	δ (ppm)	δ_d (ppm)	$1/T_1$ (s^{-1})	$1/T_2$ (s^{-1})
278	9.3	7.6	321	415
283	9.2	7.4	273	338
288	8.8	7.1	229	275
293	8.8	6.9	203	237
298	8.3	6.6	173	198
303	8.2	6.5	156	174
308	7.9	6.1	136	149
313	7.7	6.0	124	134
318	7.4	5.7	109	115
323	7.2	5.5	100	104
328	6.9	5.2	90	93
338	6.4	4.7	75	77
358	5.6	4.0	60	61

$B_0 = 18.8$ T

T (K)	δ (ppm)	δ_d (ppm)	$1/T_1$ (s^{-1})	$1/T_2$ (s^{-1})
278	5.9	4.1	359	632
283	5.6	3.8	300	517
288	5.3	3.5	246	393
293	5.1	3.3	223	335
298	4.8	3.1	182	250
303	4.6	2.9	168	221
308	4.4	2.7	141	173
313	4.2	2.5	131	158
318	4.0	2.3	112	129
333	3.5	1.8	85	93
338	3.3	1.6	75	82
358	2.6	1.0	54	56

Table VIII-15. Variable temperature ^{17}O longitudinal ($1/T_1$) and transverse ($1/T_2$) relaxation rates and chemical shifts (δ) of $[Sm(DTTA - Me)(H_2O)_2]^{-1}$ and the chemical shift of acidified water as the reference (δ_d), $B_0 = 9.4$ T and 18.8 T, pH = 5.7, $[Sm^{3+}] = 96.4$ mM

$B_0 = 9.4$ T

T (K)	δ (ppm)	δ_d (ppm)	$1/T_1$ (s^{-1})	$1/T_2$ (s^{-1})
278	7.7	7.7	304	313
283	7.5	7.5	260	267
288	7.1	7.2	216	223
293	7.1	7.0	192	196
298	6.7	6.7	163	168
303	6.4	6.5	147	151
308	6.2	6.3	127	131
313	6.0	6.0	116	118
318	5.8	5.8	102	105
323	5.6	5.6	94	96
328	5.3	5.4	84	86
338	4.9	4.9	70	72

$B_0 = 18.8$ T

T (K)	δ (ppm)	δ_d (ppm)	$1/T_1$ (s^{-1})	$1/T_2$ (s^{-1})
278	4.0	4.0	330	339
288	3.5	3.5	229	235
293	3.2	3.3	210	215
298	3.0	3.1	170	174
303	2.8	2.8	158	161
308	2.6	2.6	132	134
313	2.4	2.3	123	125
318	2.2	2.2	105	107
333	1.7	1.5	79	81
338	1.5	1.3	70	72
358	0.9	0.5	50	51

Table VIII-16. Variable temperature ^{17}O longitudinal ($1/T_1$) and transverse ($1/T_2$) relaxation rates and chemical shifts (δ) of $[Dy(DTTA - Me)(H_2O)_2]^{-1}$ and the chemical shift of acidified water as the reference (δ_d), $B_0 = 9.4$ T and 18.8 T, pH = 5.7, $[Dy^{3+}] = 104.3$ mM

$B_0 = 9.4$ T

T (K)	δ (ppm)	δ_d (ppm)	$1/T_1$ (s^{-1})	$1/T_2$ (s^{-1})
278	-2.7	7.5	327	576
283	-2.8	7.4	267	451
288	-2.8	7.2	225	361
293	-2.8	6.9	196	287
298	-2.8	6.6	167	235
303	-2.8	6.5	150	200
308	-2.8	6.1	129	167
313	-2.8	6.0	118	145
318	-2.8	5.7	104	124
323	-2.8	5.5	95	112
328	-2.9	5.2	85	97
338	-2.9	5.0	71	78
358	-2.9	4.3	51	54

$B_0 = 18.8$ T

T (K)	δ (ppm)	δ_d (ppm)	$1/T_1$ (s^{-1})	$1/T_2$ (s^{-1})
278	-6.2	4.2	360	1368
283	-6.2	3.9	298	973
288	-6.2	3.6	244	745
293	-6.3	3.4	217	588
298	-6.3	3.0	179	428
303	-6.3	3.0	164	368
308	-6.3	2.7	138	274
313	-6.3	2.4	128	251
318	-6.3	2.3	109	192
333	-6.3	1.5	82	119
338	-6.3	1.4	73	100
358	-6.3	0.8	52	63

Table VIII-17. Variable temperature ^{17}O longitudinal ($1/T_1$) and transverse ($1/T_2$) relaxation rates and chemical shifts (δ) of $[Tm(DTTA - Me)(H_2O)_2]^{-1}$ and the chemical shift of acidified water as the reference (δ_d), $B_0 = 9.4$ T and 18.8 T, pH = 5.7, $[Tm^{3+}] = 93.1$ mM

$B_0 = 9.4$ T

T (K)	δ (ppm)	δ_d (ppm)	$1/T_1$ (s^{-1})	$1/T_2$ (s^{-1})
278	4.7	6.0	308	314
283	4.6	5.9	257	260
289	4.4	5.5	217	220
294	4.3	5.4	189	191
299	4.0	5.1	162	164
304	4.0	5.0	145	146
309	3.7	4.6	126	127
315	3.7	4.5	114	115
320	3.4	4.2	100	100
325	3.3	4.0	92	92
330	3.1	3.7	82	82
341	2.7	3.3	68	68
358	2.2	2.7	52	52

$B_0 = 18.8$ T

T (K)	δ (ppm)	δ_d (ppm)	$1/T_1$ (s^{-1})	$1/T_2$ (s^{-1})
278	4.9	6.3	315	335
293	4.6	5.7	197	205
298	4.2	5.3	165	173
303	4.3	5.3	152	157
308	3.9	4.9	129	134
313	4.0	4.9	123	126
318	3.7	4.5	103	106
328	3.6	4.3	89	91
338	3.1	3.7	70	72
348	2.8	3.4	62	62
358	2.6	3.0	52	52

Table VIII-18. Variable temperature ^{17}O longitudinal ($1/T_1$) and transverse ($1/T_2$) relaxation rates and chemical shifts (δ) of $[Yb(DTTA - Me)(H_2O)_2]^{-1}$ and the chemical shift of acidified water as the reference (δ_d), $B_0 = 9.4$ T and 18.8 T, pH = 5.7, $[Yb^{3+}] = 100.5$ mM

$B_0 = 9.4$ T

T (K)	δ (ppm)	δ_d (ppm)	$1/T_1 (s^{-1})$	$1/T_2 (s^{-1})$
278	4.2	6.0	292	303
283	4.1	5.8	248	258
288	4.0	5.7	208	217
293	3.8	5.5	182	189
298	3.7	5.4	156	163
303	3.5	5.1	139	145
308	3.3	4.9	121	127
313	3.2	4.7	110	114
318	3.0	4.5	98	101
323	2.8	4.3	89	92
328	2.6	4.0	80	83
338	2.2	3.7	67	70
358	1.8	3.2	48	50

$B_0 = 18.8$ T

T (K)	δ (ppm)	δ_d (ppm)	$1/T_1 (s^{-1})$	$1/T_2 (s^{-1})$
278	4.9	6.7	311	360
283	4.9	6.7	275	319
288	4.6	6.3	219	255
293	4.7	6.4	201	231
298	4.3	5.9	164	188
303	4.4	6.0	152	174
308	4.0	5.6	127	145
313	4.1	5.6	120	136
318	3.7	5.2	102	117
333	3.4	4.8	78	88
338	3.0	4.4	69	79
358	2.4	3.8	50	56

Table VIII-19. Variable pressure ^{17}O longitudinal ($1/T_1$) and transverse ($1/T_2$) relaxation rates of $[Pr(DTTA - Me)(H_2O)_2]^{-1}$, $B_0 = 9.4$ T, pH = 5.7, $[Pr^{3+}] = 103.2$ mM

P (MPa)	$1/T_1 (s^{-1})$	$1/T_2 (s^{-1})$
2.5	199.0	225.0
20	196.3	224.2
41	193.8	222.8
55	192.0	221.8
69	191.0	221.5
80	189.0	220.7
100	187.2	220.3
120	185.1	219.8
141	183.2	219.3
150	181.8	218.9
160	180.8	218.7

Table VIII-20. Variable pressure ^{17}O longitudinal ($1/T_1$) and transverse ($1/T_2$) relaxation rates of $[Nd(DTTA - Me)(H_2O)_2]^{-1}$, $B_0 = 9.4$ T, pH = 5.7, $[Nd^{3+}] = 86.5$ mM

P (MPa)	$1/T_1 (s^{-1})$	$1/T_2 (s^{-1})$
7.6	178.4	210.5
22	178.1	210.8
41	175.7	211.5
50	174.6	212.2
62	174.5	212.6
81	172.2	213.3
99	170.1	214.7
120	169.2	215.2
139	169.1	216.7
160	165.7	218.1

Table VIII-21. Variable pressure ^{17}O longitudinal ($1/T_1$) and transverse ($1/T_2$) relaxation rates of $[\text{Dy(DTTA}-\text{Me})(\text{H}_2\text{O})_2]^{-1}$, $B_0 = 9.4$ T, pH = 5.7, $[\text{Dy}^{3+}] = 103.5$ mM

P (MPa)	$1/T_1$ (s^{-1})	$1/T_2$ (s^{-1})
0.6	181.1	269.3
0.8	181.0	269.3
11	180.0	269.8
23	178.6	270.3
39	176.2	271.9
62	174.2	273.0
79	172.8	276.7
101	171.2	279.3
116	169.8	280.2
141	167.5	283.5
161	166.6	284.9

Table VIII-22. Variable pressure ^{17}O longitudinal ($1/T_1$) and transverse ($1/T_2$) relaxation rates of $[\text{Tm(DTTA}-\text{Me})(\text{H}_2\text{O})_2]^{-1}$, $B_0 = 9.4$ T, pH = 5.7, $[\text{Tm}^{3+}] = 93.1$ mM

P (MPa)	$1/T_1$ (s^{-1})	$1/T_2$ (s^{-1})
0.7	188.4	198.2
4.3	187.2	197.2
11	185.2	195.5
21	184.5	194.8
32	182.1	192.5
39	181.1	191.8
48	180.2	190.8
62	177.8	189.2
67	176.8	188.1
71	175.2	187.0
100	174.3	186.4
114	170.9	183.3
139	170.0	182.9
158	166.0	179.6

VIII.3.4 Full list of parameters obtained from the analysis of ^{1}H and ^{17}O NMR data

Table VIII-23. Full list of parameters obtained from the nonlinear least squares fit of ^{1}H and ^{17}O NMR data for $[\text{Ln(DO3A)(H}_2\text{O})_2]$ complexes. Reported errors correspond to one standard deviation obtained by statistical analysis

		Pr^{3+}	Nd^{3+}	Dy^{3+}	Tm^{3+}	Yb^{3+}
$\Delta H^{\ddagger}$	(kJ mol^{-1})	23 ± 1	40 ± 1	29 ± 1	13 ± 1	12 ± 1
k_{ex}^{298}	(10^6 s^{-1})	1.6 ± 0.1	2.9 ± 0.1	16.6 ± 0.3	3.2 ± 0.1	2.2 ± 0.1
$\Delta S^{\ddagger}$	(J mol^{-1}K^{-1})	-50 ± 2	+12 ± 2	-9 ± 3	-77 ± 3	-83 ± 3
$\Delta V^{\ddagger}$	(cm^3 mol^{-1})	-0.4 ± 0.2	-0.5 ± 0.2	-0.5 ± 0.3	-0.9 ± 0.5	-
$\tau_{R,O}^{298}$	(ps)	107 ± 4	105 ± 3	98 ± 3	93 ± 2	96 ± 3
E_R	(kJ mol^{-1})	22 ± 1	22 ± 1	21 ± 1	23 ± 1	24 ± 1
r_{LnH}	(Å)	3.43 ± 0.6	3.41 ± 0.4	3.28 ± 0.1	3.12 ± 0.1	3.11 ± 0.3
T_e	(ps)	0.5 ± 0.2	0.6 ± 0.2	0.6 ± 0.1	0.4 ± 0.1	0.5 ± 0.3
B_1	(K)	-0.2 ± 0.01	-0.2 ± 0.01	0.1 ± 0.02	0.1 ± 0.01	0.1 ± 0.01
B_2	(K^2)	38 ± 4	23 ± 2	231 ± 5	-6 ± 3	-9 ± 2

Table VIII-24. Full list of parameters obtained from the nonlinear least squares fit of ^1H and ^{17}O NMR data for $[Ln(DTTA-Me)(H_2O)_2]^-$ complexes. Reported errors correspond to one standard deviation obtained by statistical analysis

		Pr^{3+}	Nd^{3+}	Dy^{3+}	Tm^{3+}	Yb^{3+}
$\Delta H^{\ddagger}$	(kJ mol^{-1})	26 ± 1	49 ± 1	36 ± 1	13 ± 1	13 ± 1
k_{ex}^{298}	(10^6 s^{-1})	3.5 ± 0.1	5.8 ± 0.1	40.6 ± 0.9	26.7 ± 0.8	13.9 ± 0.1
$\Delta S^{\ddagger}$	(J mol^{-1}K^{-1})	-31 ± 1	+49 ± 1	+21 ± 2	-60 ± 2	-64 ± 3
$\Delta V^{\ddagger}$	(cm^3 mol^{-1})	+7.0 ± 0.2	+6.8 ± 0.2	+1.8 ± 0.2	+0.4 ± 0.4	-
$\tau_{R,O}^{298}$	(ps)	152 ± 4	156 ± 4	149 ± 6	146 ± 3	133 ± 1
E_R	(kJ mol^{-1})	24 ± 1	21 ± 1	26 ± 2	23 ± 1	23 ± 1
r_{LnH}	(Å)	3.37 ± 0.5	3.36 ± 0.7	3.28 ± 0.1	3.16 ± 0.1	3.12 ± 0.1
T_e	(ps)	0.5 ± 0.1	0.6 ± 0.1	0.7 ± 0.2	0.4 ± 0.1	0.5 ± 0.1
B_1	(K)	-0.4 ± 0.01	-0.3 ± 0.02	0.4 ± 0.02	0.3 ± 0.01	0.1 ± 0.01
B_2	(K^2)	79 ± 2	34 ± 5	104 ± 6	82 ± 4	2 ± 1

VIII.4 Appendix to chapter IV

VIII.4.1 ^1H NMR experimental data

Table VIII-25. ^1H relaxivities, r_1, of $[Gd(DTTA-Me)(H_2O)_2]^-$, T = 25°C, B$_0$ = 0.7 T (30 MHz), [Gd^{3+}] = 0.16 mM, I = 0.3 M

[DTTA − Me^{4-}]/[Gd^{3+}]	r_1 (mM^{-1} S^{-1})
1.0	7.41
2.8	7.40
4.8	7.37
6.2	7.34
8.4	7.31
10.2	7.27
11.8	7.25
13.9	7.21
16.3	7.19
17.4	7.18
19.5	7.16

Table VIII-26. ^1H relaxivities, r_1, of $[Gd(DTTA-Me)(H_2O)_xF_y]^z$, T = 25°C and 37°C, B$_0$ = 0.7 T (30 MHz), pH = 7.4, [Gd^{3+}] = 0.12 mM, I = 1.3 M

[F$^-$]/[Gd^{3+}]	25°C	37°C
0	8.10	6.25
445	7.39	5.55
814	7.15	5.30
1208	7.03	5.20
1677	6.93	5.10
2127	6.88	5.08
2507	6.95	5.02
2931	6.85	5.00
3303	6.81	5.00
3610	6.79	5.04

Table VIII-27. Variable temperature ^{1}H relaxivities, r_1, of $\left[Gd(DTTA - Me)(H_2O)_xF_y\right]^z$ at different temperatures, B_0 = 4.7 T, I = 1 M, pH = 7.4, $[Gd^{3+}]$ = 0.12 mM

$[F^-]/[Gd^{3+}]$	15°C	20°C	30°C	35°C	45°C	50°C	55°C	65°C
0	9.65	5.51	4.16	3.22	4.03	4.90	6.98	7.81
445	9.00	4.86	3.55	2.66	3.36	4.20	6.06	7.13
814	8.82	4.64	3.28	2.45	3.15	3.98	5.82	6.91
1208	8.70	4.48	3.25	2.37	3.03	3.84	5.68	6.87
1677	8.60	4.42	3.20	2.32	3.01	3.74	5.51	6.73
2127	8.62	4.33	3.11	2.29	2.93	3.73	5.44	6.67
2507	8.56	4.27	3.06	2.28	2.89	3.73	5.44	6.70
2931	8.54	4.28	3.06	2.26	2.91	3.66	5.33	6.55
3303	8.51	4.26	3.04	2.23	2.86	3.68	5.33	6.58
3610	8.50	4.25	3.03	2.22	2.84	3.63	5.31	6.57

Table VIII-28. Variable pressure ^{1}H relaxivities, r_1, of $\left[Gd(DTTA - Me)(H_2O)_xF_y\right]^z$, T = 20°C, B_0 = 9.4 T, pH = 7.4, $[F^-]/[Gd^{3+}]$ = 28, $[F^-]$ = 0.2 M

P (MPa)	r_1 (mM^{-1} s^{-1})
3	6.50
21	6.60
40	6.72
61	6.78
72	6.90
80	6.92
100	7.00
110	7.07
121	7.07
139	7.13
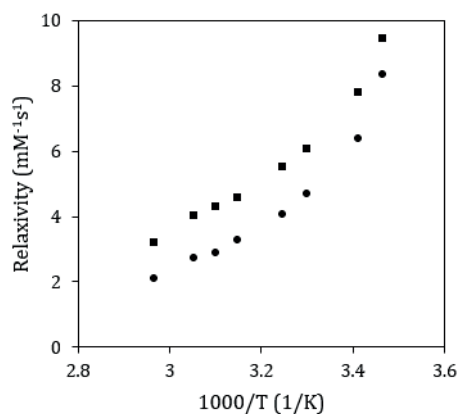
Figure VIII-1. Temperature dependence of proton relaxivities of $[Gd(DTTA - Me)(H_2O)_2]^-$ (■) and $[Gd(DTTA - Me)(H_2O)F]^{2-}$ (●) complexes, $[Gd^{3+}]$ = 0.12 mM, B_0 = 4.7 T (200 MHz), pH = 7.4.

VIII.4.2 ^{19}F NMR experimental data

Table VIII-29. Transverse ^{19}F relaxation rates ($1/T_2$) measured on free fluoride in aqueous solutions of $[Gd(DTTA - Me)(H_2O)_2]^-$ and F^-

T (K)	$1/T_2$ (s^{-1})	
	$[F]_{tot} = 0.210$ M	$[F]_{tot} = 0.313$ M
277	43	35
282	62	51
287	90	90
292	132	125
298	202	185
303	320	267
308	523	393
314	635	578
319	988	876
324	1413	1098
329	1700	1409

VIII.4.3 ^{17}O NMR experimental data

Table VIII-30. Variable temperature ^{17}O transverse ($1/T_2$) relaxation rates of $\left[Gd(DTTA - Me)(H_2O)_xF_y\right]^z$ and of the reference ($1/T_{2,d}$), $B_0 = 9.4$ T, $[Gd^{3+}] = 10$ mM

	F = 0 M		F = 0.10 M		F = 0.20 M	
T (K)	$1/T_2$ (s^{-1})	$1/T_{2,d}$ (s^{-1})	$1/T_2$ (s^{-1})	$1/T_{2,d}$ (s^{-1})	$1/T_2$ (s^{-1})	$1/T_{2,d}$ (s^{-1})
278	665	301	534	322	525	325
283	616	247	445	262	444	277
288	561	209	385	213	365	227
293	521	189	339	191	319	196
298	456	151	288	158	267	162
303	411	137	253	142	235	144
308	343	117	212	123	196	128
313	297	106	184	110	170	114
318	247	95	156	97	144	101

Table VIII-31. Variable pressure ^{17}O transverse ($1/T_2$) relaxation rates of $\left[Gd(DTTA - Me)(H_2O)_xF_y\right]^z$ and of the reference ($1/T_{2d}$), $[F^-] = 0$ M, $B_0 = 9.4$ T, $[Gd^{3+}] = 9.4$ mM

P (MPa)	$1/T_2$ (s^{-1})	$1/T_{2, d}$ (s^{-1})
2	557	206
21	565	203
31	572	202
41	575	200
61	587	197
81	595	194
91	599	193
100	606	192
120	613	189
140	623	186

Table VIII-32. Variable pressure ^{17}O transverse ($1/T_2$) relaxation rates of $[Gd(DTTA - Me)(H_2O)_xF_y]^z$ and of the reference ($1/T_{2,d}$), $B_0 = 9.4$ T, $[F^-] = 0.20$ M, $[Gd^{3+}] = 7.2$ mM

P (MPa)	$1/T_2$ (s^{-1})	$1/T_{2,d}$ (s^{-1})
3	317	197
21	321	195
40	324	192
61	329	189
72	332	188
80	333	186
100	336	184
110	339	182
121	341	181
139	344	178

Table VIII-33. Full list of parameters obtained from simultaneous fit of variable temperature ^{17}O NMR data

$k_{ex,1}^{298}$	(10^6 s^{-1})	177 ± 6
$k_{ex,2}^{298}$	(10^6 s^{-1})	24.6 ± 1.2
$\Delta H_1^{\ddagger}$	(kJ mol^{-1})	42 ± 2
$\Delta H_2^{\ddagger}$	(kJ mol^{-1})	50 ± 2
τ_v^{298}	(ps)	0.8^a
Δ^2	(10^{20} s^{-2})	0.2 ± 0.01
E_v	(kJ mol^{-1})	1^a
$A/\hbar$	(10^6 rad s^{-1})	-3.5^a

[a] fixed to the parameters obtained for $[Gd(DTTA - Me)(H_2O)_2]^-$ in chapter III

VIII.5 Appendix to chapter V

VIII.5.1 ^{1}H NMR experimental data of [Dy(DO3A)(H$_2$O)$_2$]

Table VIII-34. Variable temperature ^{1}H transverse relaxation rates and chemical shifts of [Dy(DO3A)(H$_2$O)$_2$] (1/T$_2$, δ) and of the water as the reference (1/T$_{2,d}$, δ_d), B$_0$ = 9.4 T and 18.8 T, pH = 5.7, [Dy^{3+}] = 114.7 mM

B$_0$ = 9.4 T

T (K)	δ (ppm)	δ_d (ppm)	1/T$_2$ (s^{-1})	1/T$_{2,d}$ (s^{-1})
278	4.45	6.83	730	1.44
283	4.47	6.79	604	1.46
289	4.49	6.73	491	1.46
294	4.52	6.69	415	1.47
299	4.54	6.64	338	1.48
304	4.56	6.59	283	1.47
309	4.55	6.59	229	1.49
315	4.57	6.48	190	1.49
320	4.59	6.40	152	1.51
325	4.59	6.48	127	1.51
330	4.59	6.36	103	1.53
341	4.62	6.40	74	1.56
348	4.64	6.27	63	1.60

B$_0$ = 18.8 T

T (K)	δ (ppm)	δ_d (ppm)	1/T$_2$ (s^{-1})	1/T$_{2,d}$ (s^{-1})
278	4.45	6.83	2850	3.26
283	4.47	6.78	2148	3.30
293	4.52	6.69	1466	3.40
298	4.54	6.64	1348	3.40
303	4.56	6.61	1224	3.45
308	4.58	6.55	848	3.48
313	4.60	6.51	695	3.51
318	4.60	6.50	581	3.55
328	4.63	6.43	504	3.58
338	4.65	6.36	277	3.65
348	4.67	6.30	268	3.72

Table VIII-35. Variable pressure ^{1}H transverse relaxation rates (1/T$_2$) of [Dy(DO3A)(H$_2$O)$_2$] and of the water as the reference (1/T$_{2,d}$), T = 22°C, B$_0$ = 9.4 T, pH = 5.7, [Dy^{3+}] = 86.3 mM

P (MPa)	1/T$_2$ (s^{-1})	1/T$_{2,d}$ (s^{-1})
1.2	335	2.63
6	337	2.64
22	342	2.65
39	350	2.66
62	357	2.67
79	366	2.69
101	373	2.70
119	379	2.72
140	391	2.73
161	397	2.74

VIII.5.3 ^{1}H NMR experimental data of [Dy(DTTA-Me)(H$_2$O)$_2$]$^-$

Table VIII-36. Variable temperature ^{1}H transverse relaxation rates and chemical shifts of [Dy(DTTA − Me)(H$_2$O)$_2$]$^-$ (1/T$_2$, δ) and of the water as the reference (1/T$_{2,d}$, δ_d), B$_0$ = 9.4 T and 18.8 T, pH = 5.7, [Dy^{3+}] = 104.29 mM

B$_0$ = 9.4 T

T (K)	δ (ppm)	δ_d (ppm)	1/T$_2$ (s^{-1})	1/T$_{2,d}$ (s^{-1})
278	4.89	6.83	372	1.44
283	4.90	6.79	276	1.46
289	4.94	6.73	250	1.46
294	5.04	6.69	186	1.47
299	5.00	6.64	125	1.48
304	5.10	6.59	102	1.47
309	5.10	6.59	93	1.49
315	5.06	6.48	76	1.49
320	5.06	6.40	57	1.51
325	5.21	6.48	57	1.51
330	5.16	6.36	47	1.53
341	5.29	6.40	35	1.56

B$_0$ = 18.8 T

T (K)	δ (ppm)	δ_d (ppm)	1/T$_2$ (s^{-1})	1/T$_{2,d}$ (s^{-1})
278	4.89	6.83	1363	3.26
283	4.92	6.78	1117	3.30
293	4.98	6.69	615	3.40
298	5.00	6.64	456	3.40
303	5.04	6.61	413	3.45
308	5.06	6.55	307	3.48
313	5.09	6.51	228	3.51
318	5.16	6.50	188	3.55
328	5.16	6.43	140	3.58
338	5.16	6.36	95	3.65
348	5.25	6.30	65	3.72

VIII.5.4   Full list of parameters obtained from the fit of ^{1}H NMR data

Table VIII-37. Full list of parameters[a] obtained from the fit of ^{1}H NMR data for [Dy(DO3A)(H$_2$O)$_2$] and [Dy(DTTA − Me)(H$_2$O)$_2$]$^-$

		[Dy(DO3A)(H$_2$O)$_2$]	[Dy(DTTA − Me)(H$_2$O)$_2$]$^-$
k_{ex}^{298}	(10^6 s^{-1})	19 ± 4	45 ± 10
$\Delta H^{\ddagger}$	(kJ mol^{-1})	20 ± 1	29 ± 1
B_1	(K)	-0.04 ± 0.02	0.07 ± 0.01
B_2	(K^2)	-29 ± 5	-56 ± 6
τ_R^{298}	(ps)	98[b]	149[b]
E_R	(kJ mol^{-1})	21[b]	26[b]
T_e	(ps)	0.6[b]	0.7[b]
a_{LnH}	(10^{-10} m)	3.6	3.6
D_{LnH}^{298}	(10^{-10} m^2 s^{-1})	25	25
E_{LnH}	(kJ mol^{-1})	20	20
q		2	2
C_{os}		0 − 0.25	0 − 0.25

[a] underlined parameters were fixed, [b] from Table III-1 and Table III-2

VIII.5.5 ^{1}H NMR experimental data of [Ln(AAZTAPh-NO$_2$)(H$_2$O)$_q$]$^-$

Table VIII-38. Variable temperature ^{1}H transverse relaxation rates ($1/T_2$) of $[\mathrm{Gd(AAZTAPh-NO_2)(H_2O)_2}]^-$ and of the water as the reference ($1/T_{2,d}$), $B_0 = 18.8$ T, pH = 5.7, [Gd^{3+}] = 4.3 mM

T (K)	$1/T_2$ (s^{-1})	$1/T_{2,d}$ (s^{-1})
279	77	3.25
284	70	3.30
294	56	3.39
299	49	3.40
303	45	3.45
308	40	3.47
313	37	3.50
318	32	3.55
327	24	3.58
337	19	3.65
347	15	3.70

Table VIII-39. Variable temperature ^{1}H transverse relaxation rates ($1/T_2$) of $[\mathrm{Tm(AAZTAPh-NO_2)(H_2O)}]^-$ and of the water as the reference ($1/T_{2,d}$), $B_0 = 18.8$ T, pH = 5.7, [Tm^{3+}] = 6.0 mM

T (K)	$1/T_2$ (s^{-1})	$1/T_{2,d}$ (s^{-1})
294	4.6	3.17
299	5.3	3.20
303	5.4	3.22
308	6.5	3.28
313	7.0	3.31
318	8.8	3.40
327	11.8	3.46
328	11.9	3.47
337	17.0	3.56
348	22.8	3.71
353	25.5	3.78
358	26.8	3.84
363	27.8	3.91
368	27.8	3.98

Table VIII-40. Variable temperature ^{1}H transverse relaxation rates ($1/T_2$) of $[Dy(AAZTAPh-NO_2)(H_2O)_2]^-$ and of the water as the reference ($1/T_{2,d}$), $B_0 = 9.4$ T and 18.8 T, pH = 5.7, $[Dy^{3+}] = 4.5$ mM

$B_0 = 9.4$ T		
T (K)	$1/T_2 (s^{-1})$	$1/T_{2,d} (s^{-1})$
278	28	2.61
284	36	2.63
289	46	2.63
294	56	2.64
299	66	2.65
304	73	2.64
309	76	2.66
315	74	2.66
320	67	2.68
325	60	2.68
330	47	2.70
341	28	2.73
348	20	2.75

$B_0 = 18.8$ T		
T (K)	$1/T_2 (s^{-1})$	$1/T_{2,d} (s^{-1})$
278	29	3.26
283	36	3.30
293	59	3.40
298	80	3.40
303	95	3.45
308	117	3.48
313	129	3.51
318	136	3.55
328	127	3.58
338	95	3.65
348	69	3.72

Table VIII-41. Variable pressure ^{1}H transverse ($1/T_2$) relaxation rates of $[Gd(AAZTAPh-NO_2)(H_2O)_2]^-$ and of the water as the reference ($1/T_{2,d}$), T = 20°C, $B_0 = 9.4$ T, pH = 5.7, $[Gd^{3+}] = 4.3$ mM

P (MPa)	$1/T_2 (s^{-1})$	$1/T_{2,d} (s^{-1})$
1.5	58.34	2.63
21	58.07	2.64
39	57.74	2.65
60	57.46	2.66
81	55.72	2.67
103	54.88	2.69
120	54.62	2.70
139	54.11	2.72
159	54.32	2.73

Table VIII-42. Variable pressure ^{1}H transverse ($1/T_2$) relaxation rates of $[Dy(AAZTAPh-NO_2)(H_2O)_2]^-$ and of the water as the reference ($1/T_{2,d}$), T = 18°C, $B_0 = 9.4$ T, pH = 5.7, $[Dy^{3+}] = 5.6$ mM

P (MPa)	$1/T_2 (s^{-1})$	$1/T_{2,d} (s^{-1})$
0.8	57.71	2.63
6	57.39	2.64
20	57.39	2.65
40	56.60	2.66
60	56.14	2.67
81	55.71	2.69
101	54.37	2.70
123	53.87	2.72
140	53.15	2.73
152	52.29	2.74

Table VIII-43. Variable pressure ^{1}H transverse ($1/T_2$) relaxation rates of $[\text{Tm}(\text{AAZTAPh} - \text{NO}_2)(\text{H}_2\text{O})]^-$ and of the water as the reference ($1/T_{2,d}$), T = 23°C, B_0 = 9.4 T, pH = 5.7, $[\text{Tm}^{3+}]$ = 6.0 mM

P (MPa)	$1/T_2$ (s^{-1})	$1/T_{2,d}$ (s^{-1})
5.6	4.43	2.64
20	4.48	2.65
40	4.59	2.66
60	4.65	2.67
80	4.74	2.69
99	4.79	2.70
121	4.89	2.72
140	4.92	2.73
152	4.98	2.74
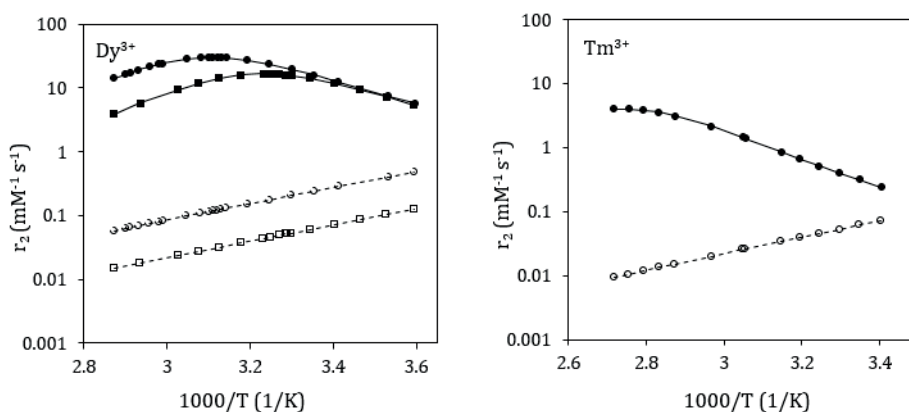
Figure VIII-2. Contribution of outer-sphere relaxivity (empty symbols) to the observed relaxivity (filled symbols) for $[\text{Ln}(\text{AAZTAPh} - \text{NO}_2)(\text{H}_2\text{O})_q]^-$, Ln = Dy^{3+} and Tm^{3+}, pH = 5.7, B_0 = 9.4 T (■) and 18.8 T (●).

VIII.5.6   Full list of parameters obtained from the fit of ^{1}H NMR data

Table VIII-44. Water exchange parameters obtained from fit of ^{1}H NMR data for $[\text{Ln}(\text{AAZTAPh} - \text{NO}_2)(\text{H}_2\text{O})_2]^-$

		Dy^{3+}	Tm^{3+}
k_{ex}^{298}	(10^6 s^{-1})	36 ± 1	46 ± 1
$\Delta H^\ddagger$	(kJ mol^{-1})	0.46 ± 0.01	0.014 ± 0.0007
B_1	(K)	0.07 ± 0.04	-0.16 ± 0.006
B_2	(K^2)	-57 ± 14	47 ± 2
T_e	(ps)	0.7^b	0.4^b
a_{LnH}	(10^{-10} m)	3.6	3.6
D_{LnH}^{298}	(10^{-10} m^2 s^{-1})	25	25
E_{LnH}	(kJ mol^{-1})	20	20
q		2	1

$^{a)}$ underlined parameters were fixed, $^{b)}$ from chapter III

VIII.5.7 ^{17}O NMR experimental data of [Gd(AAZTAPh-NO$_2$)(H$_2$O)$_2$]$^-$

Table VIII-45. Variable temperature ^{17}O longitudinal and transverse relaxation rates and chemical shifts of $[Gd(AAZTAPh - NO_2)(H_2O)_2]^-$ (1/T$_1$, 1/T$_2$, δ) and of the water as the reference (1/T$_{1,d}$, 1/T$_{2,d}$, δ_d), B$_0$ = 18.8 T, pH =5.4, [Gd^{3+}] = 4.3 mM

T (K)	δ (ppm)	δ_d (ppm)	1/T$_1$ (s^{-1})	1/T$_{1,d}$ (s^{-1})	1/T$_2$ (s^{-1})	1/T$_{2,d}$ (s^{-1})
279	6.29	6.35	267	258	366	230
284	6.02	6.14	225	218	377	210
294	5.55	5.74	167	162	401	175
299	5.11	5.38	142	137	396	152
303	5.05	5.37	130	127	392	142
308	4.56	4.97	111	109	386	125
313	4.49	4.97	103	101	377	117
318	4.14	4.64	90	88	352	103
327	3.74	4.29	75	74	308	87
337	3.15	3.73	62	61	243	72
347	2.75	3.34	53	52	196	60

Table VIII-46. Variable pressure ^{17}O transverse (1/T$_2$) relaxation rates of $[Gd(AAZTAPh - NO_2)(H_2O)_2]^-$ and of the water as the reference (1/T$_{2,d}$), T = 20°C, B$_0$ = 9.4 T, pH = 5.7, [Gd^{3+}] = 4.3 mM

P (MPa)	1/T$_2$ (s^{-1})	1/T$_{2,d}$ (s^{-1})
1.5	372	158
21	369	154
39	367	150
60	365	146
81	362	143
103	359	138
120	356	135
139	356	131
159	353	128

VIII.5.8 Full list of parameters obtained from the simultaneous fit of ^{17}O and ^1H NMR data

Table VIII-47. Water exchange parameters obtained from simultaneous fit of variable temperature ^{17}O and ^1H NMR data of $[Gd(AAZTAPh - NO_2)(H_2O)_2]^-$

k_{ex}^{298}	(10^6 s^{-1})	3.90 ± 0.1
$\Delta H^{\ddagger}$	(kJ mol^{-1})	42 ± 1
τ_R^{298}	(ps)	156 ± 3
E_R	(kJ mol^{-1})	29 ± 1
τ_v^{298}	(ps)	$\underline{31}^b$
E_v	(kJ mol^{-1})	$\underline{1}$
Δ^2	(10^{-20} s^{-2})	18 ± 1
χ	(MHz)	$\underline{7.58}$
r_{GdH}	(Å)	$\underline{3.111}$
r_{GdO}	(Å)	$\underline{2.5}$
$A/\hbar$	(10^6 rad s^{-1})	-3.5 ± 0.1
a_{LnH}	(10^{-10} m)	$\underline{3.6}$
D_{LnH}^{298}	(10^{-10} m^2 s^{-1})	$\underline{25}$
E_{LnH}	(kJ mol^{-1})	$\underline{20}$
q		$\underline{2}$

[a] underlined parameters were fixed, [b] fixed to the value reported for $[Gd(AAZTA)(H_2O)_2]^-$ in ref 3

VIII.6   Appendix to chapter VI

VIII.6.1 $^{35/37}$Cl NMR experimental data of LnCl$_3$

Table VIII-48. Variable temperature ^{35}Cl NMR longitudinal ($1/T_1$) and transverse ($1/T_2$) relaxation rates of GdCl$_3$, B_0 = 9.4 T, [Cl$^-$] = 6.7 m, [Gd^{3+}] = 0.10 m

T (K)	$1/T_1$ (s^{-1})	$1/T_2$ (s^{-1})
278	88	108
280	82	104
284	75	98
285	71	94
289	66	89
290	64	87
294	60	83
299	53	77
304	50	74
309	45	70
315	42	69
320	39	66
325	37	66
330	35	65
341	32	65

Table VIII-49. Variable temperature ^{37}Cl NMR longitudinal ($1/T_1$) and transverse ($1/T_2$) relaxation rates of GdCl$_3$, B_0 = 9.4 T, [Cl$^-$] = 6.7 m, [Gd^{3+}] = 0.10 m

T (K)	$1/T_1$ (s^{-1})	$1/T_2$ (s^{-1})
278	55	70
280	52	67
285	46	62
289	41	58
294	37	54
299	33	50
304	31	49
309	28	46
315	27	45
320	25	45
325	23	44
330	22	44
341	20	45

Table VIII-50. Variable temperature ^{35}Cl NMR longitudinal ($1/T_1$) and transverse ($1/T_2$) relaxation rates of GdCl$_3$, B_0 = 9.4 T, [Cl$^-$] = 6.7 m, [Gd^{3+}] = 0.21 m

T (K)	$1/T_1$ (s^{-1})	$1/T_2$ (s^{-1})
278	104	146
280	98	140
284	91	134
285	86	129
289	79	123
290	78	122
294	73	118
299	65	111
304	61	109
309	56	105
315	54	104
320	50	103
325	48	103
330	46	103
341	43	106

Table VIII-51. Variable-temperature ^{37}Cl NMR longitudinal ($1/T_1$) and transverse ($1/T_2$) relaxation rates of $GdCl_3$, $B_0 =$ 9.4 T, $[Cl^-] = 6.7$ m, $[Gd^{3+}] = 0.21$ m

T (K)	$1/T_1$ (s^{-1})	$1/T_2$ (s^{-1})
278	65	95
280	60	92
284	56	88
285	54	84
289	50	81
290	49	80
294	46	77
299	41	74
304	38	72
309	35	70
315	34	69
320	31	68
325	30	69
330	29	70
341	27	73

Table VIII-52. Variable temperature ^{35}Cl NMR longitudinal ($1/T_1$) and transverse ($1/T_2$) relaxation rates of $DyCl_3$, $B_0 =$ 9.4 T, $[Dy^{3+}] = 1.99$ m

T (K)	$1/T_1$ (s^{-1})	$1/T_2$ (s^{-1})
278	708	757
280	668	723
284	620	669
285	596	654
289	560	611
290	548	601
294	522	577
299	480	545
304	450	526
309	429	510
315	415	509
320	394	509
325	384	517
330	371	530
341	356	563

Table VIII-53. Variable temperature ^{37}Cl NMR longitudinal ($1/T_1$) and transverse ($1/T_2$) relaxation rates of $DyCl_3$, $B_0 =$ 9.4 T, $[Dy^{3+}] = 1.99$ m

T (K)	$1/T_1$ (s^{-1})	$1/T_2$ (s^{-1})
278	433	487
280	417	462
284	386	428
285	374	430
289	349	402
290	342	392
294	326	371
299	299	357
304	288	353
309	268	351
315	259	354
320	247	356
325	243	368
330	231	391
341	223	419

VIII.6.2 $^{35/37}$Cl NMR experimental data of Ln(ClO$_4$)$_3$

Table VIII-54. Variable temperature ^{35}Cl NMR longitudinal (1/T$_1$) and transverse (1/T$_2$) relaxation rates of Dy(ClO$_4$)$_3$, B$_0$ = 9.4 T, [Dy^{3+}] = 2.01 m

T (K)	1/T$_1$ (s^{-1})	1/T$_2$ (s^{-1})
278	25.1	25.8
280	23.5	24.3
284	21.9	22.7
285	21.0	21.8
289	19.7	20.7
290	19.3	20.3
294	18.3	19.4
299	16.9	18.2
304	16.1	17.4
309	15.0	16.6
315	14.6	16.3
320	13.9	15.9
325	13.5	15.7
330	13.1	15.5
341	12.6	15.5

Table VIII-55. Variable temperature ^{37}Cl NMR longitudinal (1/T$_1$) and transverse (1/T$_2$) relaxation rates of Dy(ClO$_4$)$_3$, B$_0$ = 9.4 T, [Dy^{3+}] = 2.01 m

T (K)	1/T$_1$ (s^{-1})	1/T$_2$ (s^{-1})
278	15.4	15.9
280	14.8	15.3
285	13.2	14.0
289	12.3	13.5
299	10.6	12.0
309	9.6	11.3
320	8.7	11.0
325	8.6	10.8
330	8.3	10.6
341	8.0	10.9

VIII.6.3 ^{17}O NMR experimental data of $Ln(ClO_4)_3$

Table VIII-56. Variable temperature ^{17}O longitudinal $(1/T_1)$ and transverse $(1/T_2)$ relaxation rates and chemical shifts (δ) of $Nd(ClO_4)_3$ and the chemical shift of $La(ClO_4)_3$ as the reference (δ_d), $B_0 = 9.4$ T and 18.8 T, pH < 3, $[Nd^{3+}] = 0.50$ m

$B_0 = 9.4$ T

T (K)	δ (ppm)	δ_d (ppm)	$1/T_1$ (s^{-1})	$1/T_2$ (s^{-1})
278	44.7	8.5	278	285
280	44.1	8.4	258	264
283	43.4	8.2	229	235
285	43.0	8.2	218	223
289	42.3	8.0	197	201
290	42.2	8.0	189	194
294	41.6	7.8	173	178
299	40.4	7.6	150	153
304	39.8	7.4	135	138
309	38.7	7.1	118	121
315	38.0	7.0	108	110
320	37.0	6.7	96	98
325	36.4	6.6	88	90
330	35.4	6.3	79	81
341	34.0	5.9	67	68
355	31.3	5.3	55	56

$B_0 = 18.8$ T

T (K)	δ (ppm)	δ_d (ppm)	$1/T_1$ (s^{-1})	$1/T_2$ (s^{-1})
280	44.5	8.7	265	290
285	43.7	8.6	231	253
289	42.5	8.3	196	215
294	42.1	8.3	178	195
299	40.8	7.9	152	167
303	40.5	7.9	143	155
308	39.2	7.5	123	134
313	39.1	7.6	116	126
318	37.8	7.2	101	110
332	36.1	6.9	80	86
336	35.0	6.6	72	78
355	32.6	5.9	55	58

Table VIII-57. Variable temperature ^{17}O longitudinal ($1/T_1$) and transverse ($1/T_2$) relaxation rates and chemical shifts (δ) of $Nd(ClO_4)_3$ and the chemical shift of $La(ClO_4)_3$ as the reference (δ_d), $B_0 = 9.4$ T and 18.8 T, pH < 3, $[Nd^{3+}]$ = 1.05 m

$B_0 = 9.4$ T

T (K)	δ (ppm)	δ_d (ppm)	$1/T_1$ (s^{-1})	$1/T_2$ (s^{-1})
278	86	10.9	306	321
280	85	10.8	288	302
283	84	10.6	260	273
285	83	10.6	246	257
289	82	10.4	222	233
290	81	10.4	215	225
294	80	10.3	197	206
299	78	10.0	170	178
304	77	9.9	155	161
309	75	9.7	135	141
315	74	9.5	124	129
320	72	9.3	110	114
325	71	9.2	102	105
330	70	8.9	91	94
341	67	8.6	78	80
355	63	8.0	65	67

$B_0 = 18.8$ T

T (K)	δ (ppm)	δ_d (ppm)	$1/T_1$ (s^{-1})	$1/T_2$ (s^{-1})
280	85	11.0	292	351
285	84	10.9	259	311
289	82	10.6	217	259
294	81	10.7	202	238
299	79	10.3	171	201
303	78	10.4	161	188
308	76	10.0	140	162
313	76	10.1	131	152
318	73	9.8	116	133
332	70	9.5	91	104
336	69	9.2	83	93
355	64	8.6	63	69

Table VIII-58. Variable temperature ^{17}O longitudinal ($1/T_1$) and transverse ($1/T_2$) relaxation rates and chemical shifts (δ) of $Nd(ClO_4)_3$ and the chemical shift of $La(ClO_4)_3$ as the reference (δ_d), $B_0 = 9.4$ T and 18.8 T, pH < 3, $[Nd^{3+}]$ = 1.48 m

$B_0 = 9.4$ T

T (K)	δ (ppm)	δ_d (ppm)	$1/T_1$ (s^{-1})	$1/T_2$ (s^{-1})
278	122	12.7	354	376
280	121	12.6	329	350
283	120	12.5	295	314
285	118	12.4	278	297
289	117	12.3	251	267
290	116	12.3	244	259
294	115	12.2	224	237
299	112	11.9	192	203
304	110	11.8	175	184
309	107	11.6	152	160
315	106	11.5	139	147
320	103	11.3	123	129
325	102	11.2	114	120
330	99	11.0	101	105
341	96	10.6	86	90
355	93	10.0	80	83

B$_0$ = 18.8 T

T (K)	δ (ppm)	δ_d (ppm)	1/T$_1$ (s^{-1})	1/T$_2$ (s^{-1})
280	123	12.8	334	423
285	121	12.8	295	369
289	118	12.5	249	311
294	117	12.5	227	281
299	114	12.2	194	240
303	113	12.3	182	222
308	110	11.9	157	192
313	109	12.0	148	179
318	106	11.7	129	157
332	102	11.5	103	121
336	99	11.2	92	109
355	94	10.7	70	81

Table VIII-59. Variable temperature ^{17}O longitudinal (1/T$_1$) and transverse (1/T$_2$) relaxation rates and chemical shifts (δ) of Nd(ClO$_4$)$_3$ and the chemical shift of La(ClO$_4$)$_3$ as the reference (δ_d), B$_0$ = 9.4 T and 18.8 T, pH < 3, [Nd^{3+}] = 2.05 m

B$_0$ = 9.4 T

T (K)	δ (ppm)	δ_d (ppm)	1/T$_1$ (s^{-1})	1/T$_2$ (s^{-1})
278	161	15.1	422	450
280	159	15.1	392	418
283	157	15.0	351	374
285	156	14.9	331	353
289	154	14.8	298	317
290	153	14.8	289	307
294	151	14.7	265	281
299	147	14.5	227	240
304	145	14.4	206	217
309	142	14.2	178	188
315	140	14.1	163	172
320	136	13.9	144	151
325	134	13.9	133	139
330	131	13.7	119	124
341	127	13.4	101	105
355	120	13.1	80	83

B$_0$ = 18.8 T

T (K)	δ (ppm)	δ_d (ppm)	1/T$_1$ (s^{-1})	1/T$_2$ (s^{-1})
280	159	15.2	402	507
285	157	15.2	354	444
289	153	14.9	298	373
294	151	15.0	273	334
299	148	14.7	231	284
303	146	14.8	216	263
308	142	14.5	185	226
313	141	14.6	174	211
318	138	14.4	152	184
332	132	14.2	119	140
336	129	13.9	108	125
355	121	13.5	81	91

Table VIII-60. Variable temperature ^{17}O longitudinal ($1/T_1$) and transverse ($1/T_2$) relaxation rates and chemical shifts (δ) of $Dy(ClO_4)_3$ and the chemical shift of $La(ClO_4)_3$ as the reference (δ_d), $B_0 = 9.4$ T and 18.8 T, pH < 3, $[Dy^{3+}]$ = 0.49 m

$B_0 = 9.4$ T

T (K)	δ (ppm)	δ_d (ppm)	$1/T_1$ (s^{-1})	$1/T_2$ (s^{-1})
278	-195	8.5	349	616
280	-194	8.4	325	570
283	-192	8.2	294	506
285	-190	8.1	278	477
289	-188	8.0	251	422
290	-187	7.9	243	410
294	-185	7.8	223	369
299	-181	7.5	191	312
304	-178	7.4	175	279
309	-174	7.1	154	241
315	-172	7.0	142	218
320	-169	6.7	126	189
325	-167	6.5	117	174
330	-163	6.3	106	154
341	-158	5.9	91	128
355	-152	4.0	80	103

$B_0 = 18.8$ T

T (K)	δ (ppm)	δ_d (ppm)	$1/T_1$ (s^{-1})	$1/T_2$ (s^{-1})
280	-192	8.7	398	1404
285	-189	8.6	347	1192
289	-185	8.2	290	958
294	-183	8.2	265	856
299	-178	7.9	223	694
303	-177	7.9	208	635
308	-173	7.5	179	526
313	-172	7.6	170	486
318	-168	7.2	148	408
332	-161	6.9	117	298
336	-158	6.6	106	260
355	-150	5.9	82	179

Table VIII-61. Variable temperature ^{17}O longitudinal ($1/T_1$) and transverse ($1/T_2$) relaxation rates and chemical shifts (δ) of $Dy(ClO_4)_3$ and the chemical shift of $La(ClO_4)_3$ as the reference (δ_d), $B_0 = 9.4$ T and 18.8 T, pH < 3, $[Dy^{3+}]$ = 1.05 m

$B_0 = 9.4$ T

T (K)	δ (ppm)	δ_d (ppm)	$1/T_1$ (s^{-1})	$1/T_2$ (s^{-1})
278	-437	10.9	478	886
280	-433	10.8	444	816
283	-427	10.6	395	723
285	-423	10.5	375	678
289	-418	10.4	338	606
290	-417	10.4	329	579
294	-412	10.2	302	527
299	-402	10.0	261	464
304	-397	9.9	239	416
309	-387	9.6	210	354
315	-383	9.5	194	322
320	-374	9.3	174	283
325	-370	9.1	162	259
330	-362	8.9	149	232
341	-351	8.5	129	194
355	-332	8.1	120	165

B₀ = 18.8 T

T (K)	δ (ppm)	δ_d (ppm)	$1/T_1$ (s^{-1})	$1/T_2$ (s^{-1})
280	-429	11.0	561	2051
285	-421	10.9	466	1686
289	-411	10.6	430	1419
294	-407	10.6	388	1275
299	-398	10.3	329	1076
303	-394	10.4	306	987
308	-385	10.0	251	840
313	-381	10.1	248	777
318	-373	9.7	217	663
332	-358	9.5	173	487
336	-351	9.2	157	424
355	-329	8.6	121	274

Table VIII-62. Variable temperature ^{17}O longitudinal ($1/T_1$) and transverse ($1/T_2$) relaxation rates and chemical shifts (δ) of $Dy(ClO_4)_3$ and the chemical shift of $La(ClO_4)_3$ as the reference (δ_d), B₀ = 9.4 T and 18.8 T, pH < 3, [Dy^{3+}] = 1.48 m

B₀ = 9.4 T

T (K)	δ (ppm)	δ_d (ppm)	$1/T_1$ (s^{-1})	$1/T_2$ (s^{-1})
278	-641	12.7	599	1026
280	-635	12.7	557	960
283	-626	12.5	496	853
285	-621	12.4	469	814
289	-613	12.3	425	733
290	-610	12.3	410	701
294	-603	12.2	377	639
299	-590	12.0	328	549
304	-581	11.9	298	493
309	-569	11.6	263	430
315	-561	11.5	243	395
320	-549	11.3	219	344
325	-542	11.2	204	317
330	-531	11.0	187	283
341	-514	10.7	163	240
355	-485	9.9	150	202

B₀ = 18.8 T

T (K)	δ (ppm)	δ_d (ppm)	$1/T_1$ (s^{-1})	$1/T_2$ (s^{-1})
280	-629	13	714	2280
285	-617	13	656	1835
289	-605	12	554	1619
294	-596	13	496	1449
299	-583	12	427	1251
303	-576	12	391	1169
308	-564	12	328	972
313	-559	12	315	901
318	-547	12	274	758
332	-524	12	218	538
336	-515	11	138	454
355	-486	11	71	283

Table VIII-63. Variable temperature ^{17}O longitudinal ($1/T_1$) and transverse ($1/T_2$) relaxation rates and chemical shifts (δ) of $Dy(ClO_4)_3$ and the chemical shift of $La(ClO_4)_3$ as the reference (δ_d), $B_0 = 9.4$ T and 18.8 T, pH < 3, $[Dy^{3+}]$ = 2.01 m

$B_0 = 9.4$ T

T (K)	δ (ppm)	δ_d (ppm)	$1/T_1$ (s^{-1})	$1/T_2$ (s^{-1})
278	-881	15.0	800	1248
280	-872	14.9	744	1176
283	-861	14.8	662	1053
285	-854	14.7	619	984
289	-842	14.7	559	890
290	-839	14.6	540	861
294	-829	14.5	497	793
299	-810	14.3	427	675
304	-798	14.2	384	626
309	-781	14.1	339	536
315	-769	14.0	311	473
320	-754	13.8	280	422
325	-743	13.7	262	389
330	-728	13.5	240	355
341	-705	13.2	206	288
355	-668	12.8	170	234

$B_0 = 18.8$ T

T (K)	δ (ppm)	δ_d (ppm)	$1/T_1$ (s^{-1})	$1/T_2$ (s^{-1})
280	-863	15.1	995	2736
285	-849	15.0	871	2297
289	-830	14.8	732	1930
294	-821	14.8	662	1747
299	-802	14.5	551	1477
303	-794	14.7	526	1385
308	-776	14.3	454	1187
313	-769	14.5	418	1077
318	-752	14.2	360	905
332	-721	14.0	289	719
336	-707	13.7	262	650
355	-668	13.3	202	463

Table VIII-64. Variable temperature ^{17}O longitudinal ($1/T_1$) and transverse ($1/T_2$) relaxation rates and chemical shifts (δ) of $Yb(ClO_4)_3$ and the chemical shift of $La(ClO_4)_3$ as the reference (δ_d), $B_0 = 9.4$ T and 18.8 T, pH < 3, $[Yb^{3+}]$ = 0.50 m

$B_0 = 9.4$ T

T (K)	δ (ppm)	δ_d (ppm)	$1/T_1$ (s^{-1})	$1/T_2$ (s^{-1})
278	-15.0	8.6	325	351
280	-14.9	8.4	303	325
283	-14.8	8.2	264	283
285	-14.6	8.2	250	268
289	-14.5	8.0	224	239
290	-14.5	8.0	216	230
294	-14.4	7.8	197	209
299	-14.2	7.6	168	178
304	-14.1	7.4	152	160
309	-13.9	7.1	131	139
315	-13.8	7.0	120	125
320	-13.6	6.7	105	110
325	-13.6	6.6	97	101
330	-13.4	6.3	86	89
341	-13.3	5.9	73	75
355	-13.1	5.5	55	56

$B_0 = 18.8$ T

T (K)	δ (ppm)	δ_d (ppm)	$1/T_1$ (s^{-1})	$1/T_2$ (s^{-1})
280	-14.6	8.7	302	404
285	-14.4	8.6	268	350
289	-14.3	8.3	222	281
294	-14.1	8.3	204	254
299	-14.0	7.9	171	209
303	-13.7	7.9	160	193
308	-13.7	7.6	136	162
313	-13.4	7.6	129	152
318	-13.4	7.2	112	130
332	-13.0	6.9	87	100
336	-13.0	6.6	79	89
355	-12.6	5.9	59	65

Table VIII-65. Variable temperature ^{17}O longitudinal ($1/T_1$) and transverse ($1/T_2$) relaxation rates and chemical shifts (δ) of Yb(ClO$_4$)$_3$ and the chemical shift of La(ClO$_4$)$_3$ as the reference (δ_d), $B_0 = 9.4$ T and 18.8 T, pH < 3, [Yb^{3+}] = 1.08 m

$B_0 = 9.4$ T

T (K)	δ (ppm)	δ_d (ppm)	$1/T_1$ (s^{-1})	$1/T_2$ (s^{-1})
278	-41	11.0	414	454
280	-41	10.9	387	422
283	-40	10.8	352	383
285	-40	10.7	325	353
289	-39	10.6	292	316
290	-39	10.5	283	306
294	-39	10.4	258	277
299	-38	10.2	216	232
304	-37	10.0	196	210
309	-36	9.8	161	171
315	-36	9.7	154	162
320	-35	9.4	133	141
325	-35	9.3	123	129
330	-34	9.1	109	114
341	-33	8.7	92	95
355	-32	8.2	75	77

$B_0 = 18.8$ T

T (K)	δ (ppm)	δ_d (ppm)	$1/T_1$ (s^{-1})	$1/T_2$ (s^{-1})
280	-39	11.2	395	541
285	-39	11.1	347	459
289	-38	10.8	288	374
294	-37	10.8	262	334
299	-37	10.4	220	276
303	-36	10.5	204	253
308	-36	10.2	174	214
313	-35	10.2	164	198
318	-35	9.9	142	170
332	-33	9.6	111	128
336	-33	9.3	98	113
355	-31	8.8	73	82

Table VIII-66. Variable temperature ^{17}O longitudinal ($1/T_1$) and transverse ($1/T_2$) relaxation rates and chemical shifts (δ) of $Yb(ClO_4)_3$ and the chemical shift of $La(ClO_4)_3$ as the reference (δ_d), $B_0 = 9.4$ T and 18.8 T, pH < 3, $[Yb^{3+}]$ = 1.50 m

$B_0 = 9.4$ T

T (K)	δ (ppm)	δ_d (ppm)	$1/T_1$ (s^{-1})	$1/T_2$ (s^{-1})
278	-58	12.8	528	528
280	-57	12.7	484	524
283	-56	12.6	427	467
285	-56	12.5	400	434
289	-55	12.4	356	386
290	-55	12.3	343	370
294	-54	12.2	311	336
299	-53	12.0	262	279
304	-52	11.9	235	251
309	-51	11.7	201	214
315	-51	11.6	183	193
320	-50	11.4	159	168
325	-49	11.3	146	153
330	-48	11.0	130	136
341	-47	10.7	108	112
355	-45	10.3	80	83

$B_0 = 18.8$ T

T (K)	δ (ppm)	δ_d (ppm)	$1/T_1$ (s^{-1})	$1/T_2$ (s^{-1})
280	-57	12.9	504	665
285	-56	12.8	429	557
289	-55	12.6	358	458
294	-54	12.6	321	408
299	-53	12.3	270	337
303	-52	12.4	249	307
308	-51	12.0	212	260
313	-51	12.1	198	240
318	-50	11.8	171	207
332	-48	11.6	132	154
336	-47	11.3	117	137
355	-44	10.8	86	98

Table VIII-67. Variable temperature ^{17}O longitudinal ($1/T_1$) and transverse ($1/T_2$) relaxation rates and chemical shifts (δ) of $Yb(ClO_4)_3$ and the chemical shift of $La(ClO_4)_3$ as the reference (δ_d), $B_0 = 9.4$ T and 18.8 T, pH < 3, $[Yb^{3+}]$ = 2.05 m

$B_0 = 9.4$ T

T (K)	δ (ppm)	δ_d (ppm)	$1/T_1$ (s^{-1})	$1/T_2$ (s^{-1})
278	-89	15.1	712	752
280	-88	15.1	656	693
283	-87	15.0	581	616
285	-86	14.9	547	578
289	-85	14.8	481	510
290	-84	14.7	462	486
294	-83	14.7	416	441
299	-81	14.5	347	366
304	-80	14.4	309	325
309	-78	14.2	261	276
315	-77	14.1	236	248
320	-75	13.9	201	211
325	-74	13.8	186	195
330	-73	13.7	164	172
341	-70	13.4	134	139
355	-67	13.0	110	114

$B_0 = 18.8$ T

T (K)	δ (ppm)	δ_d (ppm)	$1/T_1$ (s^{-1})	$1/T_2$ (s^{-1})
280	-87	15.2	685	843
285	-86	15.2	584	711
289	-84	14.9	477	579
294	-82	15.0	429	515
299	-81	14.7	351	425
303	-80	14.8	325	388
308	-78	14.5	273	327
313	-77	14.6	255	302
318	-75	14.3	217	258
332	-72	14.1	165	192
336	-70	13.9	146	169
355	-66	13.5	106	120

Table VIII-68. Variable pressure ^{17}O longitudinal ($1/T_1$) and transverse ($1/T_2$) relaxation rates of $Nd(ClO_4)_3$, $B_0 = 9.4$ T, pH < 3, $[Nd^{3+}] = 2.05$ m

P (MPa)	$1/T_1$ (s^{-1})	$1/T_2$ (s^{-1})
1.3	245	264
12	247	267
21	248	269
39	251	272
61	254	276
80	257	279
101	261	283
120	264	287
140	267	291
162	271	295

Table VIII-69. Variable pressure ^{17}O longitudinal ($1/T_1$) and transverse ($1/T_2$) relaxation rates of $Dy(ClO_4)_3$, $B_0 = 9.4$ T, pH < 3, $[Dy^{3+}] = 2.03$ m

P (MPa)	$1/T_1$ (s^{-1})	$1/T_2$ (s^{-1})
1.1	472	783
4	476	784
11	477	778
21	480	782
40	486	778
62	491	775
83	496	772
100	503	771
118	508	770
134	513	770
152	518	768
162	520	767

VIII.6.4 ^{17}O NMR experimental data of LnCl$_3$

Table VIII-70. Variable temperature ^{17}O longitudinal (1/T$_1$) and transverse (1/T$_2$) relaxation rates and chemical shifts (δ) of NdCl$_3$ and the chemical shift of LaCl$_3$ as the reference (δ_d), B$_0$ = 9.4 T and 18.8 T, pH < 3, [Nd^{3+}] = 0.50 m

B$_0$ = 9.4 T

T (K)	δ (ppm)	δ_d (ppm)	1/T$_1$ (s^{-1})	1/T$_2$ (s^{-1})
278	45.8	10.7	300	307
280	45.3	10.6	278	285
283	44.8	10.5	250	257
285	44.3	10.4	235	241
289	43.7	10.3	212	218
290	43.5	10.3	206	212
294	43.0	10.2	188	194
299	41.8	10.0	161	166
304	41.2	9.9	146	150
309	40.1	9.6	127	130
315	39.5	9.5	116	120
320	38.5	9.3	102	105
325	37.9	9.2	95	97
330	36.9	8.9	85	87
341	35.5	8.5	71	73
348	34.6	8.3	65	67

B$_0$ = 18.8 T

T (K)	δ (ppm)	δ_d (ppm)	1/T$_1$ (s^{-1})	1/T$_2$ (s^{-1})
278	46.1	10.9	304	333
283	45.3	10.7	261	287
293	43.5	10.4	196	216
298	42.3	10.2	165	185
303	41.9	10.0	152	169
308	40.7	9.8	131	148
313	40.3	9.7	122	137
318	39.2	9.5	107	121
328	38.0	9.2	90	101
338	36.4	9.0	74	83
348	35.1	8.7	64	71

Table VIII-71. Variable temperature ^{17}O longitudinal ($1/T_1$) and transverse ($1/T_2$) relaxation rates and chemical shifts (δ) of $NdCl_3$ and the chemical shift of $LaCl_3$ as the reference (δ_d), $B_0 = 9.4$ T and 18.8 T, pH < 3, [Nd^{3+}] = 1.02 m

$B_0 = 9.4$ T

T (K)	δ (ppm)	δ_d (ppm)	$1/T_1$ (s^{-1})	$1/T_2$ (s^{-1})
278	15.6	87.0	355	369
280	15.5	86.2	330	344
283	15.4	85.4	300	312
285	15.3	84.4	280	292
289	15.3	83.2	253	264
290	15.2	83.0	247	258
294	15.2	82.0	227	236
299	15.0	79.9	193	202
304	14.9	78.8	176	183
309	14.7	76.8	152	159
315	14.6	75.8	140	146
320	14.4	73.9	122	127
325	14.3	72.9	114	119
330	14.0	71.2	102	107
341	13.7	68.6	86	90
348	13.5	67.0	75	78

$B_0 = 18.8$ T

T (K)	δ (ppm)	δ_d (ppm)	$1/T_1$ (s^{-1})	$1/T_2$ (s^{-1})
278	87	15.8	366	425
283	86	15.7	317	370
293	83	15.3	239	278
298	80	15.2	200	232
303	80	15.0	185	216
308	77	14.9	159	186
313	77	14.8	148	174
318	74	14.6	129	151
328	73	14.4	110	128
338	69	14.1	90	105
348	67	13.9	78	93

Table VIII-72. Variable temperature ^{17}O longitudinal ($1/T_1$) and transverse ($1/T_2$) relaxation rates and chemical shifts (δ) of $NdCl_3$ and the chemical shift of $LaCl_3$ as the reference (δ_d), $B_0 = 9.4$ T and 18.8 T, pH < 3, [Nd^{3+}] = 1.45 m

$B_0 = 9.4$ T

T (K)	δ (ppm)	δ_d (ppm)	$1/T_1$ (s^{-1})	$1/T_2$ (s^{-1})
278	117	19.7	416	435
280	116	19.6	389	407
283	115	19.5	353	370
285	114	19.4	329	346
289	113	19.3	297	312
290	112	19.4	289	303
294	110	19.3	265	278
299	109	19.1	226	237
304	107	19.0	204	215
309	105	18.8	177	187
315	104	18.8	163	171
320	102	18.5	143	150
325	101	18.5	132	138
330	99	18.3	118	124
341	96	17.9	99	104
348	94	17.7	90	94

B$_0$ = 18.8 T

T (K)	δ (ppm)	δ_d (ppm)	1/T$_1$ (s^{-1})	1/T$_2$ (s^{-1})
278	117	19.9	420	500
283	115	19.7	367	435
293	111	19.4	275	324
298	109	19.3	230	276
303	107	19.2	214	254
308	106	19.0	183	221
313	104	18.9	171	204
318	103	18.8	148	180
328	100	18.6	126	151
338	97	18.4	103	126
348	94	18.2	89	106

Table VIII-73. Variable temperature ^{17}O longitudinal (1/T$_1$) and transverse (1/T$_2$) relaxation rates and chemical shifts (δ) of NdCl$_3$ and the chemical shift of LaCl$_3$ as the reference (δ_d), B$_0$ = 9.4 T and 18.8 T, pH < 3, [Nd^{3+}] = 1.80 m

B$_0$ = 9.4 T

T (K)	δ (ppm)	δ_d (ppm)	1/T$_1$ (s^{-1})	1/T$_2$ (s^{-1})
278	135	23.0	496	523
280	134	22.9	456	483
283	133	22.8	408	432
285	132	22.7	380	403
289	131	22.7	340	361
290	131	22.7	331	350
294	130	22.6	303	319
299	130	22.5	257	272
304	124	22.4	232	245
309	124	22.3	198	210
315	120	22.2	184	194
320	119	22.0	160	170
325	117	21.9	149	156
330	115	21.7	132	139
341	112	21.4	120	126
348	109	21.2	115	120

B$_0$ = 18.8 T

T (K)	δ (ppm)	δ_d (ppm)	1/T$_1$ (s^{-1})	1/T$_2$ (s^{-1})
278	137	23.2	486	598
283	134	23.1	421	518
293	129	22.8	315	388
298	128	22.7	262	327
303	126	22.6	242	295
308	124	22.5	206	256
313	122	22.3	192	236
318	121	22.2	166	205
328	117	22.0	140	171
338	113	21.8	114	138
348	108	21.7	99	119

Table VIII-74. Variable temperature ^{17}O longitudinal ($1/T_1$) and transverse ($1/T_2$) relaxation rates and chemical shifts (δ) of DyCl$_3$ and the chemical shift of LaCl$_3$ as the reference (δ_d), B$_0$ = 9.4 T and 18.8 T, pH < 3, [Dy^{3+}] = 0.52 m

B$_0$ = 9.4 T

T (K)	δ (ppm)	δ_d (ppm)	$1/T_1$ (s^{-1})	$1/T_2$ (s^{-1})
278	-193	10.8	422	728
280	-191	10.7	389	671
283	-188	10.6	348	594
285	-186	10.5	327	560
289	-184	10.4	293	498
290	-184	10.4	284	482
294	-181	10.3	260	439
299	-177	10.1	223	377
304	-175	10.0	202	339
309	-171	9.7	176	290
315	-169	9.6	162	264
320	-165	9.4	142	225
325	-163	9.3	132	205
330	-159	9.0	118	179
341	-154	8.7	101	147
355	-147	8.2	87	120

B$_0$ = 18.8 T

T (K)	δ (ppm)	δ_d (ppm)	$1/T_1$ (s^{-1})	$1/T_2$ (s^{-1})
280	-189	11.0	446	1574
285	-186	10.9	384	1335
289	-182	10.6	322	1079
294	-180	10.6	291	969
299	-175	10.3	242	794
303	-174	10.3	226	735
308	-170	10.0	193	621
313	-168	10.1	183	580
318	-164	9.7	158	487
332	-158	9.5	125	351
336	-154	9.2	112	301
355	-146	8.6	86	200

Table VIII-75. Variable temperature ^{17}O longitudinal ($1/T_1$) and transverse ($1/T_2$) relaxation rates and chemical shifts (δ) of DyCl$_3$ and the chemical shift of LaCl$_3$ as the reference (δ_d), B$_0$ = 9.4 T and 18.8 T, pH < 3, [Dy^{3+}] = 1.03 m

B$_0$ = 9.4 T

T (K)	δ (ppm)	δ_d (ppm)	$1/T_1$ (s^{-1})	$1/T_2$ (s^{-1})
278	-391	15.7	633	1080
280	-387	15.6	585	980
283	-382	15.5	518	855
285	-379	15.4	489	803
289	-374	15.3	438	717
290	-372	15.3	423	691
294	-367	15.3	387	626
299	-359	15.1	330	532
304	-353	15.0	299	477
309	-345	14.8	259	406
315	-340	14.7	237	366
320	-332	14.5	206	311
325	-328	14.4	194	287
330	-321	14.1	174	254
341	-310	13.8	149	210
355	-292	13.3	120	165

B₀ = 18.8 T

T (K)	δ (ppm)	δ_d (ppm)	$1/T_1$ (s^{-1})	$1/T_2$ (s^{-1})
280	-381	15.9	646	2320
285	-376	15.8	563	1904
289	-367	15.5	466	1578
294	-363	15.6	424	1408
299	-354	15.2	360	1192
303	-350	15.3	325	1085
308	-342	15.0	284	923
313	-339	15.1	266	834
318	-331	14.8	234	709
332	-317	14.6	181	521
336	-310	14.3	167	440
355	-292	13.8	126	293

Table VIII-76. Variable temperature ^{17}O longitudinal ($1/T_1$) and transverse ($1/T_2$) relaxation rates and chemical shifts (δ) of DyCl$_3$ and the chemical shift of LaCl$_3$ as the reference (δ_d), B₀ = 9.4 T and 18.8 T, pH < 3, [Dy^{3+}] = 1.49 m

B₀ = 9.4 T

T (K)	δ (ppm)	δ_d (ppm)	$1/T_1$ (s^{-1})	$1/T_2$ (s^{-1})
278	-569	20.0	735	1237
280	-564	19.9	681	1143
283	-557	19.9	612	1029
285	-551	19.8	570	954
289	-543	19.7	511	857
290	-542	19.7	499	834
294	-535	19.7	456	759
299	-521	19.5	386	640
304	-514	19.4	353	584
309	-502	19.2	304	493
315	-495	19.2	280	447
320	-483	18.9	247	383
325	-476	18.8	230	351
330	-465	18.7	206	310
341	-449	18.3	178	262
355	-423	17.9	150	208

B₀ = 18.8 T

T (K)	δ (ppm)	δ_d (ppm)	$1/T_1$ (s^{-1})	$1/T_2$ (s^{-1})
280	-560	20.2	900	2821
285	-549	20.1	776	2349
289	-537	19.9	631	1993
294	-530	19.9	562	1754
299	-517	19.7	478	1439
303	-511	19.8	436	1313
308	-499	19.5	372	1121
313	-494	19.6	349	1054
318	-482	19.3	305	873
332	-461	19.1	237	631
336	-451	18.8	215	566
355	-423	18.3	162	397

Table VIII-77. Variable temperature ^{17}O longitudinal ($1/T_1$) and transverse ($1/T_2$) relaxation rates and chemical shifts (δ) of $DyCl_3$ and the chemical shift of $LaCl_3$ as the reference (δ_d), $B_0 = 9.4$ T and 18.8 T, pH < 3, $[Dy^{3+}] = 1.99$ m

$B_0 = 9.4$ T

T (K)	δ (ppm)	δ_d (ppm)	$1/T_1 (s^{-1})$	$1/T_2 (s^{-1})$
278	-750	24.7	1047	1564
280	-741	24.6	940	1410
283	-730	24.6	831	1251
285	-724	24.5	775	1164
289	-713	24.4	691	1040
290	-710	24.5	670	1007
294	-701	24.4	609	918
299	-683	24.3	516	786
304	-673	24.3	467	709
309	-656	24.1	401	600
315	-646	24.0	367	543
320	-630	23.8	322	470
325	-621	23.7	299	431
330	-607	23.6	269	387
341	-582	23.3	226	319
355	-556	22.9	170	240

$B_0 = 18.8$ T

T (K)	δ (ppm)	δ_d (ppm)	$1/T_1 (s^{-1})$	$1/T_2 (s^{-1})$
280	-732	24.9	1146	3044
285	-722	24.8	1009	2636
289	-703	24.6	829	2196
294	-695	24.7	750	2028
299	-677	24.5	613	1705
303	-670	24.6	563	1588
308	-653	24.3	483	1317
313	-646	24.4	447	1227
318	-630	24.2	387	1031
332	-601	24.0	301	719
336	-588	23.7	270	654
355	-550	23.3	205	461

Table VIII-78. Variable pressure ^{17}O longitudinal ($1/T_1$) and transverse ($1/T_2$) relaxation rates of $DyCl_3$, $B_0 = 9.4$ T, pH < 3, $[Dy^{3+}] = 1.98$ m

P (MPa)	$1/T_1 (s^{-1})$	$1/T_2 (s^{-1})$
1	492	817
11	493	807
26	493	797
40	495	792
59	495	774
79	496	757
94	498	748
113	499	738
130	500	726
150	501	715
162	502	709

VIII.7　　　References

(1)　　Pinkerton, A. A.; Rossier, M.; Spiliadis, S. *J. Magn. Reson.* **1985**, *64*, 420.
(2)　　Bleaney, B. *J. Magn. Reson.* **1972**, *8*, 91.
(3)　　Aime, S.;　Calabi, L.; Cavallotti, C.; Gianolio, E.; Giovenzana, G. B.; Losi, P.; Maiocchi, A.; Palmisano, G.; Sisti, M. *Inorg. Chem*. **2004**, 43, 7588.

Curriculum Vitae

SHIMA KARIMI

EDUCATION

2012 - 2016	**PhD in Chemical and Biochemical Engineering** Swiss Federal Institute of Technology in Lausanne (EPFL), Switzerland
2009 - 2012	**MSc in Chemical and Biochemical Engineering** Swiss Federal Institute of Technology in Lausanne (EPFL), Switzerland
2004 - 2009	**BSc in Chemical Engineering** Sharif University of Technology, Iran

WORK EXPERIENCE

2012 – 2016
(4 years)

Swiss Federal Institute of Technology in Lausanne (EPFL), Switzerland – PhD Researcher
- **Research** – Study of water exchange and relaxivity of lanthanide complexes and aqua ions. The work resulted in 7 publications (6 published and 1 under review).
- **Project Management** – Directed 7 research projects in total. Managed multiple projects at a time.
- **Data Analysis** – Used Matlab and Excel to analyse vast data sets from over 300 scientific studies.
- **Teaching** – Over 700 hours of teaching in chemistry, physics and chemical engineering, taught 300 students in total. Supervised 4 master students' thesis and semester projects.
- **Laboratory Management** – Responsible for laboratory safety, mentoring of students on security guidelines and safety issues, participated in meetings with the university safety commission.

2011 – 2012
(7 months)

University of Manchester, United Kingdom – Research Scientist
- Research on hydrophilic nanoparticulate polymeric systems for biomedical and pharmaceutical applications. The work resulted in a publication in *Biomaterials*.

2010
(4 months)

Medipol SA, Switzerland – R&D Intern
- Independently directed a project to develop and charecterise biodegradable nanoparticles for drug delivery.
- Responsibilities included laboratory work, data mining and data analysis.

2008
(3 months)

Iranian Central Oil Fields Company, Iran – R&D Intern
- Carried out de-bottlenecking studies for gas pipelines using Pipesym and Hysis software packages.

CONFERENCES

- The 5th edition of GPOL conference, Klingenthal, Alsace, June 2014: Poster presentation.
- COST TD1004 ACTION, Athens, Greece, September 2013: Poster presentation.

PUBLICATIONS

- **Karimi, S**.; Lapicorey, G.; Bouvier, P.; Helm, L. in preparation.
- **Karimi, S**.; Tei, L.; Botta, M.; Helm, L. *Inorg. Chem.* **2016**, 55, 6300.
- **Karimi, S**.; Hunter, G.; Moriggi, L.; Platas-Iglesias, C.; Helm, L. *Inorg. Chem.* **2016**, 55, 6231.
- **Karimi, S**.; Helm, L. *Inorg. Chem.* **2016**, 55, 4555.
- Fontes, A.; **Karimi, S**.; Helm, L.; Ferreira, P. M.; André, J. P. *Eur. J. Inorg. Chem.* **2015**, 2015, 4798.
- Fontes, A.; **Karimi, S**.; Helm, L.; Yulikov, M.; Ferreira, P. M.; André, J. P. *Eur. J. Inorg. Chem.* **2015**, 2015, 1579.
- Boros, E.; **Karimi, S**.; Kenton, N.; Helm, L.; Caravan, P. *Inorg. Chem.* **2014**, 53, 6985.
- Almalik, A.; **Karimi, S**.; Ouasti, S.; Donno, R.; Wandrey, C.; Day, P. J.; Tirelli, N. *Biomaterials* **2013**, 34, 5369.

HONOURS, AWARDS & ACHIEVEMENTS

- **BASF Monthey SA Prize**: Awarded the best master project prize in Chemical and Biochemical Engineering, 2012.
- **Masters Project Abroad Scholarship Award**: Awarded a grant by the WISH Foundation at EPFL in the goal of fostering the success of talented women scientists and engineers, 2011.
- Top ranked student for three consecutive academic years at Sharif University.
- Ranked in top 0.1% for the Iranian National University Entrance Exam, 2004.
- Accepted into the National Organisation for Development of Exceptional Talents (NODET), 1997.

SKILLS

- Technical Skills: NMR spectroscopy, dynamic light scattering, uv/vis, cytotoxicity assessment, confocal microscopy.
- Software skills: Matlab, Origin, Excel, Word, PowerPoint, Chemistry software (Topspin; MestReNova; ChemDraw).
- Languages: English (fluent), Persian (native).